4-22-2021 9:00 AM

Differential Effects of KIM-1 in Subcutaneous and Orthotopic Renca Models of Kidney Cancer

Demitra M. Yotis DY, *The University of Western Ontario*

Supervisor: Gunaratnam, Lakshman, *The University of Western Ontario*

A thesis submitted in partial fulfillment of the requirements for the Master of Science degree in Microbiology and Immunology

Abstract

Renal Cell Carcinoma (RCC) is the most common and fatal type of kidney cancer. Over 30% of patients that are diagnosed with RCC exhibit metastases. Almost 88% of patients with distant metastases succumb to the disease within 5 years of diagnosis. Kidney Injury Molecule-1 (KIM-1) is a cell surface glycoprotein that is not expressed in a healthy kidney but becomes highly expressed on proximal tubular epithelial cells (PTECs) following injury. Data from the Cancer Genome Atlas (TCGA) reveals that >90% of RCC tumours express KIM-1 mRNA and that higher expression levels correlate with increased overall survival rates of patients. The pathophysiological role of KIM-1 in RCC is not well understood. Using human (786-O) and murine (RENCA) models, we recently uncovered that KIM-1 may inhibit the metastatic properties (invasion and extravasation) of RCC cells using *in vivo* and *in vitro* systems. The aim of this thesis work was to elucidate the mechanism by which KIM-1 regulates RCC tumour progression using syngeneic and pre-clinical orthotopic RENCA models.

Transcriptomic analysis of RENCA cells lacking or overexpressing KIM-1, and The Cancer Genome Atlas (TCGA), revealed significant upregulation of genes involved in extracellular matrix (ECM) interactions in association with KIM-1 expression. *In vivo,* subcutaneous implantation of RENCA tumours resulted in the development of thick, collagen dense, stromal capsules surrounding the tumours. This was observed in both immune-competent and immune-deficient mice. In a pre-clinical (orthotopic) model, KIM-1 expression inhibits primary RENCA tumour growth within the kidneys. Lastly, significant phenotypic differences in primary tumour growth, and histology were observed in between subcutaneous and orthotopic implantation of RENCA tumours.

Lay Summary

Kidney cancer comprises almost 4% of all adult malignancies and is the 8th most common type of cancer in humans. Renal Cell Carcinoma (RCC) is the most common and lethal type of kidney cancers. RCC is most lethal when it spreads to distant sites because it is resistant to many forms of anti-cancer therapy including chemo-, radio- and even modern immunotherapies. Over one third of patients have cancer that has spread at the time of diagnosis. Kidney Injury Molecule-1 (KIM-1) is a normal protein that is found in injured human kidneys and is aberrantly present in over 90% of RCC tumour samples obtained from cancer patients. Patients whose tumours have high amounts of KIM-1 seem to survive longer (due to cancer spread likely) but the reason for this is not known. The objective of my thesis was to determine how KIM-1 may protect patents with RCC from dying using genetic techniques and animal models of kidney cancer.

My work suggests that the role of KIM-1 in RCC greatly depends on the tumour model used. Overall, KIM-1 may protect patients with RCC by slowing the growth of tumours, and potentially, the spread of cancer cells to distant sites from the primary tumour. Our genetic studies suggest that KIM-1 may achieve this by altering the genes produced by the kidney tumours to produce a thick, collagen dense "capsule" around them. Further studies of these "protective" genes may help us to develop treatments for patients with RCC and potentially other cancers.

Keywords

Cancer, Renal Cell Carcinoma (RCC), Kidney Injury Molecule-1 (KIM-1), Subcutaneous, Orthotopic, Extracellular Matrix, Cancer Progression, Tumour Microenvironment, RNA-seq

Contributions Statement

The research work described in this thesis was supervised by my supervisor, Dr. Lakshman Gunaratnam, who also contributed research funds used to purchase all supplies, animals, equipment, and reagents needed to complete this work. Dr. Gunaratnam conceptualized the research, helped design the experiments and edited the thesis.

All raw TCGA human data was extrapolated and organized into a working excel spreadsheet by Audrey Champagne (CHU de Québec-Université). Audrey taught me how to analyze the data, as well as contributed the suggestion to analyze TMI signatures in correlation to KIM-1 in RCC. Audrey completed the spearman's correlation of TMI signatures and KIM-1 using KIPAN database.

Marie Sarabusky, a previous master's student within our lab generated stable Renca KIM-1^{pos} and KIM-1^{neg} cell lines for experimental use of this thesis.

All orthotopic renal surgeries were performed and supervised by Dr. Robert Gros.

Acknowledgements

First and foremost, I would like to thank my supervisor and mentor Dr. Lakshman Gunaratnam.

I was introduced to Dr. Gunaratnam while in my undergraduate studies at Wilfrid Laurier University. At that time, I had no previous wet lab experience. Every other graduate program rejected me based of this fact. Dr. Gunaratnam provided me with an opportunity and hired me as a volunteer in his lab. It was there that this journey began. For almost a year, I remained a volunteer, learning the ins and outs of daily lab life. In time, I was able to officially begin my MSc. This beginning brought with it many teachings. I credit these learnings not only to my intellectual growth, but also to my development as an individual.

Dr. Gunaratnam taught me how to analyze, learn and teach like a scientist – to think outside the box and to always think critically. He has taught me the importance of paying attention to detail and being prepared for experiments. He has also given me knowledge that I feel has benefited me greatly in these early stages of my career.

Dr. Gunaratnam, thank you for being the best supervisor a student can ask for. You took a chance on me when no one else would, and for that, I will always be grateful. Your personal success and drive to further your achievements is a true inspiration. I aspire to emulate that quality within my own journey. You have opened my eyes to a whole different world of science! Thank you for being supportive throughout my project, as well as giving great advice during hard times. I will miss our chats about science, life and the importance of work-life balance, and most of all, having a few laughs. Thank you for everything.

I would like to give a special thank you to Brad Shrum (Western University) for his great contributions to my project and all of his endless support.

Brad, you trained me to be the best version of myself in the lab. You taught me how to be a meticulous scientist (and a clean freak.) Because of how you trained me, our lab is always low on ethanol (cleaning with too much EtOH). I am grateful to have had you as a mentor and friend, your guidance and advice which shone a light in the dark when the path forward was at times unclear. Without you, I would have been lost in the lab. I will always cherish our talks about science, brainstorming cool ways of what KIM-1 is doing in RCC. I will never forget our laughs over coffee, and you making fun of my healthy eating habits. Thank you for your endless support and still being nice to me after I killed your lemon tree.

Next, I would like to thank Marie Sarabusky for her contributions to my project. Her work of generating the Renca cell lines was substantial and crucial to my project.

I would like to give a special thanks to Weihua Liu (Winnie). Winnie, you are such an amazing person to work with! Thank you for always completing my immunohistochemical staining and sectioning for me so quickly and effectively. You always know how to put a smile on my face. You have such a beautiful energy around you. Thank you for all of your help throughout my MSc.

I would like to thank Audrey Champagne (CHU de Québec-Université) for your hard work in generating the raw data files from the TCGA database. Thank you for always going above and beyond when replying to emails and answering the million questions I posed. Thank you for sitting in on zoom meetings with me for hours, helping me understand how to properly analyze clinical data. You inspired me to learn coding.

Jaclyn Diamond, thank you for being such a supportive friend. I am so grateful to have met you. I'll never forget the first time we met in MicroImm 9100. We were both ripping apart a grant application, something which made us become friends quickly. Thank you for always being there for a good laugh (or cry.) I loved our food runs and late lab nights. You made my experience in our department all the more fun. It wouldn't have been the same without you.

I would like to thank Dr. Xizhong Zhang for all of your help in the lab. Whenever we spoke, your kind nature would always put a smile on my face. You brought a great warmth to the LG lab.

Dr. Elena Tutunea-Fatan, thank you for being a helpful mentor and teaching me how to run a beautiful western blot.

Saranga Sriranganathan, you were my first friend in the LG lab. You are one of the most gentle and kindhearted people I know. Even when lab days were rough, you always brought a smile to my face. I will never forget us walking all the way to UH or the Natural Science Building to grab snacks and chat. You brought a special light into the LG lab, always making everyone smile and feel happy (even when you had been experiencing 100 failed western blots!). Thank you for letting me make fun of you and your KIM-1 struggles – I don't know anyone else who would be able to do 8 western blots a week. Thank you for always finding the positives in life.

Ji Yun Lee, thank you for being such an amazing mentor and friend. I aspire to be as kind as you. Thank you for always helping me, especially with math problems (even though we are both equally horrible at math.) You are such a kind and supportive friend. My favorite memories of us were obsessing over congee and nails, as well as talking tea at SDRI. I hope that like you, all the data I ever touch turns into **** significance.

Jasper Lee, also known as potato. Where do I begin with you? I will never forget the philosophical talks we had in the lab and in our car rides back and forth to Toronto. Thank you for being such an amazing friend. You brought a special vibe - you really knew how to brighten up a room and make everyone laugh. I am so proud and honored to share our academic accomplishments from LG lab together on our paper.

Bahar Entezari, I am so happy I met you. When Brad hired you, I had a feeling we were going to be good friends. Thank you for always being my rock. I will miss our days of working out at the Recreation Centre, walking to the lab and eating our meal prep at SDRI while running experiments. Thank you for encouraging me to be the best I can be. You inspired me to work harder, lift heavier, run faster and most importantly to try new things.

Shabitha Arumugarajah, I am so happy Dr. G hired you this year! Thank you for the endless support you have given me throughout my tough times. You have been such an amazing and selfless friend. Thank you for helping me with all my experiments and staying late with me when I needed help – by late, I mean this girl stayed until 3am just to help me! I am eternally grateful to have met you and I am so excited to see what you achieve in the future.

Thank you Rangi for being such a kind-hearted soul within our SDRI lab. Thank you for also staying late with me in lab to help make reagents for some of my final experiments. You have been an invaluable advisor to me in and out of the lab. I am grateful to have shared this past year with you.

Thank you Varunavee for being such a sweet and lovely person to work alongside. Your perseverance and hard work are inspiring and contagious. You are one of the most inspiring individuals I have met, and you have endless potential. I am so excited to hear about your future; you will do amazing things.

Rachel Creighton, I am so grateful to have met you. Your success in the Dekoter lab always pushed me to want to achieve great things. Your selflessness as a friend inspires me to be a gentler and kinder human. My favorite memories of us are working out early in the mornings, rushing to lab and then coming back and having lunch breaks together. We were attached at the hip! I wouldn't have had it any other way.

Thank you, Angus Scott for your support and being there for milestones throughout my MSc career. From my first committee meeting to my final talk, you pushed me to do my best.

I would also like to thank my advisory committee members Dr. Steven Kerfoot and Dr. Greg Dekaban for all of their support and guidance throughout my MSc training. Thank you for giving up your time to help me progress through graduate school. Your insights and knowledge of the scientific pursuit greatly impacted the success of my research. You are both such inspiring role models to me. I am grateful to have worked with you in my experience as a graduate student.

Dr. Kerfoot, thank you for all of your help with my microscopy experiments - you taught me how to properly fix my tissue and get the most beautiful images for my thesis. I would also like to thank you for your help with the widefield microscope when I experienced so many technical difficulties. I will never forget your support and kind words.

Dr. Dekaban, thank you very much for your guidance and feedback over the last two years. You always pushed me to want to be better, work harder and think more critically. Your advice helped me complete the circle with my last findings using human RCC data.

A big thank you to the entire Microbiology and Immunology Department, both students and faculty. This was an amazing experience; I am so happy to have had experienced graduate school here in our department. I have made countless friends and great memories.

I would like to personally thank all the mice I have worked with in my MSc. Thank you for making the sacrifice to allow my research to be completed. Thank you, little furry pals, for not

biting me and being cooperative while I inject you (most of the time). On a more serious note, while we made every effort to minimize animal life lost, none of our medical discoveries would have been possible without ethically conducted animal research. I know that the Gunaratnam Lab will continue to make every effort to minimize animal suffering and life lost.

Last but certainly not least, I would like to extend the warmest and biggest shoutout to my friends and family who have been here with me since day one. To my friends, who have always supported my love of science. I knew I could rely on you for your support.

Thank you to my amazing Mom and Dad - Dianne and George Yotis, for their unconditional love and support. Thank you for believing in me even when I thought I had no chance of pursuing my dream. Thank you for sending me all the way to London to volunteer for a year, financially helping me to work here and gain research experience. I'll never forget when my Dad gave me this piece of advice when I started volunteering in the LG lab "make sure you show up first and leave last." That's exactly what I did.

Lastly, I would like to recognize my grandmother, Flavia. My grandmother passed away of metastatic RCC when I was young. She was such a strong and beautiful woman, and I wish she could be here today to witness my small contribution to the field of RCC. In honor of her life, I would like to dedicate this MSc thesis to her. I had the option to choose a different project when I entered the Gunaratnam lab but decided to stick with this one for her. I am so grateful I had the opportunity to study a disease that directly affected one of my family members.

Table of Contents

List of Tables

List of Figures

List of Appendices

Abbreviations

AIM Apoptosis Inhibitor of Macrophages
AKI Acute Kidney Injury
Acid BLI Bioluminescence Imaging
BALB/c Bagg Albino (inbred research mouse strain)
ccRCC Clear Cell Renal Cell Carcinoma
cDNA Complementary Deoxyribose Nucleic Acid
CD44 Cluster Differentiation 44
COL6A1 Collagen 6 Subunit A 1
COL6A2 Collagen 6 Subunit A 2
CKD Chronic Kidney Disease
CO_2 Carbon Dioxide
CTLA-4 Cytotoxic T Lymphocyte Antigen 4
CXCL-8 CXC Chemokine Ligand 8
DAMPs Danger Associated Molecular Patterns
ddH_2O Double Distilled H_2O
DEPC Diethyl Pyrocarcbonate
DMEM Dulbecco's Modified Eagle Medium
ECM Extracellular Matrix EFA6
FBS Fetal Bovine Serum
GAPDH Glyceraldehyde phosphate dehydrogenase
Gα12/13 Alpha subunit of the G protein G12
GEM Genetically Engineered Mouse
GTP Guanosine Triphosphate
GTPase Guanosine Triphosphatase
HAV Hepatitis A
HAVCR1 Hepatitis A Virus Cellular Receptor 1
HIF Hypoxia Inducible Factor
HRP Horse Radish Peroxidase
IFN-γ Interferon Gamma
IGF Insulin Growth Factor
IL-1β Interleukin 1 Beta
IL-2 Interleukin 2
IL-6 Interleukin 6
IL-8 Interleukin 8
IL-10 Interleukin 10
IL-12 Interleukin 12
iNOS Inducible Nitric Oxide Synthase
NOS2 Nitric Oxide Synthase 2
NK Natural Killer
KIM-1 human and murine Kidney Injury Molecule-1
KIM-1^{pos} Kidney Injury Molecule-1 Positive
KIM-1^{neg} Kidney Injury Molecule-1 Negative
MCP-1 Macrophage chemokine protein -1
MOI Multiplicity of Infection

mTOR Mammalian Target of Rapamycin
NK Natural Killer
ORF Open Reading Frame
PDGF Platelet-derived Growth Factor
PBS Phosphate Buffered Saline
PD-1 Programmed Cell Death Protein 1
PDL-1 Programmed Cell Death Ligand 1
PLP Periodate-Lysine-Paraformaldehyde
PtdSer Phosphatidylserine
PTEC Proximal Tubular Epithelial Cell
Rag1 Recombinase Activation Gene 1
RCC Renal Cell Carcinoma or Renca Renal Cell Adenocarcinoma
RIPA Radioimmunoprecipitation assay
RNA-Seq Ribonucleic Acid Sequencing
RT-PCR Real Time-Polymerase Chain Reaction
SEM Standard Error of Mean
SCID Severe Combined Immunodeficient
STAT-3 Signal Transducer and Activator of Transcription 3
SQ-Unilat Subcutaneous Unilateral
SQ-Bilat Subcutaneous Bilateral
TCGA The Cancer Genome Atlas
TGF-β1 Transforming Growth Factor beta-1
TNFα Tumour Necrosis Factor Alpha
TIM-1 T Cell Immunoglobulin and Mucin Domain 1
TME Tumour Microenvironment
TMI Tumour Matrisome Index
Tregs T Regulatory Cells
uCr Urine Creatnine
VEGF/VEGFA Vascular Endothelial Growth Factor (A)
VHL von Hippel-Lindau
WT Wild type
γδ Gamma Delta

Chapter 1

1. Introduction

1.1 Cancer

Cancer is defined as a group of diseases that is caused by abnormal cells undergoing uncontrolled proliferation within any part of the human body that has the potential to invade nearby tissues or spread to distant tissues. Tumours consist of a (solid) collection of cells which can be benign or malignant. Malignant tumours are made up of cancerous cells which can cause death by infiltrating or destroying normal (local or distant) tissues (World Health Organization, 2018). Globally, cancer is the second leading cause of death – 1 in 6 deaths are caused by cancer (World Health Organization, 2018). According to the American Cancer Society in 2020, 1,806,590 new cancer cases were reported, with a total of 606,520 deaths (Siegel, Miller and Jemal, 2020). The Canadian Cancer Society, in 2019, estimated that nearly 1 in 2 Canadians will be diagnosed with cancer within their lifetime. In 2019 alone, it was estimated that 220, 400 new cases of cancer were expected to be diagnosed in Canada. Out of these expected cases, males have a slightly higher incident rate than females, with numbers at 113,000 cases vs 107,400 cases respectively. The risk of developing cancer in Canada has increased significantly with our aging population (Canadian Cancer Statistics Advisory Committee, 2019). Genetic alterations to cellular DNA and/or environmental effects are believed to be central to the development of many types of cancer. Unhealthy diets, physical inactivity, drug and alcohol abuse are all environmental factors that have been linked to an increased incidence of cancer worldwide. Various chronic infections can increase the risks of cancer development. For example, chronic infections such as with Helicobacter pylori and human papillomavirus (HPV) can result in the

development of pyloric and cervical cancer, respectively. One of the most common causes of death from cancer is the process of metastasis (World Health Organization, 2018). Metastasis is the process by which cells within a primary tumour break away from their originating boundary of growth, travel and inhabit local (neighboring) or distant tissues, resulting in the growth of a secondary tumour.

Hanahan and Weinberg famously proposed the six characteristics needed for cancer progression. These have been coined the hallmarks of cancer (Hanahan and Coussens, 2012). The six fundamental hallmarks of cancer include: sustained cell proliferation signaling, evading tumour and/or growth suppressors (e.g., immune system), invasion and metastasis, immortal replication, induction of angiogenesis and lastly resisting cell death. All of the listed hallmarks are key characteristics present in the vast majority of human cancers. These hallmark properties allow cancers to promote site specific inflammation, genetic instability leading to additional mutations, and evasion of immune destruction. These processes also allow for the cancerous cells to recruit non-neoplastic cells to the site of malignancy (e.g., macrophages), in order to benefit the cancer's progression. Critically investigating these mechanisms for specific cancers, allows us to have a better understanding of pathogenesis of that cancer and, to in turn, create higher efficacy treatments.

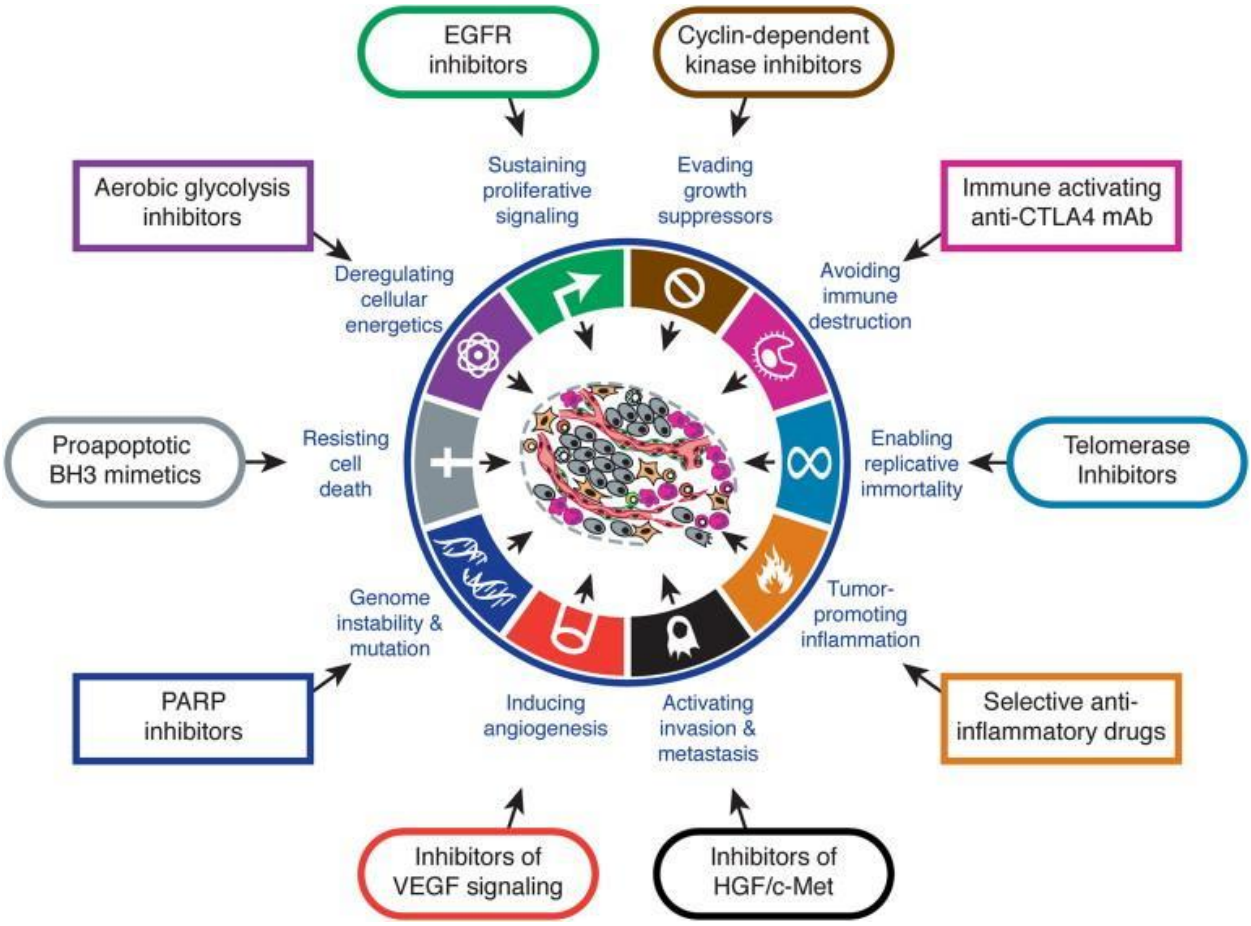

Figure 1. Hallmarks of Cancer
The six original hallmarks of cancer (Hanahan and Weinberg) along with newly found mechanisms that contribute to progression and metastasis (adapted with permission from Hanahan and Weinberg, 2011). Diagram including potential cancer therapeutics that can help combat the above mechanisms to benefit cancer treatment.

1.2 Renal Cell Carcinoma

Kidney cancer has been identified as the 8th most common form of cancer, causing 179,386 deaths globally in 2020 alone (Globocan, 2020). Renal cell carcinoma (RCC) is the most common form of kidney cancer, compromising up to 85%-90% of all cases (Chang *et al.*, 2016). RCC has the highest mortality rate out of all genital and urinary cancers. The Canadian Cancer

Statistics 2019 found from the approximate 100,000 new cases of cancer, renal and pelvic cancers have affected 4.2% and 2.3% of males and females, respectively (Canadian Cancer Statistics Advisory Committee, 2019). RCC is characterized as being a highly immunogenic cancer – where RCC tumours are recognized as foreign and elicit a strong adaptive immune response against it. By definition, the occurrence of RCC implies that these tumours evade the host's immune system. The survival rates vary greatly depending on the progression and presence of metastasis. If RCC is detected early while still being localized to the affected kidney (contained within the Gerota's fascia), surgical resection can be curative, although recurrence occurs in 20%-40% of those who have undergone surgical management (Chin *et al.*, 2006). Patients with distant metastases (metastatic RCC) have significantly reduced survival rates (American Cancer Society, 2016). Specifically, approximately 12% of patients with advanced disease die within 5 years of initial diagnoses (Choueiri and Motzer, 2017).

1.2.1 RCC Subtypes and Histological Properties

Histological analysis of RCC tumours is extremely important in determining patient prognosis as it aids not only in the diagnosis but also provides information about the histopathological type of RCC. Nephrectomy is used to make a tissue diagnosis before embarking on treatment. On rare occasions, percutaneous biopsy of small renal masses is undertaken if there is a high degree of suspicion of a metastatic lesion to the kidney from another type of cancer (Sahni and Silverman, 2009).

RCC is classified using histology into subtypes; Clear Cell Carcinoma (ccRCC) compromising ~75%, Papillary RCC (pRCC) compromising ~10%, Chromophobe RCC compromising ~5%, and lastly Collecting Ducts and Medullary RCC compromising each ~1% (Cairns, 2011; Li and

Kaelin, 2011). Up to 5% of RCC remain unclassified. The cellular morphology of ccRCC is characterized by cells with a lipid-rich cytoplasm. For pRCC, subtype 1 consists of spindle-shaped cells surrounding a basal membrane, and subtype 2 consists of spindle-shaped cells with visually prominent nuclei and an eosinophilic granular cytoplasmic space. Collecting Duct RCC histologically will present abnormal cells infiltrating the walls of the collecting ducts, causing a significant desmoplastic reaction. Lastly, Medullary RCC represents neoplasms localized to the distal nephron, characterized by hyperchromatic nuclei (Muglia and Prando, 2015).

1.2.2 Staging

Staging studies are crucial to developing a therapeutic plan for affected patients. A variety of imaging modalities are used to determine the size of the tumour as well as the extent of local and regional involvement. The most widely used is the (The American Joint Committee on Cancer (AJCC), 2017) Tumour, Node, Metastasis (TNM) (anatomic) staging system and it is used for staging all histological variants of RCC. The anatomic extent of disease is the most consistent predictor of prognosis in patients with RCC. In early stages – classified as either stage I or II - tumours can be any size (<7cm stage I, >7cm stage II) in diameter but are localized to the affected kidney only. Stage III is characterized by tumours of an undefined size within the affected kidney and metastasis to regional lymph nodes and/or into the major veins or perinephric tissues (but not beyond the Gerota's fascia of the kidney or into the ipsilateral adrenal gland) (Reznek, 2004). Lastly, stage IV is characterized by tumours that have spread beyond the Gerota's fascia to nearby tissues including the ipsilateral adrenal gland (Sandock, Seftel and Resnick, 1997). When metastatic disease is suspected at initial presentation, pathologic confirmation is obtained prior to starting therapy. The most common sites of metastasis are the lungs (29-54%), bones (16-31%), liver (8-30%), renal fossa and brain (2-10%)

(Shao *et al.*, 2019). Although approximately 65% of tumours are limited to the kidney (Stage I-III) at initial diagnosis, over 20% of these patients will experience a relapse after receiving definitive treatment (Shao *et al.*, 2019).

1.2.3 Risk Factors and Causes

A number of established risk factors exist for the development of RCC and include both genetic and environmental factors. A number of hereditary kidney cancer syndromes have been described including autosomal dominant polycystic kidney disease, Tuberous Sclerosis Complex and Von Hippel-Lindau disease (Gnarra *et al.*, 1994; Keith *et al.*, 1994; Yang *et al.*, 2014). The most common genetic alteration found in patients with sporadic RCC is the mutation of the von Hippel-Lindau tumour suppressor gene, also known as the VHL gene. Similar to many genes, VHL is co-dominantly expressed. In familial RCC, gene alterations of one inherited allele causes patients to exhibit VHL disease predisposing them for RCC tumour growth. In sporadic RCC, both alleles of the VHL gene are functional at birth, yet bi-allelic gene alterations occur postnatally causing the spontaneous development of RCC (Ma *et al.*, 2001).

The VHL gene is located on chromosome 3p region and encodes for the VHL protein. VHL protein acts as a tumour suppressor gene by regulating cellular division and preventing increased proliferation (Gnarra *et al.*, 1994). The VHL protein is mostly commonly known to form a stable protein complex with elongin C and B, as well as proteins Cul-2 and RBX-1 (Pause *et al.*, 1997). This VHL protein complex functions as a ubiquitin-protein ligase, that has many downstream effector targets. In normoxic, healthy conditions - where the VHL gene is unaltered – the VHL protein complex is able bind to the hydroxylated form of hypoxia inducible factor 1-alpha (HIF-1α) or hypoxia inducible factor 2-alpha (HIF-2α) and target the subunit for degradation via

ubiquitination. Under conditions of hypoxia, HIF-2α escapes ubiquitination by VHL as it is not hydroxylated by oxygen-dependent prolyl hydroxylases (Groulx and Lee, 2002). Under conditions where the VHL gene is altered and non-functional, the VHL protein complex is unable to bind to hydroxylated HIF-1α and thus unable to target the complex for destruction. Due to this, HIF-1α becomes continuously expressed on cells leading to the enhancement of downstream HIF transcription factors, also acting as a positive feedback loop. Overall, increased HIF transcripts result in cellular dysregulation. For example, HIF-2α enhancement mimics hypoxic cellular conditions activating apoptotic and glycolytic pathways, while increased HIF-2α enhances angiogenesis and cell proliferation. Inactivation of VHL results in upregulation of VEGF, which results in increased metabolism and angiogenesis (Verine *et al.*, 2010). Overall, the HIF-2α transcripts together with the malignant tumour microenvironment (TME) resulting from excess VEGF drive the development and progression of RCC (Rechsteiner *et al.*, 2011).

1.2.4 Treatments for RCC

1.2.4.1 Surgery

As of today, there is no therapy for RCC that is guaranteed to be curative, but some patients have experienced complete and permanent remission. The field has seen many advancements in therapeutics owing to recent breakthroughs in cancer immunology. Treatments options for RCC range from surgical resection to non-targeted (older) drugs, to molecular targeted therapies, to novel immunotherapies and various combinations of these which are currently being tested in clinical trials. The most successful and tried form of treatment for localized RCC (stage I-III) is surgical resection, either through partial or radical nephrectomy. This consists of the removal of only a portion of the kidney containing the tumour, removal of one affected kidney, or removal of the affected kidney along with nearby lymph nodes and adrenal gland, respectively (National

Cancer Institute, 2020). Unfortunately, surgery has major limitations as a primary treatment. Nephrectomy is indicated for patients with tumours contained within the kidney's Gerota's fascia (stages I-III) (Reznek, 2004). Radical or partial nephrectomy have been found to improve patients' 5-year survival rate. However, in patients that present with metastatic RCC, surgery alone is not a feasible form of treatment, and is only used in order to reduce painful symptoms or as cytoreductive treatment in combination with systemic therapy (De Vivar Chevez, Finke and Bukowski, 2014).

1.2.4.2 Targeted Therapies

Decades of research into the pathogenesis of clear cell RCC (the most common subtype), including the discovery of the roles of HIF-2α and VEGF, have led to the development of a myriad of molecular targeted therapies for patients with RCC (Cho *et al.*, 2016; Choueiri and Kaelin, 2020). Instead of enhancing mechanics of the immune system to combat disease, molecular targeted therapies attack or inhibit mechanisms that assist directly in cancers progression (see hallmarks of cancer above). These include inhibiting processes such as angiogenesis and increased proliferation. The knowledge of the crucial role of mammalian target of rapamycin (mTOR) and vascular endothelial growth factor (VEGF) (or its receptor) in the progression and metastases of RCC have greatly improved treatments of metastatic RCC (Heng, Kollmannsberger and Chi, 2010). mTOR is a highly conserved protein kinase that regulates cell proliferation, apoptosis, along with various signaling biological pathways within the body. mTOR is a downstream effector of the PI3-K/Akt/mTOR pathway. This signaling pathway is activated in RCC tumours, playing a significant role in cell proliferation, tumour metabolism, and immune cell differentiation also creating a positive feedback loop. Initiating the PI3-K/Akt/mTOR pathway is caused by the extracellular binding of growth factors which initiate

activation of tyrosine kinase receptors (Porta, Paglino and Mosca, 2014). This interaction mediates intracellular PI3-K to phosphorylate PIP2 into PIP3. PIP3 then binds to the activated PDK1/2 complex which downstream binds to Akt at its PH domain, allowing activation through phosphorylation (Battelli and Cho, 2011). When Akt is in its activated state, it has the ability to inhibit the tumour suppressor complex TSC1/TCS2. Downstream, this complex inhibits Rheb GTPase – a crucial player in the inhibition of mTOR signaling pathway in cancer. With inhibition of the tumour suppressor TSC1/TCS2 complex and Rheb, mTOR signaling allows for anabolic proliferation and dysregulation of cellular functions (Huang and Manning, 2008). Allosteric inhibitors of mTOR such as temisirolimus and everolimus, have shown significant anti-tumour effects in patients with advanced staged RCC. Combination strategies also increase efficacy and overall patient response.

Another targeted therapy commonly used in RCC treatment is anti-VEGF. VEGF is identified as an important mediator in the development and progression of RCC, as it greatly impacts tumour vascularity and thus metabolism (Stitzlein, Rao and Dudley, 2019). Specifically, HIF transcription factors target genes such as VEGF, PDGF, IGF, and TGF-α which directly implicate alterations in angiogenesis, glucose transport, apoptosis, cell signaling, and pH regulation. Various multi-kinase inhibitors such as sorafenib, are able to inhibit VEGF, PDGF, c-Kit receptor tyrosine kinases and show positive results in reduction of disease in metastatic RCC patients, with feasible toxicity (Larkin and Eisen, 2006).

1.2.4.3 Immunotherapies

Other forms of treatment involve the use of immunotherapies. Immunotherapy is a form of treatment which uses the patient's own immune system to target and potentially destroy the

cancer. Immunotherapies are an integrated form of therapy for RCC yet have shown positive results due to RCCs immunogenic nature. In the early 1990's, Interleukin-2 (IL-2) and IFNγ were the first cytokine specific treatments used to treat metastatic RCC. These two cytokines were chosen because: IL-2 promotes T-cell activation and effector function; and IFNγ triggers activation of T-cells, enhances antigen presentation by antigen-presenting cells and promotes activation of macrophages (Tau and Rotherman, 2001). In 1992 the FDA approved high-dose IL-2 as a treatment for advanced RCC (Rosenberg, 2007). Patients experienced overall response rates of up to 25%, although IL-2 was not well-tolerated amongst patients due to its toxicity at high doses. Later on, IFNγ was tested as a monotherapy for metastatic RCC patients. Clinical trials began using low-to-moderate doses of IFNγ – as they were deemed more biologically effective in previous *in vivo* experiments rather than higher doses. Early-stage clinical trials consisted of doses at 100μg/patient administered once per week, resulting in promising outcomes where the total response rate was 30%, and well tolerated by patients (Aulitzky *et al.*, 1989). In trials with patients with later stage disease, there was found to be no significant difference between both response and survival rates when comparing placebo to treatment. Hence, IFNγ as a monotherapy was not further investigated for RCC treatment. With these promising results, combination therapy of IL-2 and IFNγ began to be administered to RCC patients. Although these results were positive, only a small fraction of patients responded to the therapy, albeit incompletely (Escudier *et al.*, 1993).

More recently, the field has seen the emergence of ground-breaking immunotherapies that target T cell checkpoints (e.g. programmed cell death ligand-1 (PDL-1) and programmed cell death-1 (PD-1) and/or CD80/CD86 and cytotoxic lymphocyte antigen 4 (CTLA-4)). The agents are primarily monoclonal antibodies that block inhibitory signaling by the ligand-receptors pairs.

PD-1 is a receptor expressed on antigen presenting cells of the immune system, and when bound by its ligand PDL-1 – commonly found on antigen presenting cells and some cancer cells (Weinstock and McDermott, 2015) – suppresses T cell activation, allowing the tumour to escape immune destruction primarily through the exhaustion of cytotoxic $CD8^+$ T cells (Lu *et al.*, 2019). These immunotherapies have shown favorable results in in clinical trials when delivered as a monotherapy or in combination with other immunotherapies (anti-CTL-4) (Motzer *et al.*, 2018). Therapy was associated with an increase in intratumoural T-cell tracking, reduced immunosuppressive cytokines and T-regulatory cells, as well as an increase in anti-angiogenic properties (Weinstock and McDermott, 2015). In the process of T cell activation/priming, two positive activating signals must take place between T cell and antigen presenting cells (APCs) to allow for the success of T-cell priming. Stimulatory signal consists of the T-Cell Receptor (TCR) to the Major Histocompatibility Complex (MHC) presenting the unknown peptide, along with CD28 engagement on T-cells to CD80/CD86 on the APC. During times of autoreactivity (Boehncke and Brembilla, 2019), CTLA-4 on T-cells will bind to CD80/CD86 on the surface of APCs sending a inhibitory signal, rendering the T cell to become inactive (Buchbinder and Desai, 2016). CTLA-4 - an inhibitory molecule binds to CD80/CD86 (B7-1/B7-2) with much greater affinity than CD28 on T cells, and when engaged delivers an inhibitory signal to activated T cells (Pardoll, 2012). In cancer, blocking the inhibitory signal between CTLA-4 and CD80/CD86 has been found to enhance both priming and activation of T cells and various immune cells (Tang *et al.*, 2018). Thus, using monoclonal agonist antibody anti-CTLA-4 (Ipilimumab) as an immunotherapy in RCC, has been shown to increase T cell effector functions resulting in enhanced anti-tumour immunity (Seidel, Otsuka and Kabashima, 2018). Combination therapy with both anti-PD1 and anti-CTLA-4 antibodies was shown to have

synergistic effects on anti-tumour immunity, being able to increase overall response rates against malignancies (Motzer *et al.*, 2018). Although this therapy has been shown to cause progression-free outcomes with increased overall survival, there is still a major limitation of patient-patient variation in response (Cairns, 2011). Also, the overall response rates have been low (Weinstock and McDermott, 2015).

1.2.5 Patient Immune Profile or Immune Microenvironment

To enhance potential treatments, patient profiles have been examined to comprehend the immunological mechanisms throughout the clinical stages of RCC. Many clinical studies have evaluated patient serum for cytokine levels, indicative of the immune phenotype and tumour microenvironment present. A recent clinical study aimed to find differences in tumour-associated interleukins (IL) and cytokines from collected metastatic RCC patients treated with IL-2 immunotherapy and compare the results of serum from healthy donors. This study aimed to find differences in immunomodulatory cytokines such as IL-10, IL-6, IL-12, IL-8, and IL1β, as well as tumour necrosis factor-alpha (TNFα). Results found higher levels of cytokines that implement an immunosuppressive effect; increased IL-8, IL-6, and c-reactive protein. Patients found to have an immunosuppressive cytokine profile correlated directly with an overall reduced survival rate (Guida *et al.*, 2007).

1.2.6 The Tumour Microenvironment (TME)

The tumour microenvironment (TME) is made up of cancer cells, stromal tissue, and surrounding extracellular matrix. The immune system plays a fundamental role in shaping the TME. Intense study of the complex interactions between cancer cells and the host immune response has led to novel therapies that serve to block tumour progression. This interaction often

creates an environment that promotes tumour progression throughout all stages of malignancy. In immunogenic cancers, similar to RCC, the TME contains a vast variety of immune cells such as $CD8^+$ T cells, γδ T cells, along with fibroblasts, and endothelial cells (Hanahan and Coussens, 2012). The types of immune cells (e.g. T cells, innate lymphoid cells, macrophages etc.) within the TME are believed to be dependent on cell-cell communications between the RCC cells, the extracellular matrix and immune cells. Various studies investigating the transcriptomic profile of human RCC tumours have allowed for a clearer understanding of the components within RCC TME. This information has helped us to understand why RCC is able to evade immune destruction, despite being a highly immunogenic cancer. Immune signatures that are commonly observed in RCC are the expression of tumour promoting checkpoint inhibitors PD1, PDL1, and CTLA-4. Histopathologic and transcriptomic analysis of RCC tumours has identified three distinct immune profiles : 1) T cell enriched tumours that are infiltrated with an abundant quantity of T-Lymphocytes; 2) Non-infiltrated tumours that have a scarcity of infiltrating immune cells, and 3) Heterogenous tumours that are composed of diverse amounts of immune cells alongside the malignant cells. RCC tumours follow the phenotype of 1) or 3) – being a cancer with one of the highest T cell infiltrates and/or having tumours with heterogenous immune profile containing diverse types immune cells. Despite this immunogenic feature of RCC tumours – many patients succumb to the disease. A majority of RCC patients present with a heterogenous immune profile – although seemingly beneficial to patients - outcomes of this TME result in the poorest survival. The abundance of antigen presenting machinery also does not have clear correlations with tumour progression. Thus, analyzing specific immune cell effector functions along with their abundance can better help understand why these highly infiltrated tumours are able to evade immune destruction immunogenic. RCC tumour immune infiltrates

contain vast levels of mainly $CD8^+$ T cells, neutrophils, macrophages, and plasmacytoid Dendritic Cells (pDC). Higher frequencies of cytotoxic cells such as $CD8^+$ T cells within the TME is a characteristic that would seem to be extremely beneficial to patients, yet with RCC, high correlations of $CD8^+$ T cells alone do not correlate to increased survival. Instead, a higher ratio between cytotoxic and immune regulatory cells improve survival; specifically, the balance between $CD8^+$ T cells and T regulatory cells (Tregs) is shifted to CD8+ T cells. Tregs are a specialized immune cell able to suppress T cell proliferation and activity; known to inhibit autoimmunity, yet in cancer are able to suppress anti-tumour T cell immunity (Romano *et al.*, 2019). Heterogenous RCC tumours have significant changes when compared to T cell enriched profiles, suggesting that the T cell enriched tumours have distinct gene alterations that cause this unique immune profile (Şenbabaoğlu *et al.*, 2016). The enhancement of the T cell enrichment in RCC tumours could be due to genomic alterations that generate neoantigens or make existing antigens more immunogenic (Germano *et al.*, 2017) .

Another common phenotype observed in the TME of multiple cancer types is the abundance of extracellular matrix (ECM). ECM is a crucial component of the TME – able to influence tumour cell activity and biosynthesis (Xu *et al.*, 2019). A major component of the ECM are the collagens present (Nissen, Karsdal and Willumsen, 2019). Several mutated genes influence the interaction between cancer cells and the elements compromising the ECM, which can contribute to increased production of collagen (Xu *et al.*, 2019). Collagen activity such as degradation and re-deposition within a tumour can affect several processes in cancer progression such as infiltration, invasion, migration, and angiogenesis. The role of collagen in cancer has been found to have a paradoxical effect by both promoting and inhibiting tumour progression throughout cancer development (Fang *et al.*, 2014). In vitro studies have shown that collagen deposition is able to

inhibit lymphocyte locomotion in both human melanoma and RCC (Applegate, Balch and Pellis, 1990). In human lung tumours, collagen deposition is directly related to decreased intratumoural cytotoxic $CD8^+$ T cells – specifically, collagen is found to induce $CD8^+$ T cell exhaustion through collagen receptor interaction of LAIR1. More importantly, this study also revealed that increased collagen deposition is able to promote immune checkpoint blockade PD-1/PDL-1 resistance (Peng *et al.*, 2020). On the other hand, hypermethylation thus inactivation of specific collagen genes such as collagen type 1 α 2 (COL1A2), increase invasive capabilities of human bladder cancer (Mori *et al.*, 2009). Specifically, the role of collagen on RCC tumour progression is not fully understood. Using both TCGA database and histological analysis of ccRCC human tumours have revealed that collagen type 23 α 1 (COL23A1) correlates with larger tumour sizes and decreased overall survival, respectively (Xu *et al.*, 2017). Tumour tissue bank analysis has also implicated collagen type 6 α 1 (COL6A1) to be a predictive marker for overall survival of ccRCC patients (Wan *et al.*, 2015). Although RCC immune profiles and TME associated genes of interest (COL23A1 and COL6A1) have been classified, the mechanisms that occur to differentiate these microenvironments are not well understood. In order to combat this disease, we must elucidate the cellular mechanisms that cultivate a malignant TME in RCC tumours.

1.2.7 Murine Models for Renal Cell Carcinoma

A variety of murine models are used to study the *in vivo* progression and metastasis of RCC. Murine models of RCC have been found to accurately reflect human disease and can be used widely in experiments investigating primary and secondary tumour progression, as well as therapeutic treatment evaluation (Murphy and Hrushesky, 1973). Three types of animal models

that are widely used in the *in vivo* research of RCC are syngeneic models, xenograft models, and genetically engineering mouse models (GEM).

1.2.7.1 Syngeneic & Genetically Engineered Mouse (GEM) Models of RCC

The two major types of cancer models are the spontaneous and transplanted tumour models. Recent breakthrough in our understanding of genetic defects in clear cell RCC has led to the development of new spontaneous models of murine RCC (Harlander *et al.*, 2017). However, the vast majority of RCC research has relied on transplant models in mice (Sobczuk *et al.*, 2020). Syngeneic models are the transplantation of a cancer cell line that has the same genetic background as the host (mouse). One of the most widely used murine syngeneic models of RCC is the Renca model where the murine RCC cell line is transplanted into BALB/c *Wild-type* mice. This mouse model is syngeneic because Renca is a murine RCC cell line that was derived from a BALB/c mouse that spontaneously developed a renal malignancy (Murphy and Hrushesky, 1973). There are many advantages to using the syngeneic mouse model – they are more economical and simplistic. Syngeneic models have been crucial to developing and studying the mechanism of novel immunotherapeutics for RCC, including immune check-point inhibitors. For instance, this model allows for the investigation of how the immune system interacts with the cancer – this has permitted investigations of tumour immune profiling as well as tumour microenvironmental changes that occur in RCC. Another commonly used murine model is genetically engineered mouse (GEM) models. The GEM models are created by introducing genetic alterations of possible genes of interest thought to be involved in the progression of disease. This can include one or more genes that can be deleted, mutated, or overexpressed (Sobczuk *et al.*, 2020).

1.2.7.2 Xenografts

Another tumour transplant mouse model that is commonly used is the xenograft model. Here human derived cell lines or tissues are implanted into either humanized or immune deficient mice. These models can be differentiated in two forms of experimental use: xenografts using conventional cell lines, or xenografts using patient derived specimens. Commonly used mice for xenograft implantation are Rag1-/- deficient mice, severely compromised immunodeficient (SCID) mice, or nude mice (lack thymi and hence T cells). Each murine model has an insufficient adaptive immune response, allowing for neo-antigens of the human derived transplanted cell lines to pass immune surveillance and create a tumour (Richmond and Yingjun, 2008). Xenografts are more clinically relevant because they utilize human cells, yet are limiting due to genetics and histology poorly reflecting human cancers (Becher and Holland, 2006).

1.2.7.3 Limitations of Murine Models

Each tumour model has its advantages and disadvantages, but as a whole, they have aided scientists to better understand the biology of RCC. Some are more clinically relevant and better suited for testing potential therapies. Unfortunately, a vast majority of kidney cancer cell lines are not compatible with syngeneic and GEM murine models. Many syngeneic models are used within rodents such as mice and rats, yet poorly reflect the development and progression of human cancers. The mouse models that correlate best with clinical findings in patients are the xenograft and GEM models as they mimic the genetic alterations and/or histological properties of human RCC (Sobczuk *et al.*, 2020). Although, GEM models often poorly predict human tumour response to therapy (Richmond and Yingjun, 2008). Another major pitfall of the syngeneic mouse model is that the stromal component of TME observed within the tumour

model is made of mouse cells. Due to this, tumour microenvironmental studies may not accurately represent that of the human RCC TME.

1.2.7.4 Subcutaneous vs. Orthotopic (pre-clinical) Models of RCC

Syngeneic, xenograft, and GEM models can all undergo cancer cell line injections using different methods of implantation. Subcutaneous delivery is the most common form of cancer cell line implantation – it is the process of injecting cancer cells in the space underneath the skin and above the muscle, commonly within the flanks of mice. Although this model allows for the easy establishment and monitoring of tumours over the skin using calipers, this mode of implantation does not reflect the natural microenvironment of human RCC. A more clinically relevant model of RCC is the orthotopic model – here RCC cell lines are implanted into the kidney (where RCC originates in the human body). Orthotopic injections can be performed with syngeneic, xenograft, and GEM mouse models (Richmond and Yingjun, 2008). Orthotopic implantations have been shown to mimic primary tumour progression, local invasion and spontaneous metastases to distant organs such as the lymph nodes, lungs and liver as observed in human RCC (Salup, Herberman and Wiltrout, 1985).

1.3 Kidney Injury Molecule-1

Kidney injury molecule-1 (KIM-1), also known as hepatitis A virus cellular receptor 1 (HAVCR1) or T cell immunoglobulin receptor mucin domain 1 (TIM-1) , is a cell-surface receptor (Han *et al.*, 2002). KIM-1 belongs to the TIM family of glycoproteins which are type-1 transmembrane proteins consisting of an extracellular immunoglobulin like IgV domain, a hyper-glycosylated mucin domain, a transmembrane domain and an intracellular cytoplasmic domain. KIM-1 is expressed on various human tissues and cell types including the kidney, liver, lung,

spleen, T cells and B cells– possessing multiple functions including its involvement in acute kidney injury and repair, hepatitis A virus infection, T cell trafficking and autoimmunity (Bonventre, 2009; Zheng *et al.*, 2019). In the kidney, KIM-1 is not expressed during a healthy state but is the most upregulated protein following acute kidney injury (Ichimura *et al.*, 1998). KIM-1 is specifically expressed on the apical surface of proximal tubule epithelial cells (PTECs) immediately following kidney injury (Bonventre, 2008; Ajay *et al.*, 2014). Interestingly, KIM-1 undergoes spontaneous and accelerated (with more injury) ectodomain shedding releasing the cleaved or soluble KIM-1 into the lumen of the kidney, ultimately ending up in the blood and urine of affected patients (Gandhi *et al.*, 2014). This makes KIM-1 a sufficient clinical biomarker for kidney injury in the urine and plasma of humans, mice, and rats (Sabbisetti *et al.*, 2014).

1.3.1 Function of KIM-1 in the Kidney

The IgV portion of KIM-1 contains an ion-dependent ligand binding domain that forms an active site for recognition of the membrane phospholipid, phosphatidylserine (PtdSer) (Santiago *et al.*, 2007) – "eat me" signal - that is expressed on the outer surface of early necrotic and apoptotic cells. KIM-1 is a scavenger receptor that is able to recognize other "eat me" signals on apoptotic cells such as oxidized low-density lipoproteins (LDL) (Ichimura *et al.*, 2008). Thereby, KIM-1 enables PTECs to engulf apoptotic cells, promoting repair and regeneration of the renal tubules following acute kidney injury (Yang *et al.*, 2015; O. Z. Ismail *et al.*, 2016). Binding of KIM-1 to apoptotic cells triggers intracellular signaling via its cytosolic domain to inhibit NF-kB activation and downregulate Toll-like receptor 4 expression (Yang *et al.*, 2015). The clearance of necrotic cells, which predominate after acute kidney injury, is also facilitated by KIM-1 expressing PTECs, but this requires the opsonin, Apoptosis Inhibitor of Macrophages (AIM), which is appears in the tubules through glomerular filtration of blood. Within the tubules, AIM opsonizes

necrotic debris and cells, subsequently allowing KIM-1 to bind to AIM and engulf the debris via KIM-1/PTEC mediated phagocytosis (Arai *et al.*, 2016). This rapid clearance of dead cells prevents excess inflammation build up and the release of danger associated molecular patterns (DAMPs) from the apoptotic cells (Kobayashi *et al.*, 2007).

1.3.2 KIM-1 in RCC

KIM-1 expression is elevated in approximately 80%-90% of human RCC patients, specifically expressed in both clear cell RCC and papillary RCC – two of the most common forms of RCC (Han *et al.*, 2005; Lin *et al.*, 2007). Both of these subtypes of RCC have allowed for the non-invasive surveillance and early detection of RCC development through detectable levels of soluble/shed KIM-1 in patients plasma and urine (Han *et al.*, 2002). Urinary KIM-1 is significantly upregulated in RCC patients prior to surgical nephrectomy, and subsequently reduced either with notable reduction or complete absence of urine KIM-1 post-nephrectomy (Zhang *et al.*, 2014). Recent studies have also shown that as early as 5 years before initial diagnosis of RCC, KIM-1 is upregulated in the plasma of patients (Scelo *et al.*, 2018).

The pathophysiological role of KIM-1 in human RCC is not well known. There have been several studies that have proposed conflicting roles for KIM-1 in RCC. Research by Scelo and Muller et al., 2018 found that increased plasma concentrations of KIM-1 were associated with worse survival rates in RCC patients (Scelo *et al.*, 2018). Another study by Cuadros et al., 2014, studied intrinsic mechanisms involved in the progression of RCC. Specifically, this study analyzed the human RCC cell line, 769-P where KIM-1 is basally overexpressed, by silencing its expression and reported that KIM-1 directly activates IL-6/STAT-3/HIF-1α axis, in turn possibly driving angiogenesis and tumour progression. Moreover, this study found that KIM-1

activation of IL-6/STAT-3/HIF-1, is dependent on KIM-1 ectodomain shedding (Cuadros *et al.*, 2014).

1.4 Rationale, Objective and Hypothesis

1.4.1 Rationale

Renal cell carcinoma (RCC) is the most common and lethal type of kidney cancer (Cohen and McGovern, 2005). RCC originates within the proximal convoluted tubules of the kidney, and can metastasize to the adrenal gland, nearby lymph nodes, and distant organs such as the lungs. Despite the fact that RCC is characterized as a highly immunogenic cancer, >30% of patients present with (local or distant) metastatic disease at initial diagnosis, with >88% of these patients dying within 5 years (Decastro and McKiernan, 2008; Choueiri and Motzer, 2017). As of today, there is no cure for RCC, and the current treatments are inadequate.

The primary form of treatment for localized RCC is surgical resection of the tumour. Although this treatment is very common, the method is problematic for metastatic RCC. Current treatments for metastatic RCC include immunotherapies (Motzer *et al.*, 2019) and targeted therapies (e.g. sunitinib) that focus on immune checkpoints (Motzer *et al.*, 2013). There is a strong demand for novel therapeutics for metastatic RCC, as the cancer is highly resistant to many existing therapies. Immunotherapies such as anti-PDL-1/PD1 (Weinstock and McDermott, 2015), anti-CTLA-4 (Seidel, Otsuka and Kabashima, 2018), and targeted therapies such as mTOR (Everilimus (Donskov *et al.*, 2020)) and VEGF (Sunitinib (Ravaud *et al.*, 2016)) inhibitors, have been shown to reduce tumour progression and overall survival of patients with RCC (Vachhani and George, 2016). The most promising treatment to date for metastatic RCC

are blocking antibodies targeting the immune checkpoints aimed at enhancing anti-tumour immunity in patients: PDL-1 (Nivolumab), PD-1L (Avelumab) and CTLA-4 (Ipilimumab) (Motzer *et al.*, 2015, 2018). Unfortunately, response rates and major improvement in overall survival have been limited.

A characteristic of RCC is the cell surface expression of Kidney Injury Molecule-1 (KIM-1). KIM-1. Although KIM-1 is known to play an anti-inflammatory and reparative role in acute kidney injury, its specific role in RCC (including metastasis) are unclear. Analysis of The Cancer Genome Atlas (TCGA) database has shown that >90% of all patients with RCC express KIM-1, additionally correlating with overall increased survival (Lee and Gunaratnam, 2019).

Recent findings from our team have demonstrated that tumour associated KIM-1 inhibits metastasis. Specifically, we found that KIM-1 expression on murine Renca, and human 786-O cells inhibits extravasation and invasion *in vitro*. KIM-1 expressing human 786-P cells were found to have a significant reduction in extravasation capability in an *in vivo* CAM model. Moreover, using an experimental metastasis model, we found that KIM-1 expressing Renca, and 786-O cells had significantly reduced metastasis to the lungs, independent of adaptive immunity. Lastly, we identified two pro-metastatic, invasion, and adhesion genes, Rap1 and RAB27b, that may be downregulated by KIM-1. Overall, our findings reveal a novel inhibitory role of KIM-1 in the metastatic cascade of RCC (Lee and Gunaratnam, 2019). These previous findings suggest that KIM-1 may be playing a beneficial role for RCC patients. Further determining the pathophysiological role of KIM-1 in RCC progression, may provide new insights into its pathogenesis and potentially identify KIM-1 as a therapeutic target.

1.4.2 Objective and Hypothesis

The objective of this study was to further understand the pathophysiological role of KIM-1 in RCC tumour progression. Based on preliminary clinical findings from TCGA database, we hypothesized that KIM-1 expression on RCC inhibited tumour growth and progression. To study this, we generated murine RCC Renca cell lines to overexpress KIM-1 (KIM-1^{pos}) or to not express KIM-1 (KIM-1^{neg}) through lentiviral transduction, and further investigate *in vitro* and *in vivo* effects.

1.4.3 Specific Aims

The aims outlined in the work of this thesis are: 1) To evaluate whether KIM-1 expression alters Renca tumour growth within immune competent syngeneic BALB/c mice. 2) Characterize the TME of KIM-1^{pos} vs KIM-1^{neg} Renca tumours. And 3) Investigate potential mechanisms and downstream targets of KIM-1. We hypothesize that KIM-1 inhibits primary tumour growth in our subcutaneous immune competent model, that KIM-1 alters the TME allowing for a greater anti-tumour immune response, and lastly that KIM-1 expression is able to inhibit primary tumour growth through downstream targets similar to those found within human RCC.

Chapter 2

2. Methods and Materials

2.1 Generation of KIM-1 Expressing Stable Cell Line Using Lentiviral Particles

A previous master's student from our laboratory generated our mouse cell lines utilized for the aims of this thesis. The mouse Renca adenocarcinoma cell line (Murphy and Hrushesky, 1973) known as Renca (CRL-2947) was purchased from American Type Culture Collection (ATCC) and transduced with Lentiviral Open Reading Frames (ORF) particles containing empty vector or encoding the mouse KIM-1 gene, *Havcr1*. The generation of these cell lines are described in detail elsewhere. Briefly, lentiviral ORF particles containing a vector coding the mouse KIM-1 gene transcript (MR203831L3V; Origene, Rockville, MD), was used to implement the overexpression of KIM-1 to generate Renca KIM-1^{pos} cells. Control Lentiviral ORF particles containing the same vector without the presence of the mouse KIM-1 gene transcript (PS100092V; Origene, Rockville, MD), was used as a control to generate Renca KIM-1^{neg} cells. The lentiviral particle concentration used for transduction was determined using multiplicity of infection (MOI) ratios. The desired MOI refers to the number of virion infectious particles to the number of cells that are needed for stable transduction. The total number of cells per well was multiplied by the desired MOI to get the total transducing units (TU). The TU was then divided by the viral titre, known as the total TU/ml that is specific to the purchased virus. This calculation provided us with an optimal volume of virus to use for the desired MOI on our Renca cells.

Methods for the following were performed previously by our team and was essential to the success of this project. Renca cells were seeded in a 6-well plate and incubated for 24h at 37°C and 5% (v/v) CO_2 in complete Dulbecco's Modified Eagle Medium (DMEM; Lonza, Walkersville, MD) with 10% (v/v) fetal bovine serum (FBS; Cat No. 12483020, Thermo Fisher Scientific, Waltham, MA), 1% (v/v) 200uM L-glutamine (Cat No. 25-030-081, Thermo Fisher Scientific, Waltham, MA), 1% (v/v) 100X sodium pyruvate (Cat No. 11360070, Thermo Fisher Scientific, Waltham, MA), 1% (v/v) 100X non-essential amino acids (Cat No. 11-140-050, Thermo Fisher Scientific, Waltham, MA) until 75% confluency had been reached. After 24 h, complete DMEM was aspirated and replaced with fresh complete DMEM, supplemented with 8 ug/mL polybrene solution (Santa Cruz Biotechnology), along with either mouse-KIM-1 encoded lentiviral ORF particles and/or control lentiviral ORF particles. Cells were incubated with polybrene solution and lentiviral ORF particles for 24h at 37°C and 5% (v/v) CO_2. After 24h, medium was aspirated and replaced with fresh complete DMEM. After 72h post-transduction the complete DMEM was aspirated and replaced with 1mL of complete DMEM supplemented with 2ug/ml of puromycin dihydrochloride (Sigma-Aldrich, Oakville, CA) per well. Replacement of culture medium containing puromycin dihydrochloride occurred every 2-3 days for two weeks post-transduction. After sufficient replication and subculture of positively selected cells, both KIM-1^{pos} and KIM-1^{neg} Renca cells were trypsinized (Trypsin-EDTA [0.25%, Cat No. 25200072, Thermo Fisher Scientific, Waltham, MA]) and collected to confirm KIM-1 gene and protein expression, respectively (Lee and Gunaratnam, 2019).

2.1.2 Cell Culture

Renca cells (KIM-1^{pos} and KIM-1^{neg}) were maintained according to culture methods recommended by ATCC Renca cells in antibiotic free complete Dulbecco's Modified Eagle Medium (DMEM; Lonza, Walkersville, MD) as defined above. Stable cell lines were maintained with 2µg/mL of puromycin dihydrochloride. Cell culture medium was aspirated and replaced every 2-3 days with fresh complete DMEM plus 2µg/mL puromycin dihydrochloride where required. Renca cells were sub-cultured every 4-5 days using Trypsin-EDTA.

2.2 Protein Extraction

Cells were seeded in 10cm^2 culture dishes (Cat No. 10062-880, VWR, Pennsylvania, USA) with complete cell culture medium. Cells were incubated at 37°C and 5% (v/v) CO_2 for 24h until reaching ~90% confluency. Prior to cell lysis, Radioimmunoprecipitation assay buffer (RIPA [RIPA Lysis Buffer System; sc-24948; Santa Cruz Biotechnology]) was prepared by combining 10ul of sodium orthovanadate, 10µl of PMSF solution, and 10ul of protease inhibitor solution for every 1mL of complete RIPA buffer needed (sc-24948; Santa Cruz Biotechnology). Once cells have reached ~90% confluency, cell medium was aspirated and cells were washed with cold 1 x PBS (PBS; 137 mM NaCl, 2.7 mM KCl, 4.3 mM Na2HOP4, 1.47 mM KH2PO4, pH 7.4) for 5 minutes on ice. Cold 1 x PBS was aspirated, and cells were prepared lysed using. For 100mm culture dishes, 1mL complete RIPA buffer was evenly placed on the monolayer of cells while on ice for 5 minutes, gently agitating the solution occasionally. Using a cell scrapper, cells were collected from the dish and carefully transferred into microcentrifuge tubes. Lysates were then centrifuged at 4°C at ~12,000 x g for 20 minutes. After centrifugation was complete, protein

supernatants from samples were collected and isolated into fresh microcentrifuge tubes for further analysis.

2.2.1 Western Blot

Whole cell lysates were collected and analyzed for protein purity and concentration using the Pierce BCA Protein Assay Kit (Cat No. 23225, Thermo Fisher Scientific, Waltham, MA). Protein concentrations were determined and compared to the concentrations of protein standards provided with the kit. Lysate samples were diluted with appropriate amounts of H_2O, to generate a total concentration of 50µg of protein per sample. Loading dye was prepared by combining 190µl 6x sodium dodecyl sulphate (SDS) protein loading buffer (Laemmli buffer) with 10µl of β-mercaptoethanol. Subsequently, 6µl of prepared loading dye solution were added to each sample to reduce disulphide bonds. Samples were then boiled for 5 minutes at 95°C to further denature protein structures. Samples were then loaded onto 10% SDS-polyacrylamide gels. Protein samples were then separated based on charge-to-mass ratio and then transferred onto a polyvinylidene difluoride membrane (Millipore, Billerica, MA) for 50 minutes at 90 V (Bio-Rad, Hercules, CA). After 50 minutes, membranes were blocked with a 3% (w/v) BSA (bovine serum albumin; Cat No. AD0023, Bio Basic, Markham, ON) solution made in 1 x TBST (Tris-buffered saline, in 1mL of 0.2% Tween-20Cat No. BP337-500, Fisher Bioreagents, Waltham, MA). Membranes were then incubated overnight at 4°C on a rotational shaker with either goat anti-mouse KIM-1 primary antibody (1:2000; Cat No. AF1817, R& D Systems, Minneapolis, MN) or anti-human KIM-1 (AKG; [Han *et al.*, 2002]) targeting the extracellular domain of KIM-1. Glyceraldehyde phosphate dehydrogenase (GAPDH) was used (loading control) was detected using anti-mouse GAPDH (65C) antibody (1:1500; Santa Cruz Biotechnology). After overnight

incubation, membranes were then washed 4 times on a rotational shaker in 1 x TBST with changes every 7 minutes. Membranes were then incubated with appropriate secondary antibodies conjugated with horseradish peroxidase (1:20000; Jackson Immunoresearch Laboratories, West Grove, PA) in 3% BSA blocking buffer for 1h in the dark, at room temperature. After secondary antibody incubation and washing in 1 x TBST for 5 minutes for 3 times, proteins were then visualized using Luminata Forte Western HRP Substrate (EMD Milipore) and developed on the Licor C-digital imaging device. Western blot images were captured using Image Studio Lite.

2.3 RNA Isolation

Cell and tissue RNA were extracted on ice using TriZol Isolation Reagent (Cat No. 15596018; Life Technologies) using approximately 500µl-1mL per sample depending on cell confluency and/or tissue size, respectively. For every 500µl of TriZol, 100µl of chloroform was added to facilitate phase separation. Samples were briefly vortexed and incubated on ice for 10 minutes before centrifugation at ~ 12,000 x g for 20 minutes at 4°C. After centrifugation and phase separation had occurred, the aqueous layer was removed carefully and placed into a fresh microcentrifuge tube. For every 500µl of TriZol, 100µl of isopropanol was added to the aqueous layer to facilitate precipitation of RNA. Samples were briefly vortexed and incubated on ice for 10 minutes before centrifugation at ~ 12,000 x g for 10 minutes at 4°C. Supernatants were removed from the samples and discarded. Pellets were washed with 70% ethanol (EtOH) diluted in Diethyl Pyrocarbonate (DEPC) -treated H_2O (RNase free water) and centrifuged at ~ 7,500 x g for 5 minutes at 4°C. Supernatant was removed from samples and discarded. RNA pellets were resuspended in DEPC-treated H_2O and heated in a water bath at 56°C for 10 minutes. RNA was quantified and analyzed for purity using a spectrophotometer (260nm and 280nm;

MulltishkanTM GO Microplate Spectrophotometer; Thermo Fisher Scientific, Waltham, MA). One microliter of total RNA was placed onto Microplate and absorbances were used to calculate purity and concentration of RNA. One microgram of total RNA was combined with 4µL of qSCRIPT cDNA SuperMix (Quanta Biosciences, Gaithersburg, MD) to synthesize cDNA. The reaction was facilitated using a MyCycler^{TM} Thermal Cycler (Bio-Rad, Hercules, CA). cDNA was further stored at -20°C until further analyzation.

2.3.1 Real Time Quantitative PCR (RT-qPCR)

cDNA samples were used to perform RT-qPCR using SYBR green reagents (Thermo Fisher Scientific, Waltham, MA). Reaction mixtures were placed in a v-shaped 96-well plate, each well containing 10µL of SYBR green, 4.6µL of DEPC-treated water, 5µl of diluted cDNA in DEPC-treated water (ratio 1:10), and 0.2µL of both 10µM forward and reverse strand primers made by myself. Various primers were used to detect varying gene transcriptions in both cell lines and tissues shown in Table 1. Target genes were normalized using GAPDH to counterbalance any PCR variations present. Relative gene expression was calculated using 2- ΔΔCT method.

2.3.2 RNA Sequencing

Renca cell line preparation for RNA sequencing was performed by Brad Shrum. Previously generated data showing discrepancies between our Renca cells [KIM-1^{pos} and KIM-1^{neg}] (Lee and Gunaratnam, 2019), was re-analyzed for this project. RNA sequencing was performed by London Genomics Centre with the help of Dr. Rob Hegele at the Robarts Research Institute at Western University. RNA was extracted and isolated, with subsequent cDNA synthesis performed as described above on both KIM-1^{pos} and KIM-1^{neg} Renca cell lines. Illumina sequencing adapter sequences were used, and libraries were sequenced using the Illumina

NextSeq 500 sequencer (Illumina Inc., San Diego, CA). All sequence data was generated and analyzed by Partek Flow Software (Partek Inc., St. Louis, MO). Stringencies for data analysis was instilled within the bioinformatic pipeline to only compare genes with a p-value < 0.05, and to exclude fold changes between 1.5 and -1.5. Differential genes were analyzed through gene enrichments; allowing for the grouping of like genes that comply to a specific cellular function, as well as gene pathways. Bioinformatic pipelines were further specified by exploring for functional cellular differences within both gene enrichments, and gene pathways.

2.4 The Human Cancer Genome Atlas (TCGA) Database

All raw TCGA patient data was extrapolated and organized into a working excel spreadsheet by colleague Audrey Champagne. KIPAN patient database was used to complete human RCC and KIM-1 analyses. KIPAN database contains patient information from those diagnosed with ccRCC (KIRC or Kidney Clear Cell Carcinoma), pRCC (KIRP or Kidney Papillary Carcinoma), and Chromophobe RCC (KICH or Chromophobe Carcinoma). Working spreadsheet was then filtered to select data based upon analyses needed. Data was then transferred into GraphPad/Prism 8 in order to perform statistical analyses and generate graphical representations.

2.5 Mice

Animal protocol (2018-147) outlining all the studies contained in this thesis were approved by Western University's Animal Care Committee and in compliance with the guidelines set by Canadian Council of Animal Care. Female wild-type (WT) BALB/c mice were purchased from Charles River Laboratory (Wilmington, MA). Female mice are the common model to use for oncological research (Lee *et al.*, 2018), along with having a higher tolerance to kidney injury in

comparison to male mice (Hu *et al.*, 2009). All mice were kept in shoebox cages with easy access to water and mouse chow pellets. Immune-deficient recombinase-activating gene (Rag $1^{-/-}$) null mice were purchased from Jackson Laboratory (Bar Harbor, ME) and housed in the West Valley pathogen-free barrier facility at Western University. These mice were kept in shoebox microisolator cages with easy access to water and mouse chow pellets. Mouse holding rooms were maintained at a constant temperature of 22°C with timed 12 h light and 12 h dark periods.

Experimental mice were monitored every 2-3 days for health and behavioral monitoring. All physiological and behavioral changes were monitored and recorded for all experimental animals. After experiments were complete, all mice were euthanized using CO_2. Collection of samples needed per experiments occurred post-mortem. Mouse holding rooms were maintained at a constant temperature of 22°C with timed 12 h light and 12 h dark periods.

2.6. Experimental Tumour Models

2.6.1 Subcutaneous Model of RCC Tumours

To study tumour growth of RCC cells with the overexpression of KIM-1 (Renca KIM-1^{pos}) or the absent expression of KIM-1 (Renca KIM-1^{neg}) – Renca cell lines were injected into immune competent BALB/c mice. Prior to injections, Renca cells were cultured in 15cm dishes at a seeding concentration of 1 x 10^6cells/mL in complete DMEM. Stable expression of the transduced cell lines was maintained with 2µg/mL of puromycin dihydrochloride. Medium was aspirated and replaced with fresh complete DMEM and puromycin dihydrochloride every 2-3 days until 80%-90% confluency had been reached. Once 80%-90% confluent, cells were washed

with 10mL of warmed 1xPBS, and subsequently replaced with 5mL of Trypsin-EDTA for 5 minutes in 37°C, 5% (v/v) CO_2 incubator. 10mL of complete DMEM was then added to cells to neutralize trypsin. Cells were then spray washed to remove any adherent cells from the culture dish surface. Collected cells were then centrifuged at 21°C, 400 x g, for 3 minutes. After centrifugation, the supernatant was aspirated and discarded, and cell pellets were then resuspended in complete DMEM in preparation for cell counting. Cells were counted using a 1:1 dilution; 10µL of trypan blue (0.4%) (Cat No. 97063-702, VMR International) with 10µL of suspended cells onto a hemocytometer (Fisher Scientific, Waltham, MA). Cell viability was assessed using Trypan blue exclusion and cell a viability of >95% was observed before injection. After determining the total cell number, cells were resuspended at a concentration of $1x10^6$ cells/100µL in a 1:1 ratio of 1xPBS and Corning Matrigel™ growth factor reduced (GFR) Membrane Matrix (Cat No. CB-40230C, Thermo Fisher Scientific, Waltham, MA). Cells in PBS and Matrigel™ were kept on ice to avoid solidification of matrix solution. Mice were sedated using 2% isoflurane for medium depth anesthesia following standard operating procedures prior to and during injections. Renca cells were resuspended at 1 x 10^6 cells/100µL in either 1 x PBS alone (No Matrigel™) or in a 1:1 dilution of 1 x PBS with Corning (GFR) Matrigel™ Membrane at a volume of 100µL/injection. One hundred microliters of each cell line were placed into an intermediary microcentrifuge tube, and subsequently drawn up into an 1/2 inch 28-gauge insulin syringe (Becton Dickinson, Franklin Lakes, NJ). Cells were either injected bilaterally, where Renca KIM-1^{pos} and Renca KIM-1^{neg} cells were injected into opposite flanks of the same mouse, or cells were injected unilaterally where only one cell line was given per mouse. Prior to injection, needles were inserted bevel up under the skin, and gently moved around to remove facia. This allowed for cell suspension with Matrigel™ membrane to solidify in a more unified

shape. Mice were monitored every day for the first 72h post injection, and then every 3-4 days afterwards for a duration of 21 days. Mice were then euthanized using a CO_2 chamber, and tumours were removed using sterile surgical instruments, and collected for further analysis.

2.6.2 Renal Orthotopic Model

To study tumour growth of Renca KIM-1^{pos} vs Renca KIM-1^{neg} cells in a clinically relevant model of RCC – Renca cells were injected directly into the kidney. Specifically, either Renca KIM-1^{pos} or Renca KIM-1^{neg} cells were injected orthotopically into the subcapsular region of the left kidney of 6-10-week-old female WT BALB/c mice. Prior to injections, Renca cells were cultured, collected, and counted using the methods as described above. After determining the total cell number, cells were resuspended at a concentration of 2.5 x 10^5 cells/100µL in a 1:1 ratio of 1xPBS and Corning Matrigel™ GFR Membrane Matrix. Cells in PBS and Matrigel™ were kept on ice to avoid solidification of matrix solution. Mice were given slow-release buprenorphine (0.6mg/kg, Chiron Compounding Pharmacy, Guelph, ON) analgesics, and subsequently isoflurane sedation prior to surgical injections. Mouse fur was then shaved at the region of interest on the left flank, and surgical area was sterilized with iodine solution and 70% ethanol. Skin barrier and muscle layer were incised using sterile surgical instruments. Left kidneys were exposed and 30µl of cells in Matrigel™ suspension were injected into the subcapsular region of the left kidney. All incisions were closed using sutures and staples according to our standard operating procedures outlined in animal our protocol. Mice were kept under a heat lamp until conscious and monitored 24 h post-injection, and every 2 days following. After 21 days, mice were euthanized using a CO_2 chamber, tumour bearing kidneys and lungs were removed for further analysis of primary and secondary tumour growth, respectively.

2.7 Tumour Immunofluorescence Microscopy

2.7.1 Sample Preparation

All tissue samples were fixed in Periodate-Lysine-Paraformaldehyde (PLP) solution, made one day before use. Solution was made by first preparing a phosphate buffer containing 3:1 parts monobasic sodium phosphate and dibasic sodium phosphate diluted in double distilled H_2O (ddH_2O). Phosphate buffer was autoclaved and cooled to room temperature prior to preparing complete fixative solution. Once phosphate buffer reached room temperature, L-Lysine (>98%, Cat No. L5501-25G, Sigma-Aldrich, Oakville, CA) and Paraformaldehyde (PFA, Cat No. PB0684.SIZE.500g, Bio Basic, Markham, ON) were diluted in ddH_2O and combined. Sodium Periodate (>99.8%, Cat No. 311448-100G, Sigma-Aldrich, Oakville, CA) was then added to mixture. Using the prepared phosphate buffer, the total volume was then brought up to 500mL or 1L depending on how much solution was needed. PLP was kept at 4°C, in the dark until use (Appendix A 2).

Subcutaneous and renal subcapsular experimental tumours were both collected to analyze immune infiltration using immunofluorescence. After euthanization, tissues were collected in 15mL Falcon Centrifuge tubes (Cat No. 14-959-49B, Thermo Fisher Scientific, Waltham, MA), containing 10mL of PLP. Samples incubated in PLP for a maximum of 24 h, on a rotational shaker at 4°C, in the dark. After 24 h, samples were removed from PLP and gently rinsed with phosphate buffer before subjecting tissues to a sucrose gradient. Sucrose solutions were prepared the same day to ensure no bacterial contaminations occurred. Sucrose gradients were prepared using phosphate buffer (3:1 monobasic, dibasic sodium phosphate) with (v/v) 10%, 20% and

30% sucrose (>99.5%, Cat No. S7903-250G, Sigma-Aldrich, St. Louis, MO). All samples were placed in each gradient beginning at 10%, then subsequently 20%, and 30%, for one hour at a time or until tissues sank. After completing the three sucrose gradient steps, tissues were removed from sucrose and pat dried. A freezing bath was prepared using a metal tray placed in a styrofoam box containing dry ice with 10mL of 95% (v/v) ethanol. Approximately 5mL of 2-Methylbutane Reagent (>99%) (Cat No. M32631-4L, Sigma-Aldrich, Oakville, CA) was added to the metal tray and allowed to reach the appropriate freezing temperature. Tissues were then placed in OCT compound (Cat No. 23730571, Thermo Fisher Scientific, Waltham, MA) in tissue cassettes. Tissues completely submerged in OCT compound within cassettes were placed onto metal tray until OCT compound froze around tissues. Cassettes were then wrapped in cling wrap and covered with tin foil prior to storage in the -80°C to avoid samples drying out.

2.7.2 Co-Immunofluorescence

Frozen OCT blocks containing tissue samples were sent off to Weihua Liu in the Department of Pathology at The University of Western Ontario. Samples were removed from histology tissue cassettes and placed onto a cryostat and sliced at a size of 7-10 microns. Each sample is then placed onto a positively charged glass slide (Cat No. 22-037-246, Fisher Scientific, Waltham, MA) and mounted appropriately. Fluorophore conjugated antibodies were applied to samples - $CD3^+$ (SP7) (1:200, Cat No. NB600-1441SS, Novus Biologicals), $CD4^+$ (1:200, Cat No. MABF575, Millipore Sigma, Burlington, MA), and $CD8^+$ (1:400, Cat No. 100727, Bio Legend, San Diego, CA) to analyze co-immunofluorescence ($CD3^+$, $CD3^+CD4^+$, and $CD3^+$ $CD8^+$). Tumour samples were analyzed for immune infiltrate population frequency and distribution using Cell Counter plugin in Fiji (ImageJ) Software, normalized to measured areas of focus (per square micron of tissue).

2.7.3 Immunohistochemistry

Tissue samples that were subjected to immunohistochemical staining were collected from mice, and directly placed into 15mL Falcon tubes (Cat No. 14-959-49B, Thermo Fisher Scientific, Waltham, MA) containing 10% formalin buffered solution (Cat No. HT501128-4L, Sigma-Aldrich, Oakville, CA). Tissue samples were incubated in 10% formalin for 72 h for tissue fixation. After 72 h, samples were moved from 10% formalin to 70% ethanol prior to analysis. Samples were then embedded in paraffin blocks within tissue cassettes. After hardening occurred, embedded tissues were sliced at 7-10 microns, and placed onto a positively charged glass slide. Samples were mounted properly and stained with either hematoxylin and eosin (H&E) or Masson's Trichrome staining for further analysis.

Quantification of histological sections of KIM-1^{pos} and KIM-1^{neg} Renca tumour capsules were measured using brightfield microscope analyzing for distance width measurements using NIS-Elements Nikon Software. All tumour capsules were measured at 100x and normalized to total visualized area imaged by the microscope software. Tumour capsule measurements were evaluated using distance between two points; from the inner-most to the outer-most collagen layer of the capsule. Capsules were measured at five randomized locations throughout each tumour sample, and widths were averaged for final measurements.

2.8 Statistical Analysis

All data is presented as a mean ± standard error of the mean (SEM). Normality was assessed using normality and lognormality tests. Between group differences in standard error of the means (SEM) were assessed using Student's t- or Kruskal-Wallis tests for parametric and nonparametric data, respectively. Survival was plotted using Kaplan Meir curves, and groups

compared with log-rank test. Normality Lognormality statistical analysis was used to compare matched normal vs adjacent tumour tissue from TCGA patient database. A two-tailed alpha <0.05 was considered statistically significant. Statistical analyses were performed using GraphPad Prism, version 8.

2.9 Sample Size Calculation

Sample size calculation for tumour growth studies was calculated prior to experiments to determine proper N to observe significance. N mice in each group would provide >=80% power to detect at least a 30% difference in tumour growth between groups, two-sided alpha = 0.05. N mice per group would provide >=80% power to detect at least a difference of at least xx standard deviations, two-sided alpha = 0.05).

Chapter 3

3. Results

3. 1 KIM-1 (*Havcr1*) mRNA is expressed at all stages of RCC and increases overall patient survival

To investigate how KIM-1 expression may impact the survival of patients diagnosed with RCC, we utilized The Cancer Genome Atlas (TCGA) database (https://www.cancer.gov/tcga). KIPAN patient database including data from ccRCC, pRCC, and Chromophobe RCC patients was extracted. For our analysis, the KIRC (Kidney Clear Cell Carcinoma) and KIRP (Kidney Papillary Carcinoma) databases were combined due to KIM-1 upregulation being found in only ccRCC and pRCC patients (Zhang *et al.*, 2014). I analyzed ccRCC or pRCC patient data in correlation with tumour associated KIM-1 (*Havcr1*) mRNA expression. First, I analyzed differences of KIM-1 expression between affected RCC tumours, and adjacent unaffected or normal tissue. Results showed that KIM-1 mRNA expression was significantly increased within tumours compared to normal adjacent tissue (Fig 1A). I then stratified patients according to the American Joint Committee on Cancer (AJCC) tumour-node-metastasis (TNM) staging system (Stages 1 to 4) to determine if KIM-1 expression varied with stage (The American Joint Committee on Cancer (AJCC), 2017). Compared to normal adjacent tissue, the KIM-1 mRNA expression level was significantly increased in tumours at all stages of RCC (Fig 1B). Finally, patients with tumours having KIM-1 expression in the top 50^{th} percentile had significantly improved survival compared to patients with tumours having KIM-1 expression below the 50^{th} percentile in a KIRC and KIRP combined analyses (median survival = 25% vs. 50%, respectively, $p < 0.0001$) (Fig 1C). Separate analyses of overall survival of KIRC and KIRP alone

were completed to evaluate discrepancies between tumour types. KIM-1 expression was found to significantly increase overall survival of KIRC patients (Fig 1D), but not KIRP patients (Fig 1E).

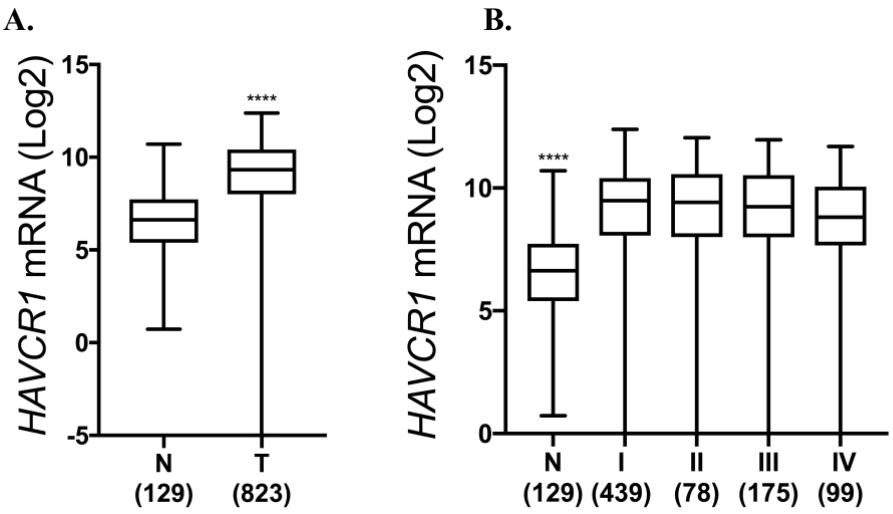

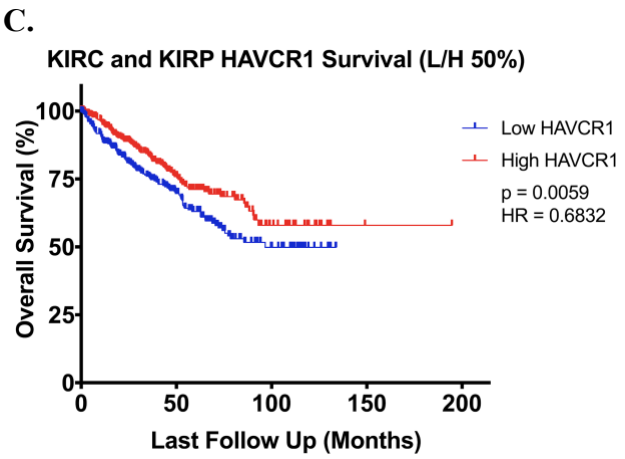

D.

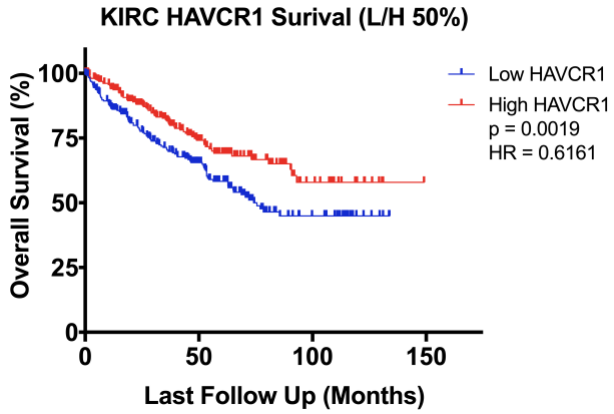

E.

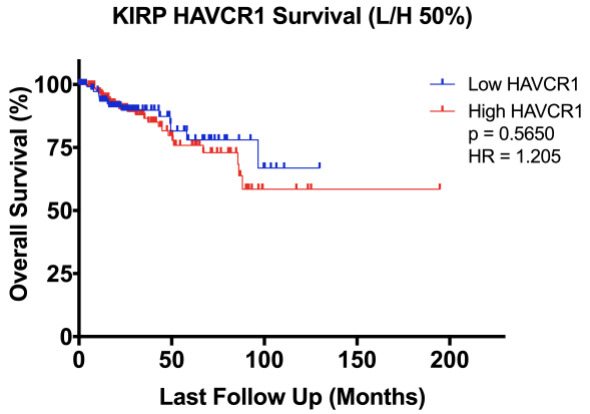

Figure 1. TCGA RNA Sequencing data reveals HAVCR1 (KIM-1) mRNA is expressed at all stages of RCC and increased expression correlates to increased survival of KIRC (Kidney Clear Cell Carcinoma) and KIRP (Kidney Papillary Carcinoma) patients.

A. Comparison of KIM-1 mRNA expression within non-paired normal adjacent tissue vs tumour tissue of KIRC and KIRP RCC patients (Normal: n = 129, Tumour: n = 823) (****, P<0.0001, Mann-Whitney *t*-test). **B.** KIM-1 mRNA expression in KIRC and KIRP RCC tumour stages vs normal adjacent tissue (Normal: n = 129, I: n = 439, II: n = 78, III: n = 175, IV: n = 99) (****, P<0.0001, Kruskal-Wallis statistical analysis). **C.** Overall KIRC and KIRP patient survival vs KIM-1 mRNA expression using 50% low/high expression cut-offs (Low: n = 376, High: n = 441) (**, p = 0.0059; Kaplan-Meier statistical analysis). **D.** Overall KIRC patient survival vs KIM-1 mRNA expression using 50% low/high expression cut-offs (Low: n = 259, High: n = 272) (**, p = 0.0019; Kaplan-Meier statistical analysis). **E.** Overall KIRP patient survival vs KIM-1 mRNA expression using 50% low/high expression cut-offs (Low: n = 117, High: n = 169) (NS, p = 0.5650, Kaplan-Meier statistical analysis).

3.2 Expression of several collagen genes is increased within human RCC tumour tissue, in comparison to normal adjacent tissue

Extracellular matrix (ECM) and collagen properties are widely studied in terms of its effects on tumour progression and metastasis (Fang *et al.*, 2014). Thus, I investigated the correlation between collagen and KIM-1 expression in RCC patients with ccRCC and pRCC from TCGA. Collagen genes of interest; *COL1A1*, *COL1A2*, *COL6A1*, *COL6A2*, and *COL23A1* were selected based off previous research of collagen in RCC (Wan *et al.*, 2015; Xu *et al.*, 2017; Majo *et al.*, 2020). First, I analyzed the expression of the above collagen genes and compared their expression in RCC tumour tissue vs normal adjacent tissue for each patient. Results showed that *COL1A1*, *COL1A2*, *COL6A1*, *COL6A2*, and *COL23A1* mRNA expression were all significantly increased within RCC tumour tissues compared to matched normal adjacent tissues (Fig 2A-E).

A.

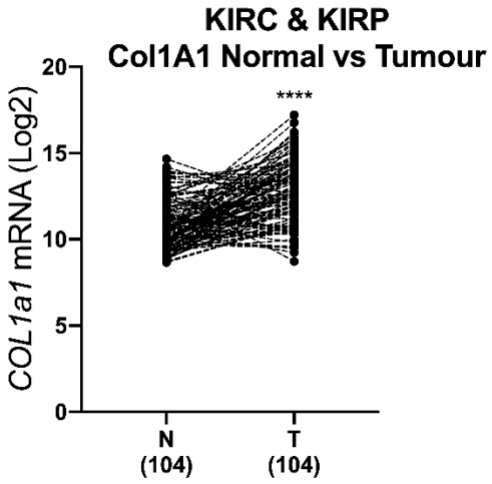

B.

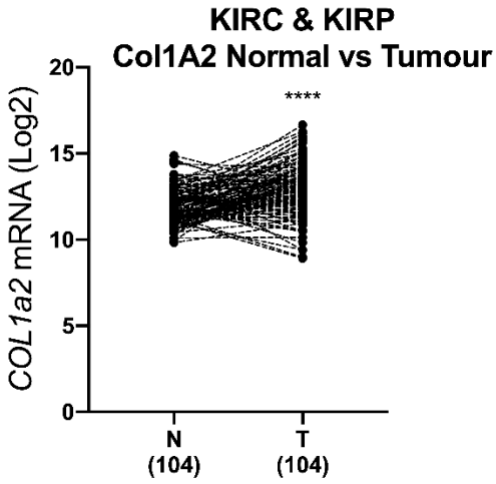

C.

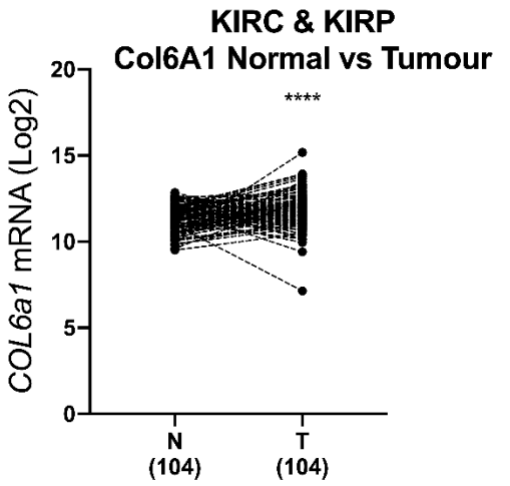

D.

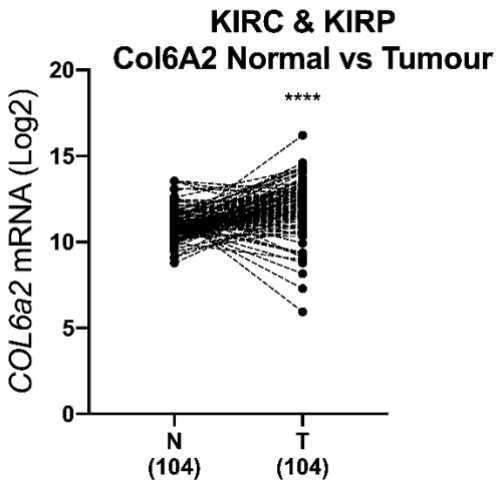

E.

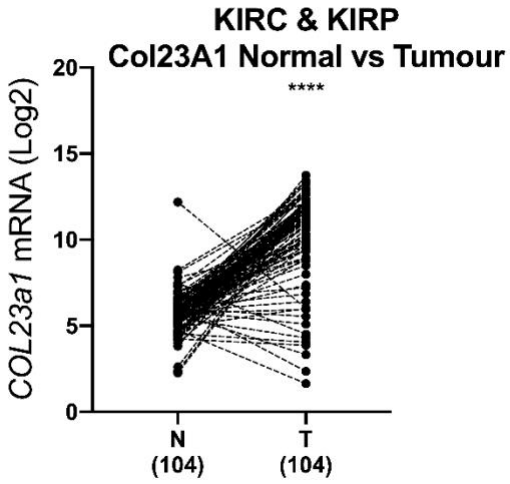

Figure 2. TCGA RNA Sequencing database reveals increased collagen mRNA expression in RCC tumour tissue vs normal adjacent tissue using KIRC (Kidney Clear Cell Carcinoma) and KIRP (Kidney Papillary Carcinoma) patient databases.

Paired comparison of normal adjacent tissue vs matched patient tumour tissues reveals several collagen genes **A.** Col1A1, **B.** Col1A2, **C.** Col6A1, **D.** Col6A2 and **E.** Col23A1 mRNA expression increased in RCC tumour tissues (n=104/group) (****, P<0.0001; Normality Lognormality statistical analysis).

3. 3 mRNA expression of KIM-1 vs serval collagen genes, have no clear correlation in human RCC patients

To investigate the relationship between KIM-1 and collagen gene mRNA expression within human RCC patients, I analyzed our previously used collagen genes of interest (*COL1A1*, *COL1A2*, *COL6A1*, *COL6A2*, and *COL23A1*) along with 29 genes selected from a group of genes termed tumour matrisome index (TMI) by Su Bin Lim and team (Lim *et al.*, 2019). The TMI was previously used to perform a multi-component analysis of ECM genes in a pan-cancer study to elucidate differential tumour immune responses. Using our previous genes of interest as well as the 29 genes within the TMI from Su Bin Lim, I analyzed correlations between collagen genes vs KIM-1 mRNA expression within human RCC patients (Lim *et al.*, 2019) (Fig 3A). TCGA RNA-seq data from KIPAN databases (KIRC, KIRP and KICH) were used in order to correlate comparative mRNA expression levels. Tumour KIM-1 expression in the top 25th percentile, and bottom 25th percentile were compared using Spearman's rank order correlation co-efficient to elucidate whether each collagen gene had a negative or positive correlation to KIM-1 (*Havcr1*). Results showed many correlations between the signature and KIM-1, yet no clear correlation trends between KIM-1 (*Havcr1*) and the TMI signatures (Fig 3B).

A.

Tumour Matrisome Index (TMI) Genes (Su Lin Bim *et al.*,)
ABI3BP
ADAMTS8
CD36
CHRDL1
COL10A1
COL11A1
COL6A6
CPB2
CTHRC1
CXCL13
CXCL2
FCN3
GREM1
HHIP
IL6
LPL
MAMDC2
MMP1
MMP12
OGN
PCOLCE2
S100A12
S100A2
SFTPA2
SFTPC
SFTPD
SPP1
TNNC1
WIF1

B.

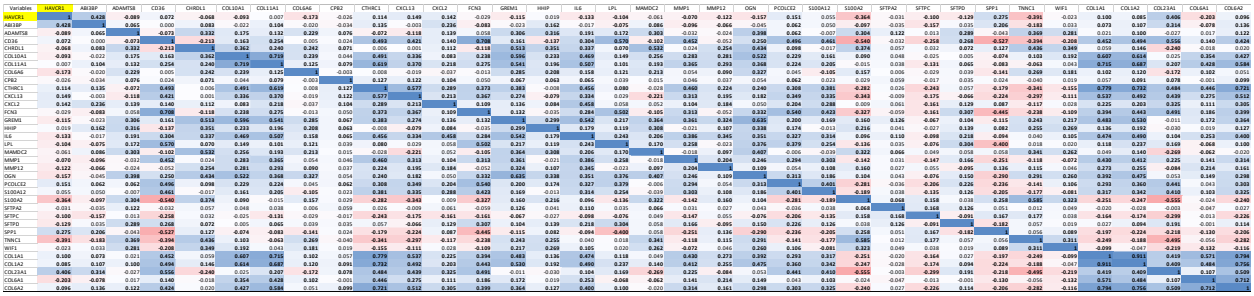

Figure 3. Correlogram examining the correlation between tumour KIM-1 and collagen signatures mRNA expression using TCGA KIPAN patient databases.

A. List of TMI genes extrapolated from Su Bin Lim and team used in correlation analysis (Lim *et al.*, 2019), along with several collagen genes of interest (*COL1A1, COL1A2, COL6A1, COL6A2* and *COL23A1*). **B.** Correlogram of Spearman's correlation matrix comparing collagen and TMI signature and collagen genes to KIM-1 mRNA expression levels in human RCC patients. Correlation co-efficient ranging from +1 to -0.5 were plotted and used to create visual comparative heat map. Perfect correlations noted as +1 or -1, for both positive and negative correlations to KIM-1 expression, respectively. Each plot in correlogram represents a gene correlation to KIM-1, for each patient analyzed (KIPAN (total): n = 1019: KIRC: n = 606, KIRP: n = 321, KICH: n = 90, N/A: n = 2 – excluded from analysis due to non-matching).

3. 4 KIM-1 expression on RCC cell does not alter their tumorigenic potential when injected bilaterally into BALB/c mice.

To investigate the role of KIM-1 expression on the growth of RCC tumours, we injected 1 x 10^6 KIM-1^{pos} and KIM-1^{neg} Renca cells into the flanks of 6-8-week-old female BALB/c mice for 21 days. Matrigel™ incorporation into injection methods influences uniformity and reproducibility of Renca tumour models by maintaining the integrity of cells after subcutaneous injection (Yu *et al.*, 2018). Cells were either resuspended in 100µL of 1 x PBS alone and/or 1:1 dilution of 1 x PBS and Corning (GFR) Matrigel™ Membrane, subcutaneously into the right flanks of 6-8-week-old female mice, to rule out any effects of Matrigel™ use on tumour development. Bilateral injection of Renca tumours allowed us to compare tumour growth between KIM-1^{pos} and KIM-1^{neg} tumours in the same host (i.e., same immune system). I did not observe any significant differences in tumour volume or mass between KIM-1^{pos} and KIM-1^{neg} tumours both without Matrigel™ (Fig 4A) or with Matrigel™ (Fig 4B).

A.

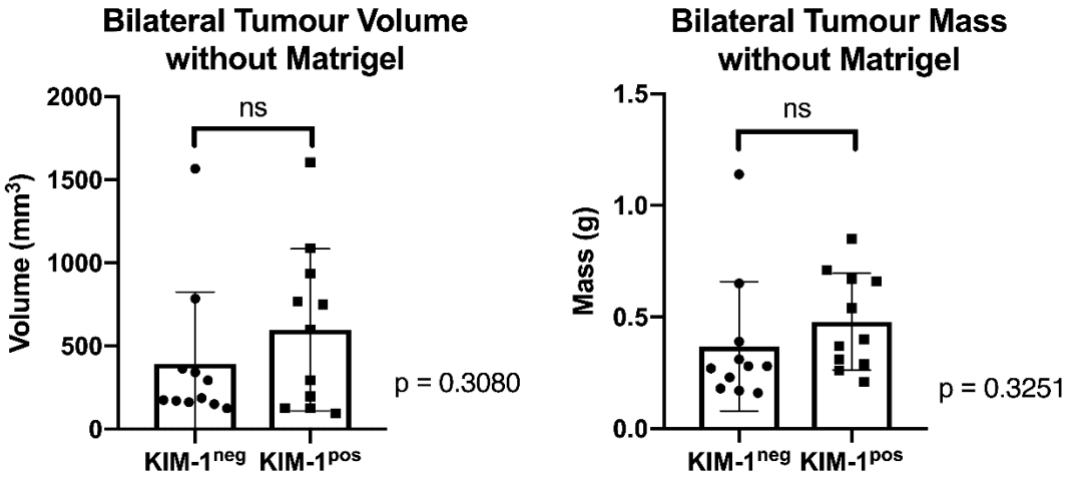

B.

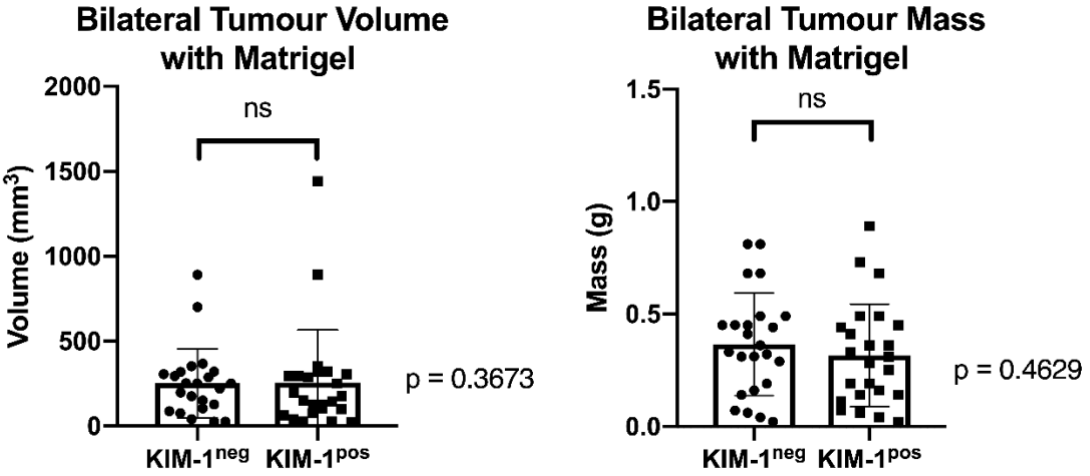

Figure 4. Mass and volumes of KIM-1^{pos} and KIM-1^{neg} Renca tumours grown SQ-Bilat.

A. KIM-1^{pos} and KIM-1^{neg} Renca tumour volume and mass, grown without Matrigel^{TM} for 21 days in 6–8-week-old female mice (n=11/group) (volume: NS, p=0.3080, mass: NS, p=0.3251). **B.** KIM-1^{pos} and KIM-1^{neg} Renca tumour volume and mass, grown with Matrigel^{TM} for 21 days in 6–8-week-old female mice (n=24/group) (volume: NS, p=0.3673, mass: NS, p=0.4629). Data is represented as mean measurement of tumour size/volume (mm^3), and mass (g) ± SEM (NS=not significant, Unpaired two-tailed t-test).

3.5 KIM-1 expression in Renca cells does not alter tumorigenic potential when injected unilaterally into BALB/c mice.

Next, I investigated whether unilateral injection methods of KIM-1^{pos} or KIM-1^{neg} Renca cells into the flanks of BALB/c mice would change the results observed in the previous experiment. I argued that if KIM-1 expression in Renca cells had any effect on the anti-tumour immune response to Renca tumours, unilateral injection of the KIM-1^{pos} and KIM-1^{neg} cells into separate mice would result in differences between the two groups. Once again, I either suspended the Renca cells in a 1 x PBS alone or a 1:1 dilution of 1 x PBS with Corning (GFR) Matrigel^{TM} Membrane. Again, I did not observe any differences between KIM-1^{pos} and KIM-1^{neg} Renca tumour volume or mass in our unilateral model both without Matrigel^{TM} (Fig 5A) or with Matrigel^{TM} (Fig 5B). Since I found no differences between SQ-Bilat or SQ-Unilat tumour volumes and masses, here on in I decided to analyze tumour specimens only with the incorporation of Matrigel^{TM} for our various models.

A.

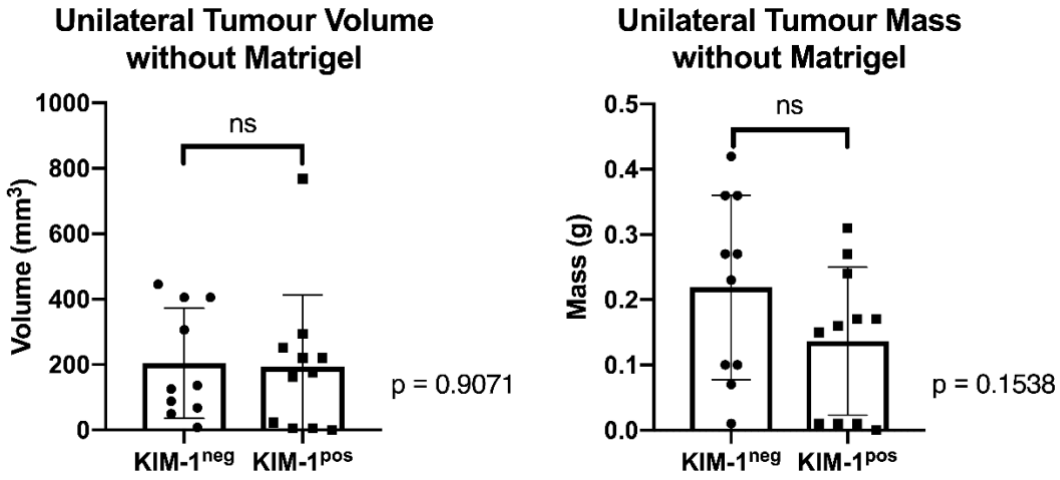

B.

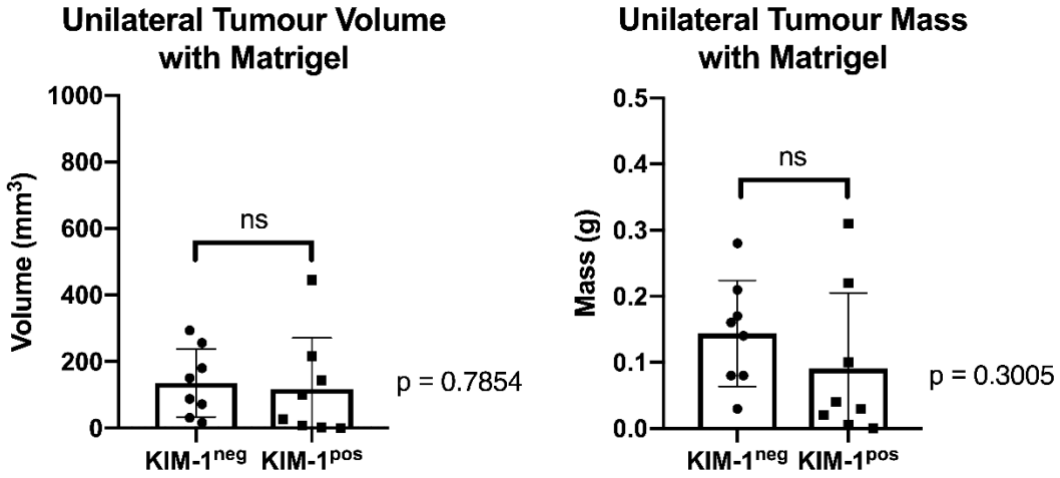

Figure 5. Mass and volumes of KIM-1^{pos} and KIM-1^{neg} Renca tumours grown SQ-Unilat.

A. KIM-1^{pos} and KIM-1^{neg} Renca tumour volume and mass, grown without Matrigel^{TM} for 21 days in 6–8-week-old female mice (KIM-1^{neg}: n=10, KIM-1^{pos}: n=11) (volume: NS, p=0.9071, mass: NS, p=0.1538). **B.** KIM-1^{pos} or KIM-1^{neg} Renca tumour volume and mass, grown with Matrigel^{TM} for 21 days in 6–8-week-old female mice (n=8/group) (volume: NS, p=0.7854, mass: NS, p=0.3005). Data is represented as mean measurement of tumour size/volume (mm^3), and mass (g) ± SEM (NS=not significant, Unpaired two-tailed t-test).

3.6 Tumour KIM-1 expression does not influence immune infiltration of lymphocytes in the subcutaneous Renca model.

To investigate the effect of KIM-1 expression on the immune response against Renca tumours, I compared the immune infiltrate between KIM-1^{pos} and KIM-1^{neg} Renca tumours grown subcutaneously within female immune competent BALB/c mice using co-immunofluorescence staining for $CD3^+$, $CD3^+CD4^+$, and $CD3^+$ $CD8^+$ cells. We examined tumours at 21 days post-injection to allow for maximal infiltration of immune cells. There were no significant differences in tumour infiltrating $CD3^+$, $CD4^+$, or $CD8^+$ immune cells between Renca KIM-1^{pos} (Fig 6A) and KIM-1^{neg} (Fig 6B) tumours (Fig 6C).

A.

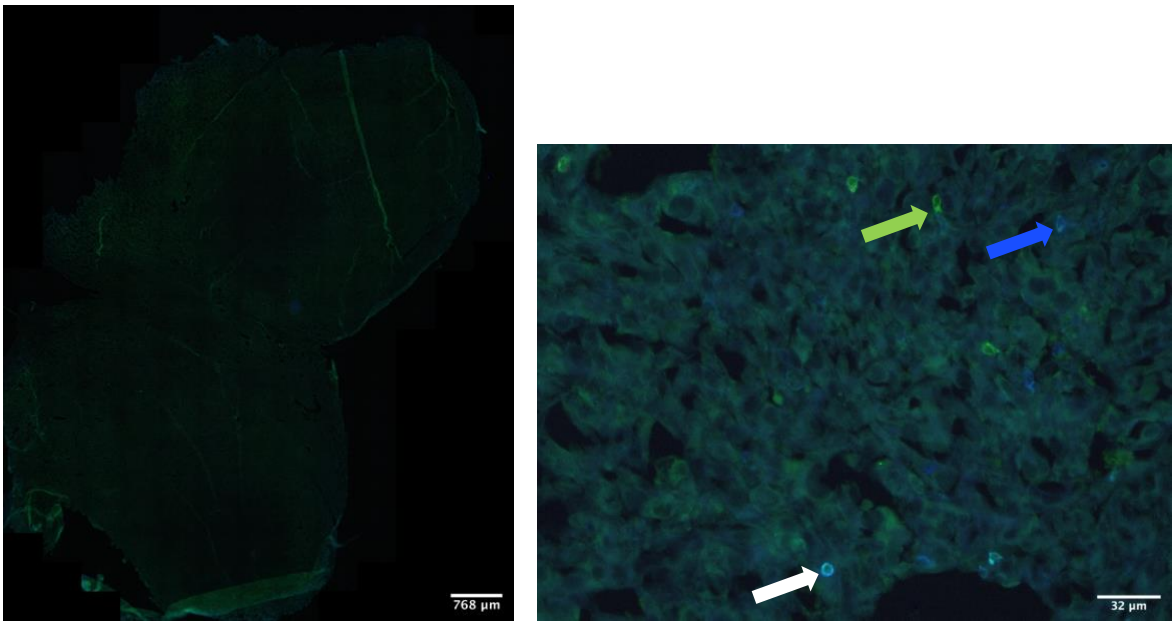

B.

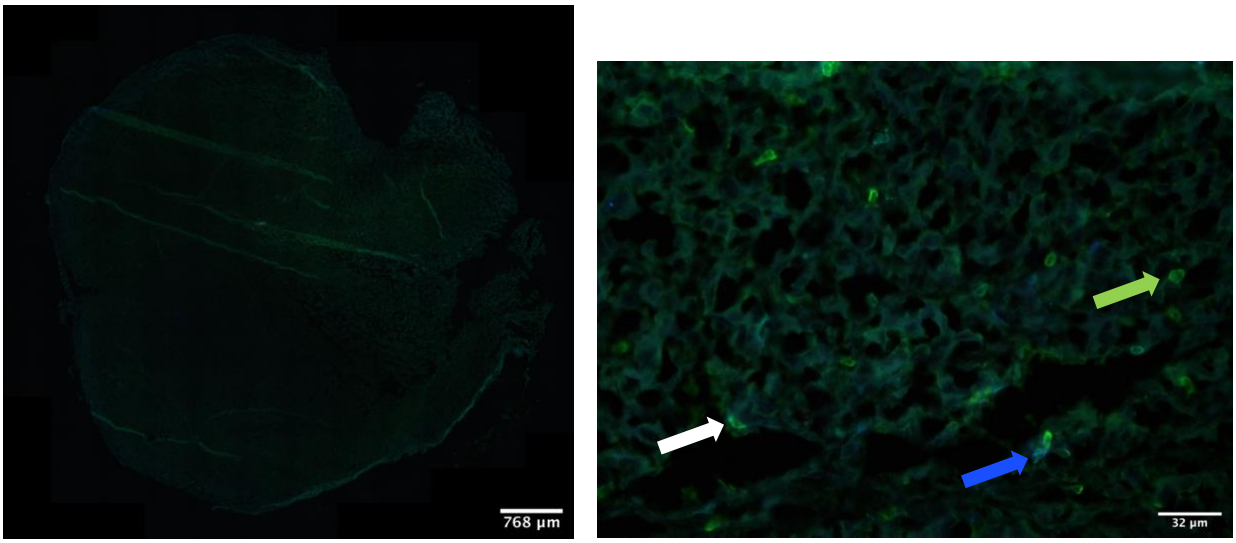

C.

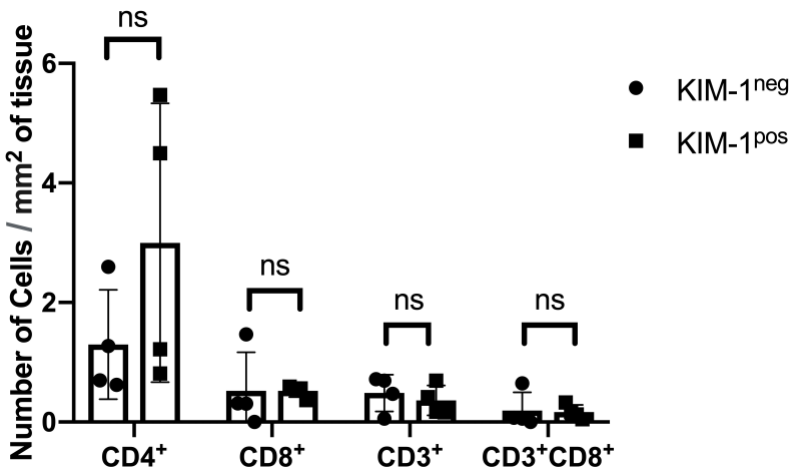

Figure 6. Co-immunofluorescence staining for $CD3^{+,}$ $CD4^{+}$ and $CD8^{+}$ invading lymphocytes in KIM-1^{pos} and KIM-1^{neg} Renca tumours 21 days after SQ-Bilat injection.

A. KIM-1^{pos} and **B.** KIM-1^{neg} Renca tumour stained with $CD3^{+}$ (green) $CD4^{+}$ (blue) $CD8^{+}$ (white) conjugated antibodies (n=4/group). **C.** Quantification of the various types of immune infiltrates counted within tumours. Designated arrows pointing to cell types [$CD3^{+}$ (green) $CD4^{+}$ (blue) $CD8^{+}$ (white)] on inlet images. All images were taken via widefield microscopy using Leica Software at 10x and 100x magnification, respectively. Immune infiltrates were enumerated using Fiji manual cell counter software. Data is represented as mean measurement of number of immune infiltrates per tissue surface area ± SEM ($CD4^{+\cdot}$ p= 0.218575, NS; $CD8^{+}$, p= 0.999170, NS; $CD3^{+}$, p = 0.859486, NS; $CD3^{+}CD8^{+}$, p=0.875091, NS. Unpaired two-tailed t-test).

3.7 KIM-1^{pos} Renca tumours are enveloped in a collagen-rich capsule.

Since I elucidated that various collagen genes are significantly upregulated in RCC patient tumours, I next examined differences in connective tissues within KIM-1^{pos} and KIM-1^{neg} Renca tumours at endpoint (21 d) by staining for collagen using Masson's Trichrome stain. KIM-1^{pos} tumours were found to be surrounded by a significantly thicker collagen dense capsule compared to the KIM-1^{neg} tumours (Fig 7A-C). Importantly, the collagen dense capsule was found to be prominent in Renca KIM-1^{pos} regardless of whether the Renca cells were injected bilaterally into either flank of the same BALB/c mice or unilaterally into independent mice (Matrigel^{TM}) (Fig 8A-C).

A.

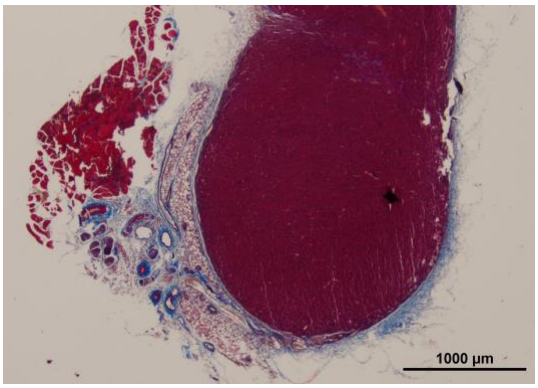

B.

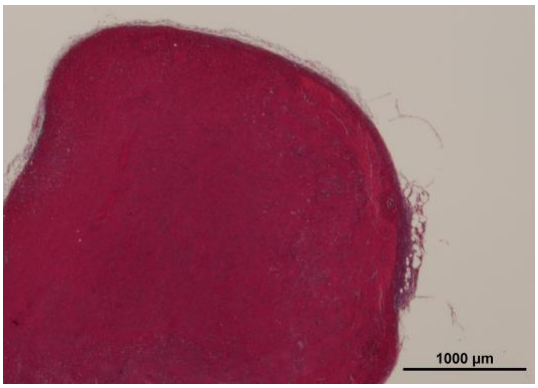

C.

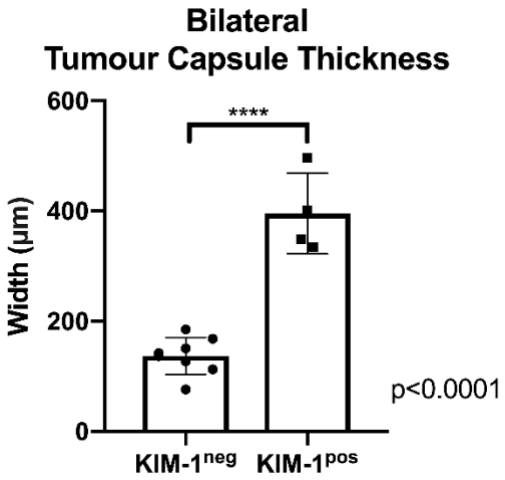

Figure 7. Collagen deposition in KIM-1^{pos} and KIM-1^{neg} Renca tumours injected SQ-Bilat in female BALB/c (WT) mice.

Micrograph of **A.** KIM-1^{pos} and **B.** KIM-1^{neg} Renca tumour stained with Masson's Trichrome elucidating the collagen stromal capsule (KIM-1^{neg}: n=7, KIM-1^{pos}: n=4). All images were taken at 100x magnification using brightfield microscopy and NIS-Elements Nikon software. **C.** Width (µm) quantification of collagen tumour capsule from KIM-1^{neg} and KIM-1^{pos} Renca tumours. Data is represented as mean measurement of tumour capsule width (µm) ± SEM (****, p<0.0001, Unpaired two-tailed t-test).

A.

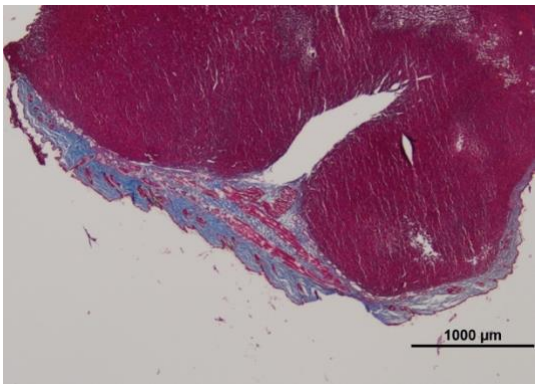

B.

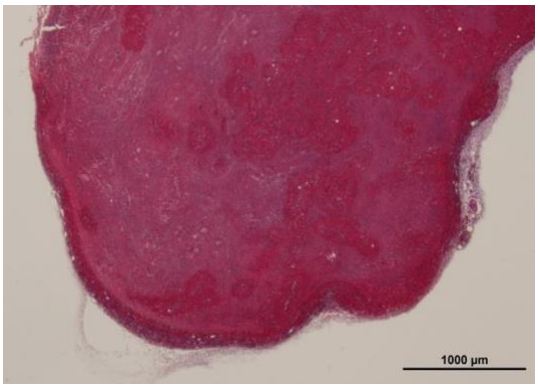

C.

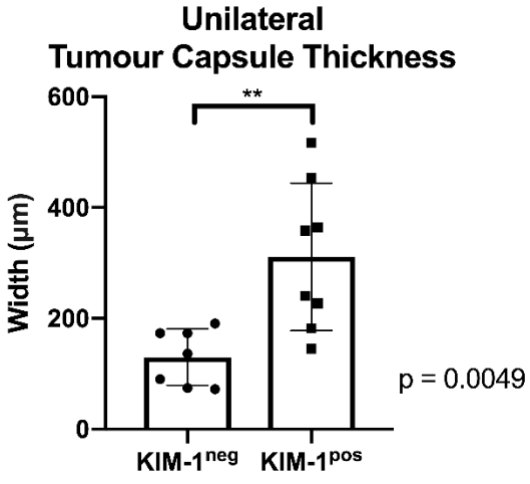

Figure 8. Collagen deposition in KIM-1^{pos} and KIM-1^{neg} Renca tumours grown SQ-Uni in female BALB/c mice.

Micrograph of **A.** KIM-1^{pos} and **B.** KIM-1^{neg} Renca tumours stained with Masson's Trichrome elucidating the collagen stromal capsule (KIM-1^{neg}: n=7, KIM-1^{pos}: n=8). All images were taken using brightfield microscopy and NIS-Elements Nikon software. **C.** Width (μm) quantification of collagen tumour capsule from KIM-1^{neg} and KIM-1^{pos} Renca tumours. Data is represented as mean measurement of tumour capsule width (μm) ± SEM (**, p = 0.0049, Unpaired two-tailed t-test).

3.8 The collagen-dense capsule surrounding KIM-1^{pos} Renca tumours does not depend on the host adaptive immune system.

To determine whether the differences in collagen dense capsule surrounding the Renca KIM-1^{pos} tumours was dependent on an intact adaptive immune system of the host, I examined KIM-1^{pos} and KIM-1^{neg} Renca tumours growth in immune deficient Rag-1$^{-/-}$ mice on the BALB/c background. Once again, the tumours were collected 21 days post-injection and sections were stained with Masson's Trichrome stain. KIM-1^{pos} Renca tumours exhibited significantly thicker collagen dense capsules in comparison to KIM-1^{neg} Renca tumours (Fig 9A-C).

A. **B.**

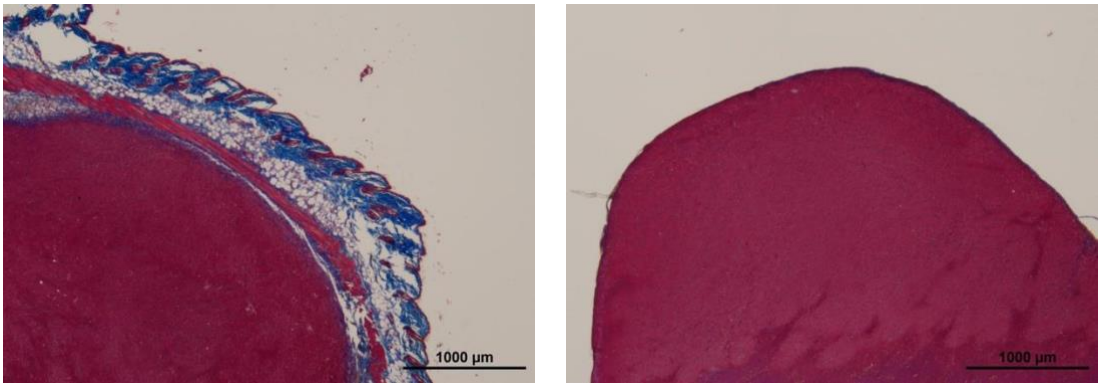

C.

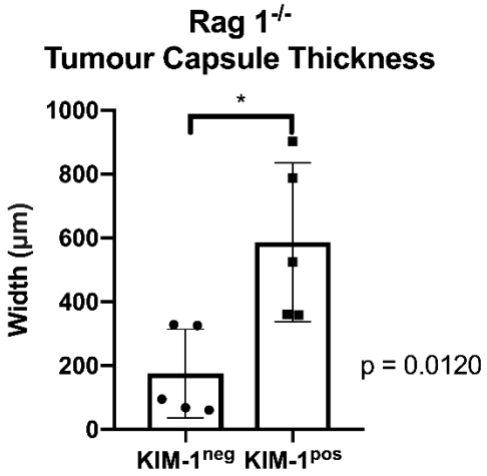

Figure 9. Collagen deposition in KIM-1^{pos} and KIM-1^{neg} Renca tumours grown SQ-Bilat in Rag1 -/- mice.

Micrograph of **A.** KIM-1^{pos} and **B.** KIM-1^{neg} Renca tumour stained with Masson's Trichrome elucidating the collagen stromal capsule (n=5/group). All images were taken at 100x magnification using brightfield microscopy and NIS-Elements Nikon software. **C.** Width (µm) quantification of collagen tumour capsule from KIM-1^{pos} and KIM-1^{neg} Renca tumours. Data is represented as mean measurement of tumour capsule width (µm) ± SEM (*, p = 0.0120, Unpaired two-tailed t-test).

3. 8 KIM-1 expression inhibits Renca tumour growth in an orthotopic model of RCC.

RCC tumours arise from the proximal tubule of the kidney and can metastasize to distant sites such as the lung. To test the role of KIM-1 on tumour growth within the kidney and on metastasis to the lungs, I orthotopically injected KIM-1^{pos} or KIM-1^{neg} Renca cells into the renal subcapsular space of BALB/c mice. Previous studies have claimed that Renca cells are able to grow in the kidney and preferentially metastasize to the lungs within 2 weeks of intra-renal injection (Feldman *et al.*, 2016). Renca cells were injected with Matrigel^{TM} into the subcapsular region of the left kidney. The volume and weights of the KIM-1^{pos} Renca tumours were significantly lower than KIM-1^{neg} Renca tumours (Fig 10). Mice injected with KIM-1^{pos} Renca

cells also had fewer metastatic lung nodules compared to mice injected with KIM-1^{neg} Renca cells, albeit this was not significant (Fig 13A-C).

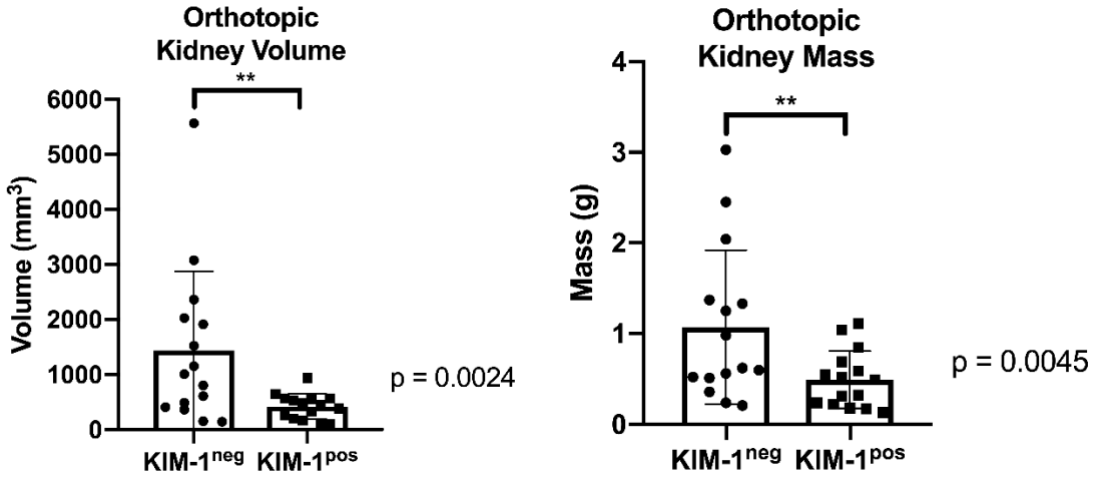

Figure 10. Volumes and weights of KIM-1^{pos} and KIM-1^{neg} Renca tumour after orthotopic injection into BALB/c mice.

Tumour bearing kidney volume and mass respectively, 21 days post orthotopic injections of KIM-1^{pos} or KIM-1^{neg} Renca cells (n=15/group). Data is represented as mean measurement of tumour size/volume (mm^3), and mass (g) ± SEM (volume, **, p = 0.0024; mass, **, p = 0.0045, Unpaired two-tailed t-test).

3. 9 KIM-1^{pos} Renca tumours do not produce a collagen rich capsule when injected orthotopically into BALB/c mice.

To investigate if orthotopic injection of KIM-1^{pos} Renca cells produce tumours with a collagen rich capsule, both KIM-1^{pos} and KIM-1^{neg} Renca tumours grown orthotopically in female BALB/c mice were subjected to Masson's Trichrome staining. Analysis of kidney bearing tumours revealed no measurable differences in capsule size between both KIM-1^{pos} and KIM-1^{neg} kidney bearing tumours (Fig 11A and B).

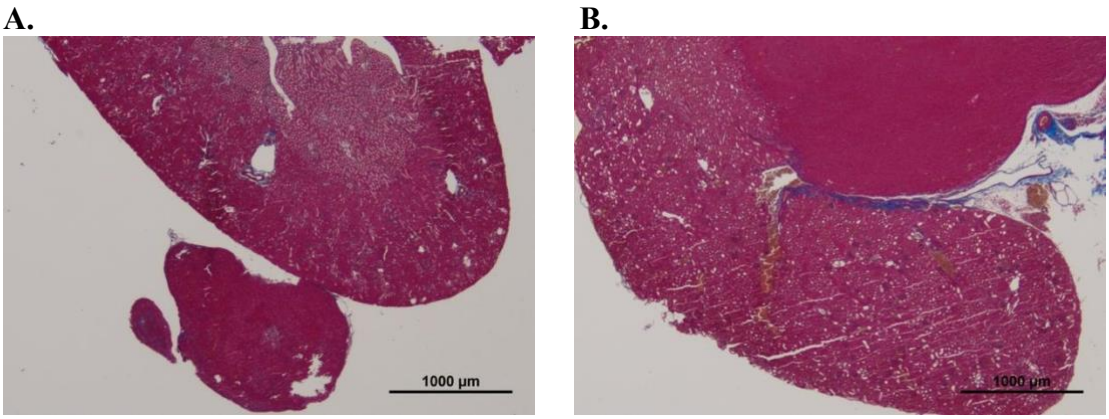

Figure 11. Collagen deposition in KIM-1^{pos} and KIM-1^{neg} Renca tumours grown orthotopically in BALB/c mice.

Micrograph of **A.** KIM-1^{pos} and **B.** KIM-1^{neg} kidney bearing Renca tumours stained with Masson's Trichrome elucidating the lack of collagen stromal capsule. All images were taken at 100x magnification using brightfield microscopy and NIS-Elements Nikon software.

3.10 Tumour KIM-1 expression does not influence immune infiltration of invading lymphocytes in the orthotopic Renca model.

Next, I investigated whether KIM-1 expression on Renca tumours had any effects on tumour infiltrating T cells in our orthotopic model. KIM-1^{pos} and KIM-1^{neg} tumour-bearing kidneys were stained for $CD3^+$, $CD3^+CD4^+$, and $CD3^+$ $CD8^+$. We examined tumours at 21 days post-injection to allow for maximal infiltration by immune cells. There were no significant differences in tumour infiltrating $CD3^+$, $CD4^+$, or $CD8^+$ T cells between Renca KIM-1^{pos} and KIM-1^{neg} tumours (Fig 12A-C).

A.

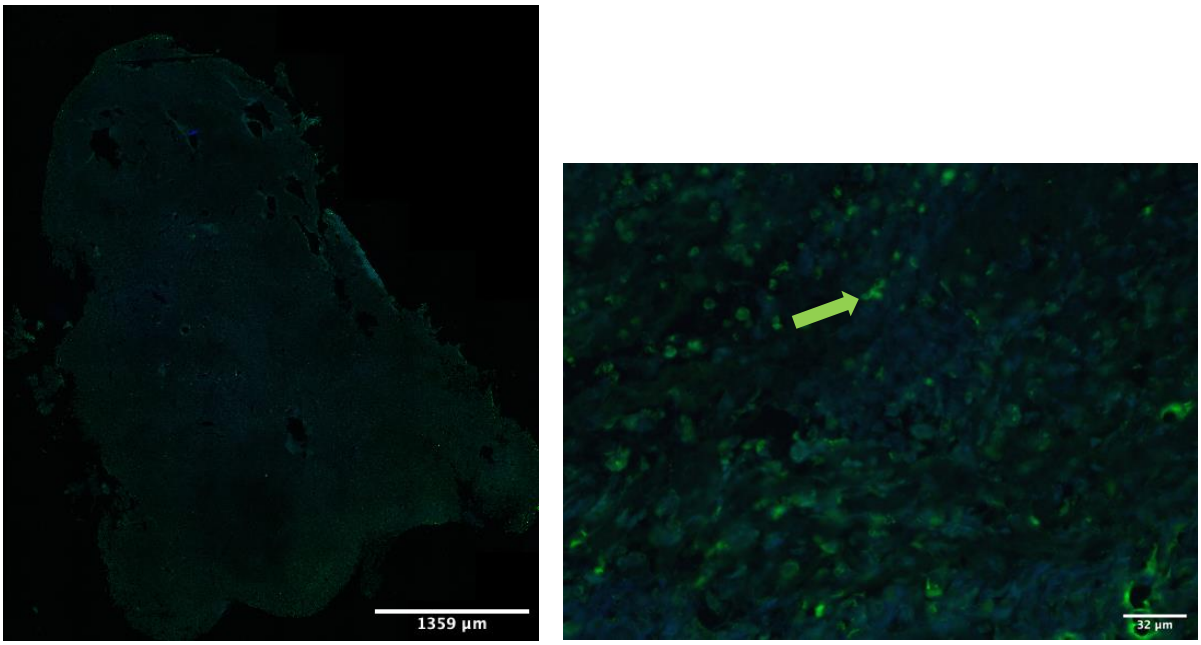

B.

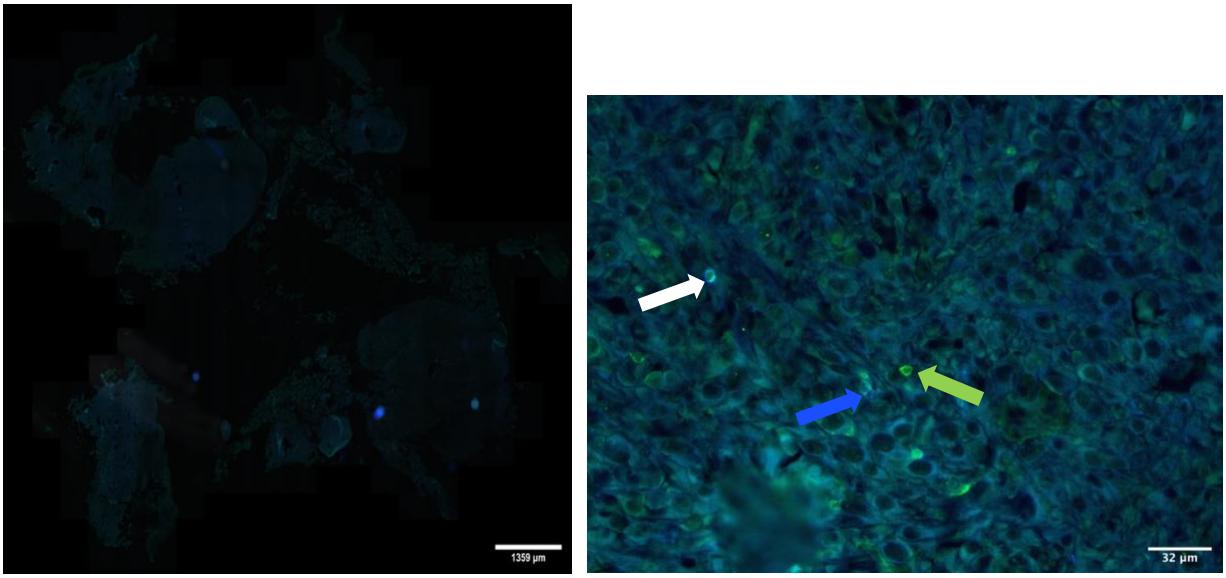

C.

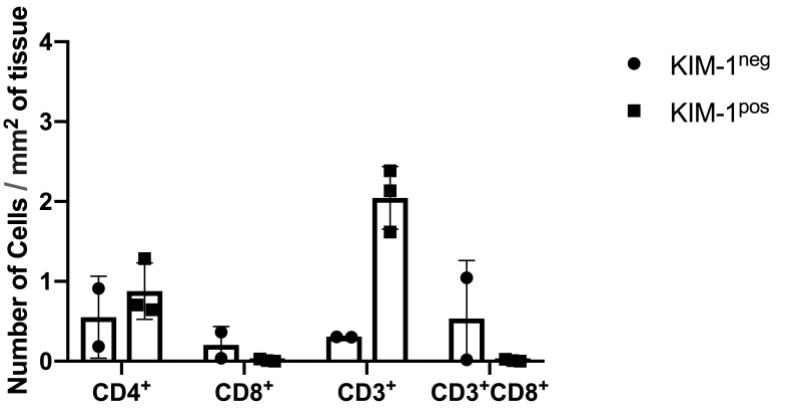

Figure 12. Co-immunofluorescence staining for $CD3^+$, $CD4^+$, and $CD8^+$ invading lymphocytes in KIM-1^{pos} and KIM-1^{neg} Renca orthotopic tumours from BALB/c mice after 21 days.

Micrographs of **A.** KIM-1^{pos} and **B.** KIM-1^{neg} Renca tumour stained for $CD3^+$ (green) $CD4^+$ (blue) $CD8^+$ (white) (KIM-1^{pos}: n=3, KIM-1^{neg}: n = 2). **C.** Quantification of the various types of immune infiltrates counted within tumours. Designated arrows pointing to cell types [$CD3^+$ (green) $CD4^+$ (blue) $CD8^+$ (white)] on inlet images. All images were taken via widefield microscopy using Leica Software at 10x and 100x magnification, respectively. Immune infiltrates were enumerated using Fiji manual cell counter software.

3. 11 KIM-1 expression does not affect spontaneous metastasis from the kidneys to lungs in the orthotopic model of RCC.

We next investigated whether KIM-1 expression had any impact on the process of metastasis from the kidney to the lungs by collecting the lungs at day 21 and examining them for metastatic nodules using microscopy. Histological examination of the lung tissues revealed no statistically significant differences in the number of metastatic nodules, as well as no differences in collagen encapsulation between mice injected orthotopically with KIM-1^{pos} or KIM-1^{neg} Renca cells (Fig 13A-C).

A.

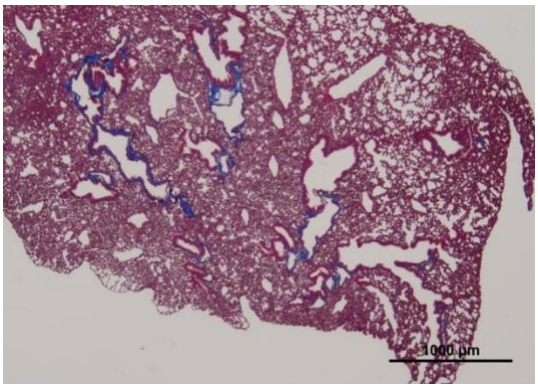

B.

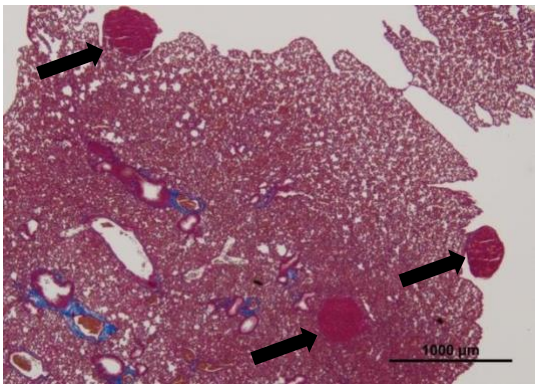

C.

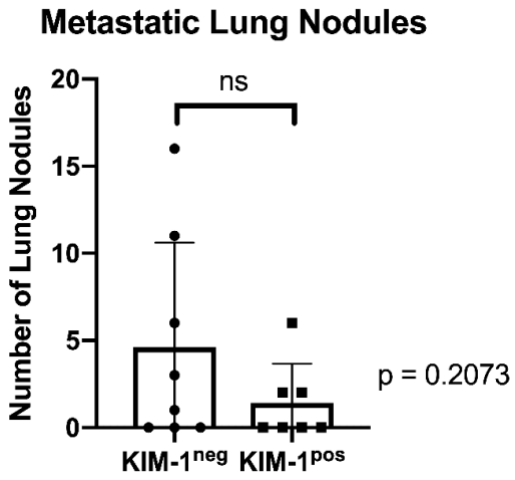

Figure 13. Number of metastatic lung nodules in BALB/c mice injected orthotopically with KIM-1^{pos} or KIM-1^{neg} Renca cells.

Micrographs of H&E-stained sections of lung tissue excised from **A.** KIM-1^{pos} and **B.** KIM-1^{neg} Renca cell treated mice (n=8/group). **C.** Quantification of metastatic lung nodules formed within both KIM-1^{pos} and KIM-1^{neg} Renca cell treated mice. Nodules were enumerated by manually counting visualized metastases. Metastases are indicated using arrows. All images were taken using brightfield microscopy and NIS-Elements Nikon software. Data is represented as mean measurement of number of metastatic nodules per tissue surface area ± SEM (NS, p = 0.2073, Unpaired two-tailed t-test).

3.12 KIM-1 expression in Renca cells promotes transcription of genes involved in the formation and interaction with extracellular matrix.

To understand how KIM-1 expression promotes the formation of collagen rich capsules by Renca tumours, I analyzed our previously generated RNA sequencing data from both KIM-1^{pos} and KIM-1^{neg} Renca cells (Lee and Gunaratnam, 2019). The most significant gene enrichment that was upregulated within the Renca KIM-1^{pos} cells was in genes involved in Extracellular Matrix Interaction ($p < 0.05$, fold change 1.96) (Fig 14A and B). This enrichment contained genes involved in the interaction and deposition of extracellular matrix (ECM). Moreover, the most significantly upregulated collagen genes within KIM-1^{pos} Renca cells was *COL6A1* and *COL6A2* (Fig 14C).

A.

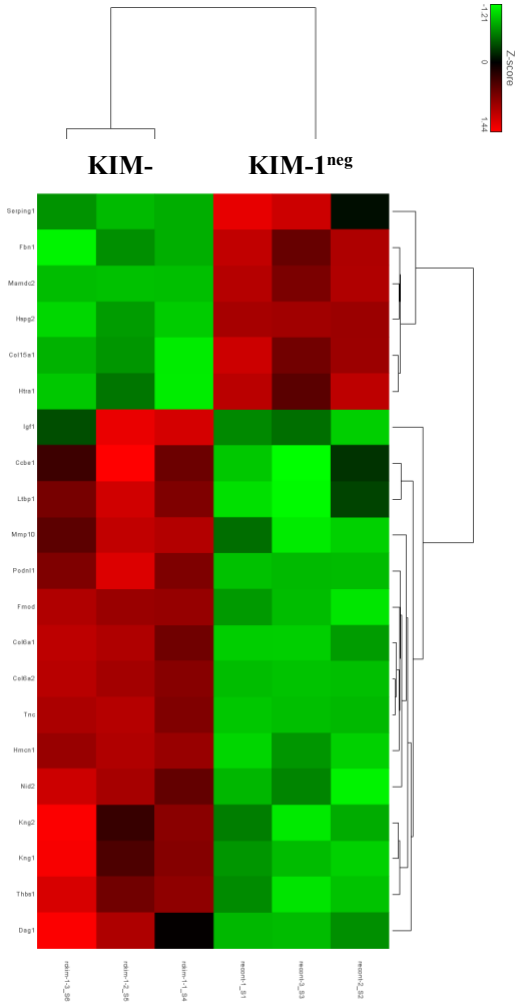

B.

Extracellular Matrix Genes Enriched in KIM-1pos Renca Cells (1.96-Fold Change)
Dag1
THBS1
Kng1
Kng 2
Nid2
Hmcn1
Tnc
Col6a2
Sema5a
Podnl1
Fmod
Adgrg6
Mmp10
Ltbp1
Ccbe1
Igf1

C.

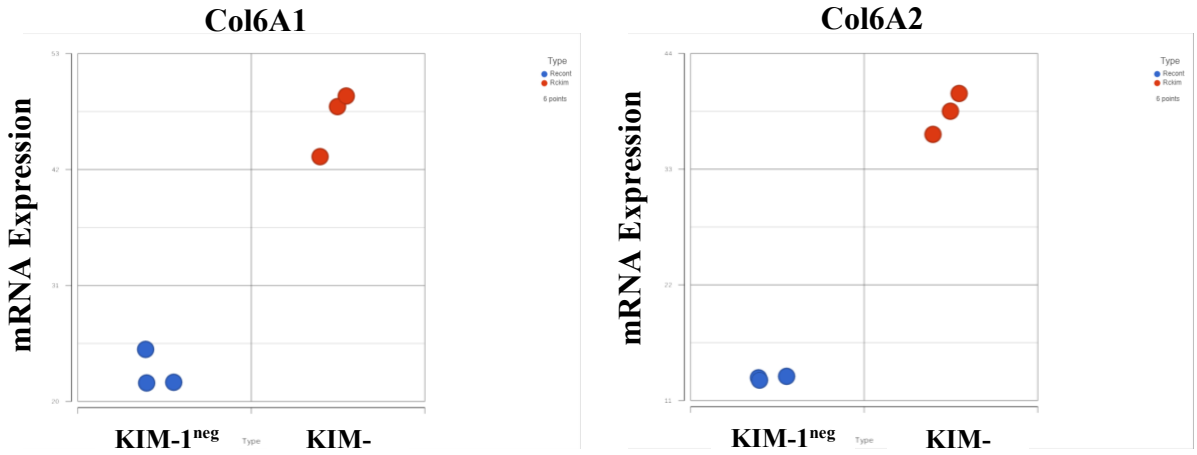

Figure 14. Illumina RNA-Sequencing transcriptomic analysis of enriched Extracellular Matrix Genes between KIM-1^{pos} and KIM-1^{neg} Renca cell lines.

A. Heat map generated from RNA Sequencing data of KIM-1^{pos} and KIM-1^{neg} Renca cell lines (n=3/group), displaying differential gene enrichment analysis of extracellular matrix (ECM) genes (p>/=0.05). Genes with increased numbers of transcripts are marked as red, while decreased are marked as green. **B.** List of ECM genes that have significant increased expression in KIM-1^{pos} Renca cells, in comparison to KIM-1^{neg} Renca cells. **C.** Collagen 6 A 1 and Collagen 6 A 2 mRNA expression level within both KIM-1^{pos} (red) and KIM-1^{neg} (blue) Renca cells.

Table 1. Mouse Oligonucleotide PCR primer sequences

Primer Sequence (5' → 3')		
Gene	**Forward Sequence**	**Reverse Sequence**
mKIM-1 (murine)	TCAGCATCTCTAAGCGTGGT	ATGTTGTCTTCAGCTCGGGA
GAPDH (murine)	AGGTCGGTGTGAACGGATTTG	TGTAGACCATGTAGTTGAGGTCA

Chapter 4

4. Discussion

4.1 Major Findings

4.1.1 KIM-1 (*Havcr1*) mRNA is expressed at all stages of RCC and increases overall patient survival

Multiple studies have identified KIM-1 as a urine or blood biomarker for the early detection of RCC (Scelo *et al.*, 2018). This was made possible through sensitive detection of shed or soluble KIM-1 (sKIM-1) in the blood plasma and urine (Scelo *et al.*, 2018) of RCC patients. Our laboratory previously showed that cell-surface KIM-1 is shed by ADAM17 or TACE in RCC cells (Gandhi *et al.*, 2014). Using the TCGA KIPAN database, specifically analyzing KIRC (Kidney Clear Cell Carcinoma) and KIRP (Kidney Papillary Carcinoma) patient databases, I was able to show that increased KIM-1 mRNA is highly upregulated in human RCC patients (Fig 1). KIM-1 expression was found to be significantly increased as early as stage I disease, with persistent expression through stages I-IV. Given that KIM-1 is only upregulated during acute kidney injury (AKI) (Han *et al.*, 2005), and the early detection of KIM-1 in the blood of RCC patients (Scelo *et al.*, 2018), these data confirm that KIM-1 is likely upregulated in early RCC lesions (Han *et al.*, 2002). The reason for this upregulation is unclear, but it is not due to VHL-loss of function (unpublished observations). In addition, higher KIM-1 expression was associated with significantly increased overall survival rates in KIRC (ccRCC) patients, yet not KIRP (papillary RCC) patients (Fig 1C, D and E). These data are in contradiction to findings reported by Scelo and team (Scelo *et al.*, 2018), that high plasma KIM-1 concentrations were associated with poorer survival. Our study, however, examined endogenous tumour KIM-1and not soluble (shed) KIM-1.

Many groups, including Dr. Gunaratnam's, have shown that during AKI, KIM-1 converts proximal tubular epithelial cells (PTECs) into semiprofessional phagocytes for clearance of apoptotic and necrotic cells of (Arai *et al.*, 2016). KIM-1 recognizes and binds to phosphatidylserine (PtdSer) – a phospholipid abundantly expressed on early necrotic and apoptotic cells – via the metal ion-dependent ligand binding site within its IgV domain (Nagata *et al.*, 2016). The clearance of dying cells leads to curtailment of inflammation and promotes tissue repair. The function of KIM-1 in RCC may be linked to its reparative role in the healthy kidney during acute injury, where an increase in KIM-1 expression reduces the amount of apoptotic or early necrotic cells formed in tumours, thereby significantly reducing tumour burden and promoting cell regeneration and repair (O. Z. Ismail *et al.*, 2016). This in turn could explain why patients with higher levels of KIM-1 expression, exhibit more favorable outcomes.

4.1.2 ECM signatures are upregulated in human RCC

Previous studies have underscored the importance of tumour stroma and ECM components in tumour progression and metastasis (Yuzhalin *et al.*, 2018). RCC is known to upregulate adhesion molecules (Chen *et al.*, 2016), moreover, several collagen genes exhibiting increased mRNA expression have been found in human RCC tumours and linked to tumour grade (Best *et al.*, 2019). Collagen genes such as Collagen 1 (*COL1*) (Majo *et al.*, 2020), Collagen 6 (*COL6*) (Wan *et al.*, 2015), and Collagen 23A1 (*COL23A1*) (Xu *et al.*, 2017) have been shown to be upregulated in RCC tumours. Collagen in cancer has been found to be both beneficial and detrimental to patients in terms of tumour progression (Fang *et al.*, 2014), although the mechanistic role of collagen in RCC is not well understood. Furthermore, chronic KIM-1 expression after AKI has been linked to kidney fibrosis *in vivo* (Humphreys *et al.*, 2013). Our analysis of the TCGA using KIRC and KIRP patient cohorts revealed that various collagen genes

(i.e. *COL1A1, COL1A2, COL6A1, COL6A2,* and *COL23A1*) were all significantly upregulated in RCC tumour tissues vs adjacent normal tissues (Fig 2). A recent study found that *Col6a1* promotes metastasis and a poorer prognosis in pancreatic cancer patients (Owusu-Ansah *et al.*, 2019). Another study found *Col23A1* is upregulated in RCC, and contributes to tumour progression (Xu *et al.*, 2017). On the other hand, down-regulation of *Col1A2* by methylation was found in both bladder (Mori *et al.*, 2009), and melanoma cancer (Bonazzi *et al.*, 2011). The role of these various collagen genes across multiple types of cancer remains controversial. When correlating KIM-1 expression to the TMI signature gene list (Lim *et al.*, 2019), along with previous collagen genes of interest (*COL1A1, COL1A2, COL6A1, COL6A2,* and COL23A1), I found no clear correlation trends between these collagen signatures and KIM-1 expression in RCC patients (Fig 3). Although, when comparing KIM-1 expression to *COL1A2, COL6A1, COL6A2*, and *COL23A1* - these were found to positively correlate to KIM-1 expression in RCC. Many of the genes within the TMI signature (Lim *et al.*, 2019) had either a significant positive or negative correlation to tumour KIM-1 mRNA – although further investigation behind the specific genes must be completed before additional conclusions can be made. Previous research has shown that during AKI, KIM-1 expression is beneficial in early acute stages of injury but chronic expression of KIM-1 promotes renal fibrosis (Humphreys *et al.*, 2013). Cell types implicated in the process of fibrosis are fibroblasts and myofibroblasts that aid in tissue remodeling and the secretion of extracellular matrix components such as collagen (Wynn, 2008). The positive correlation of collagen genes in KIM-1 expressing Renca cells may be a protective mechanism by the kidney. It may be possible that KIM-1 expression in renal malignancies causes similar effects. This would suggest that chronic KIM-1 expression leading to fibrosis, may be a dominant phenotype of KIM-1 not only in kidney injury, but possibly in RCC. However, the

exact interaction – if present – between KIM-1 and *COL1A2, COL6A1, COL6A2*, and *COL23A1* needs to be confirmed through more mechanistic studies.

4.1.3 KIM-1 does not alter tumour growth in an immune competent subcutaneous Renca model

Multiple studies have identified the subcutaneous model as a stable murine model to study RCC tumour biology (Sobczuk *et al.*, 2020). Using the bilateral and unilateral subcutaneous models, I compared the growth of KIM-1^{pos} and KIM-1^{neg} Renca tumours in immune competent mice. The bilateral model is an ideal model to use as it minimizes the genetic heterogeneity between individual mice that could cause variations in response to the same treatment. Bilateral models are better suited to studying the effect of tumours on the host immune system (e.g. immune check-point blockade) (Zemek *et al.*, 2020). I found that KIM-1 had no effect on tumour growth regardless of whether we used the bilateral or unilateral approach (Fig 4 and 5). Previous studies have found that Renca tumour growth *in vivo* had inconsistent tumour growth kinetics in the absence of Matrigel^{TM} (Yu *et al.*, 2018). Following this study, I revised my protocol to CDTRresuspend our Renca cells in growth factor reduced Matrigel^{TM} prior to both bilateral and unilateral subcutaneous injection. My studies produced consistent tumour sizes and masses with smaller standard deviations. Therefore, I am confident of my findings showing that KIM-1 expression does not alter the tumour size or mass produced by Renca cells implanted subcutaneously into immune competent mice.

4.1.4 KIM-1 expression promotes the formation of a collagen dense capsule around Renca tumours injected subcutaneously into both immune competent and immune deficient mice

Dysregulated collagen production has been linked to a more malignant phenotype in various cancers (Seager *et al.*, 2017). On the other hand, many benign tumours are known to be surrounded by a capsule consisting of connective tissue. My findings suggest that KIM-1 expression promotes transcription of various collagen genes in human RCC tumours and formation of a collagen-rich capsule surrounding the Renca tumours. Interestingly, I observed the formation of the capsule around KIM-1^{pos} Renca tumours only when injected subcutaneously but not orthotopically (Fig 7, 8 9, and 11). The use of Matrigel^{TM} did not affect these results. Some studies have suggested that the collagen rich tumour capsule directly interacts with the host immune system, and thus, the ensuing interaction strongly impacts tumour progression (Seager *et al.*, 2017). Given that the tumour capsule was present on KIM-1^{pos} Renca tumours grown in wild type BALB/c and RAG$1^{-/-}$ BALB/c mice, my data suggests that the formation of the capsule does not depend on the interaction of tumour cells and the adaptive immune system, yet is dependent on the site of injection (subcutaneous vs orthotopic). Specifically, we can assume that the collagen capsule is localized to the tumour stroma due to the interaction between tumour-associated KIM-1 and the surrounding cells of the subcutaneous microenvironment. Given that there were no differences in volume or mass between the subcutaneous KIM-1^{pos} and KIM-1^{neg} Renca tumours regardless of host immune status (WT BALB/c or Rag$1^{-/-}$ BALB/c mice), it could be argued that the capsule does not alter the T- or B cells responses against the tumours, in opposition to previous studies (Salmon *et al.*, 2012).

4.1.5 KIM-1 expression does not alter frequency or distribution of invading lymphocytes in both subcutaneous and orthotopic Renca models

The tumour microenvironment plays a key role in anti-tumour immunity (Applegate, Balch and Pellis, 1990). Intra- and extra-tumoral cell signaling, tumour and cell metabolism, and oxygenation are all factors that influence tumour progression and metastasis - can be determined by the surrounding tumour microenvironment (Henke, Nandigama and Ergün, 2020). Tumour microenvironment components can differ significantly between tumour types, but the main components are invading or surrounding immune cells, the vasculature, stromal cells and the tumour associated ECM (Anderson and Simon, 2020). In most cases, the tumour cells seem to orchestrate the surrounding cells to promote a microenvironment favorable for growth and/or metastasis (Walker, Mojares and Del Río Hernández, 2018). It is well known that tumour associated ECM (including collagen) is able to inhibit the invasion of immune cells into the tumour parenchyma and/or alter the phenotype of the invading immune cells to promote cancer progression (Maller *et al.*, 2020). Also, depending on the density of tumour associated collagen, the ECM can inhibit the positioning and migration of T cells, resulting in possible T cell exclusion from the tumour periphery (Kuczek *et al.*, 2019). Increased tumoral collagen has also been found to exhaust $CD8^+$ T cells through direct contact with T cell markers, LAIR1 (Peng *et al.*, 2020). This phenomenon has been observed in many cancers such as triple-negative breast cancer, pancreatic cancers (Kuczek *et al.*, 2019) and lung cancer (Salmon *et al.*, 2012). Organization and location of tumour associated ECM structures are commonly positioned around vasculature structures or the stromal interface. Specifically, research has shown that both perivascular and loose organized structures of the ECM in particular are where most of the intra-tumoral T cell migration occurs (Salmon *et al.*, 2012). I was able to elucidate that my KIM-1^{pos}

Renca tumours develop significantly thicker collagen dense stromal capsules. Yet, I observed no significant differences in the distribution or frequencies of invading lymphocytes within subcutaneous KIM-1^{pos} or KIM-1^{neg} Renca tumours (Fig 6). $CD4^+$ and $CD8^+$ T cells were chosen for analysis due to the compelling research that: 1) T cells are fundamental to anti-tumour immunity; 2) known exclusion or inhibitory mechanisms via collagen deposition targets both T cell subsets.

We have no concrete conclusions about the distribution or frequency of invading lymphocytes within KIM-1^{pos} and KIM-1^{neg} Renca tumours grown orthotopically (Fig 12). Due to the small sample size of my KIM-1^{neg} group, additional experiments will be required to confirm whether or not there are any real differences. Further characterization of the immune infiltrate and evaluation of the effector function of invading lymphocytes in KIM-1^{pos} vs. KIM-1^{neg} Renca tumours, may help elucidate the mechanism responsible for inhibiting tumour growth in our orthotopic model.

4.1.6 KIM-1 expression inhibits tumour growth in an orthotopic Renca model

Subcutaneous tumour models are widely used for *in vivo* cancer studies and allows for growth of the tumour below the skin to become a highly vascularized area. This allows for rapid tumour growth that is easily monitorable using calipers, permitting a rapid assessment of growth kinetics overtime (Zhang *et al.*, 2019). There are several limitations to the subcutaneous tumour model in comparison to other experimental cancer mouse models. Subcutaneous tumour models allow for the simple monitoring of biological staging yet are is not feasible for studying metastasis (Zhang *et al.*, 2019) – as it is not often observed in subcutaneous models (Gomez-Cuadrado *et al.*, 2017). Researchers have brought to light that the development of tumours in subcutaneous tissue may

not reflect the development of human cancers in native tissues (Zhang *et al.*, 2019). Therefore, orthotopic mouse models are regarded as a more clinically relevant model for the study of human cancers including progression, metastasis and therapeutic intervention. Orthotopic models have been shown to better correspond to human cancer development in terms of histology, tumour vasculature, response to therapies/treatments, and of course the metastatic cascade to nearby and distant organs (Khanna and Hunter, 2005). A recent study evaluating BB3r-targeted therapy in both subcutaneous vs orthotopic mouse models of prostate cancer, found that orthotopic models had overall higher tumour uptake, increased vascular perfusion, and lower burden of hypoxia. Overall findings from this study concluded that the tumour microenvironmental differences between subcutaneous and orthotopic models differs greatly (Zhang *et al.*, 2019). Another study recently compared the interactome profiles of gastric cancer – OE19 adenocarcinoma - using both subcutaneous and orthotopic xenograft models. Pathway analysis using RNA sequencing revealed various significantly enhanced pathways within orthotopic models in comparison to subcutaneous models. More vascular invasion were found within orthotopic models - observing increased interactions between cancer and stromal cells – with orthotopic models thought to have higher interplay with the surrounding microenvironment (Nakano *et al.*, 2018). Prior to our research, the discrepancies between subcutaneous vs orthotopic models in RCC was unknown. Overall, I am the first to uncover the major differences between subcutaneous and orthotopic mouse Renca tumour models and how they dictate the interaction between cancer cells and surrounding stromal cells. My results found that KIM-1^{pos} Renca cells create significantly smaller primary tumours in - comparison to KIM-1^{neg} Renca cells - when injected orthotopically into the subcapsular space of the kidney, but not subcutaneously, in immune competent mice (Fig 10). My results support previous evidence revealing KIM-1 as a potential protective player

in RCC (Lee and Gunaratnam, 2019), as patients with higher levels of KIM-1 expression resulted in an increased overall survival rate (Fig 1C). However, my findings also differ from that of (Cuadros *et al.*, 2013), who proposed that KIM-1 promotes tumour progression. In contrast to these studies, my findings suggest KIM-1 does not promote tumour progression, and in fact, inhibits tumour growth in my orthotopic studies.

One study investigated the differences in membrane bound tissue KIM-1 as well as soluble cleaved KIM-1, in regard to their differential effects on RCC progression. Microvascular invasion – the invasion of cancer cells into the endothelium of blood vessels – was correlated with increased tissue KIM-1 expression in clear cell RCC (ccRCC) tumours. This study also found that increased levels of soluble KIM-1 detected in the urine correlated with increased TNM staging and overall exacerbated disease progression (Mijuskovic *et al.*, 2018). Another study stated that when analyzing RCC patient plasma, higher concentrations of soluble KIM-1 were associated with poorer survival rates (Scelo *et al.*, 2018). On the other hand, the Gunaratnam laboratory has shown that KIM-1 expression on TECs is able to inhibit Gα12, subsequently inhibiting a small GTPase RhoA, which is found to increase metastatic progression of cancers (Z. O. Ismail *et al.*, 2016). Although the mechanistic correlation between KIM-1 and Gα12 expression in RCC *in vitro/in vivo* work was not further investigated. Despite these findings, the clear role of KIM-1 expression in the pathogenesis and progression of RCC remains not well understood. The discrepancy between my study and those discussed above may be explained by my studies involving multiple *in vivo* systems (subcutaneous vs orthotopic), and correlation of both *in vitro* and *in vivo* experimental data with TCGA patient database findings.

4.1.7 KIM-1 does not promote collagen capsule formation in an orthotopic Renca model

As mentioned above, previous studies have shown that orthotopic tumour models better mimic the natural biology of tumour progression (Nakano *et al.*, 2018). Surprisingly, my data showed no significant differences between KIM-1^{pos} and KIM-1^{neg} collagen capsules in our orthotopic model (Fig 11), yet in our subcutaneous model, KIM-1^{pos} Renca tumours bared significantly thicker collagen dense capsules in both immune competent and deficient mice. This discrepancy may be explained by differences in the (tumour) surrounding cells (skin vs. kidney) which the Renca cells recruit to form the microenvironment. Conceivably, the skin may be a more permissive environment for the formation of a collagen rich matrix (Cox and Erler, 2011). One study found that the adipose tissue of rats located within the subcutaneous space, strongly varied from visceral adipose tissue. This study observed subcutaneous adipose gene clusters strongly relating to ECM related genes involving collagen, cell adhesion, and proteases. Expression profiles revealed major fibril-forming collagen genes that were upregulated were Collagen I, Collagen III, Collagen V, and Collagen VI, along with the more common ECM related genes such as Lama, Fibronectin 1, and Collagen IV (Mori *et al.*, 2014). Although this study was performed in rats, previous research on adipose tissue has suggested that both mice and rats are comparable to one another (National Human Genome Research Institute, 2004). Another study found that when comparing ECM of subcutaneous tumours and *in vitro* tumour spheroids (a three-dimensional cell culture model), the subcutaneous tumours had an increased collagen content (De L Davies *et al.*, 2002) likely due to the proximity to cells within the adjacent connective and dermal adipose tissues (Wojciechowicz *et al.*, 2013). These previous findings

may give reason as to why we observed a significantly thicker collagen capsule formation in KIM-1^{pos} Renca tumours within our subcutaneous, but not orthotopic model.

4.1.8 KIM-1 does affect spontaneous metastasis of Renca cells to the lungs in an orthotopic model

Late stage RCC (III-IV) involves tumour growth into the renal vein, inferior vena cava, or to regional lymph nodes, each of which must pass the Gerota's fascia – the fibrous envelope encapsulating the kidney. Common sites of metastasis in RCC include the lungs, adrenal glands, and bones – whilst the lungs being the most common site of metastasis, found in up to 50%-60% of autopsies (Reznek, 2004). Orthotopic injection of Renca cells are widely used as a model to study the metastatic cascade of RCC (Hillman, Droz and Haas, 1994; Gomez-Cuadrado *et al.*, 2017). Although our orthotopic experiments revealed that the KIM-1^{pos} Renca tumours were considerably smaller than the KIM-1^{neg} Renca tumours, the small sample size precluded determining whether there were significant differences in the metastatic potential to the lungs between the KIM-1^{pos} or KIM-1^{neg} Renca cells (Fig 13). My data showed significantly fewer metastatic nodules compared to other studies employing Renca cells (Feldman *et al.*, 2016) where metastatic nodules compromised ~70% of lung tissue, whereas in my study both KIM-1^{pos} and KIM-1^{neg} Renca treated mice had only ~15 metastatic nodules observed per mouse. Secondary metastatic nodules also presented no differences in collagen encapsulation between groups. There are multiple potential explanations as to why I observed less metastasis in my experiments. I followed the protocol from Feldman Ret al., injecting 2 x 10^5 KIM-1^{pos} or KIM-1^{neg} Renca cells into the subcapsular space of the left kidney. This study used an endpoint for the assessment of metastases at 14 days post-injection and this resulted in sufficient primary tumour growth as well as secondary metastases compromising up to ~70% of resected lung tissue

(Feldman *et al.*, 2016). Another study by Murphy et al., injected Renca cells directly into the kidney – intrarenal implantation – to study metastatic RCC for the assessment of preclinical therapies (Murphy *et al.*, 2017). At 23 days after injection of Renca cells into the renal cortex/medulla, using BLI to assess tumour burden, this study observed significantly more metastasis than I did with subcapsular injection. Potential explanations for the low numbers of metastatic nodules in my model could be: 1) Subcapsular vs. intra-renal injection of Renca cells; 2) improper injection and leakage of cells outside the kidney; 3) reduced malignancy of our Renca cell lines upon transduction with Lentivirus. The use of luciferase expressing Renca cells may allow for more sensitive detection of metastatic foci when using real -time bioluminescent imaging (BLI).

4.1.9 KIM-1 expression increases transcription of ECM related genes in Renca cells

My data from the subcutaneous model of RCC revealed that KIM-1^{pos} Renca tumours obtain a significantly thicker collagen dense stromal capsule in comparison to KIM-1^{neg} Renca tumours, independent of adaptive immunity. Surprisingly, my orthotopic model of RCC revealed no significant differences in collagen stromal capsule formation between my tumour groups. In efforts to elucidate how KIM-1 expression may alter mechanistic pathways allowing for ECM production in our subcutaneous model, I interrogated the transcriptomic profile of KIM-1^{pos} and KIM-1^{neg} Renca cells using RNA sequencing and bioinformatic approaches. My data did not show many significant differences between our cell lines in terms of pathway analyses, yet we did detect a significant gene enrichment of genes involved in Extracellular Matrix Interactions (Fig 14). Many of the genes involved in this enrichment, are involved in extracellular matrix synthesis and deposition. These data suggests that KIM-1 expression in Renca cells may activate

a transcription factor which regulates multiple extracellular matrix related genes. I believe these findings correlate to the clinically relevant findings from TCGA between KIM-1 and collagen. Interestingly, two significantly upregulated genes that were found in the RNA Sequencing of the Renca cell lines – *COL6A1*, *COL6A2* – are also found in my TCGA data where these collagens are significantly upregulated in RCC patient and positively correlate with KIM-1 expression. These findings further validate our KIM-1 overexpression Renca model, revealing the similarities between our Renca cell lines and RCC patient transcriptomic profiles.

4. 2 Limitations

4.2.1 Subcutaneous Mouse Model

Although subcutaneous models are widely used in oncological research, there are major drawbacks of this method. Initially I had difficulties in trying to overcome the variability in tumour volume and weight differences between our KIM-1^{pos} and KIM-1^{neg} groups. As stated previously, there are many drawbacks of the model, most of which surround the microenvironment, and clinical relevance. Studies have found that subcutaneous models although non-invasive, the microenvironment implantation causes the tumour to behave as a benign tumour rather than malignant tumour, owing to the reduced propensity to form metastases (Sordat, 2017). One study found significant inconsistencies in tumour formation due to the vast variations in angiogenesis and tumour vasculature within the subcutaneous pocket where injections occur (Lwin, Hoffman and Bouvet, 2018). These studies could explain why we had difficulties obtaining consistent results with our subcutaneous model. Another study - investigating various tumour immune profiles of murine syngeneic tumour models - found that Renca cells were the only cell line within the study that needed to be injected with a growth

factor reduced basement membrane Matrigel™, in order to facilitate consistent growth patterns (Yu *et al.*, 2018). Following this protocol, I repeated my subcutaneous injections of 1 x 10^6 KIM-1^{pos} and KIM-1^{neg} Renca cells this time in a 1:1 dilution of 1x PBS and growth factor reduced Matrigel™. With this addition to my subcutaneous injection model, I was able to find data with tighter standard deviations in my tumour volumes and masses in both KIM-1^{pos} and KIM-1^{neg} tumour results. Although there was visibly less variability, incorporation of Matrigel™ did not cause uniformity in shape, resulting in abnormally shaped subcutaneous tumour growth still remaining an issue. These facts, coupled with my results, underscore the limitations of this model that are likely related to the microenvironment of the murine subcutaneous tissue.

4.2.2 Orthotopic Experimental Model

Although extremely useful and clinically relevant given the clinical cascade of human RCC, the orthotopic kidney tumour model is widely dependent on technique (Bibby, 2004). Subcapsular injections into the kidney are extremely difficult and can easily cause high variability between injections. A major drawback of orthotopic implantation is the high likelihood of leakage of the inoculate outside the kidney (Sasaki *et al.*, 2015). Although my surgeries were performed by an experienced veterinary surgeon and implemented with the use of growth factor reduced Matrigel™ in order to minimize leaking, this process can still occur late after surgery, and in some cases are unavoidable. Overall, the orthotopic model remains the most clinically relevant one despite its technical limitations.

4.2.3 Renca Cell Line

Renca cells are perhaps the most commonly used murine cell lines for *in vivo* RCC studies. They are naturally derived from a spontaneous renal adenocarcinoma that arose in a BALB/c mouse,

making the cell line syngeneic when injected into BALB/c mice. Renca cell lines are known to not fully reflect the genetics of human RCC, although they importantly possess the VHL (Von Lippen Lindau) deletion – causing epithelial mesenchymal transition (EMT) and HIF-1 α stabilization – which accurately represent the biology of human RCC tumours (Wolf, Kimryn Rathmell and Beckermann, 2020). Despite the overall concrete research that supports the use of Renca cell lines, I experienced several problems with our subcutaneous models (as stated above) that could be due to our cell line of choice. Yu et al. studied the tumour immune profiles of Renca tumours in different syngeneic mouse models and found Renca cells to be highly immunogenic - able to elicit an adaptive immune response (Yu *et al.*, 2018). Renca tumours are known to be highly infiltrated by immune cells from both the myeloid and lymphoid lineages (Wolf, Kimryn Rathmell and Beckermann, 2020). Interestingly, they found that the tumour immune profile depended on the size of the tumours *in vivo*. Through RNA sequencing, they found that smaller tumours (~100mm^3) had more immune cell infiltrates (including T cells, macrophages, and NK Cells), while larger tumours (~500mm^3 – 2000mm^3) contained more myeloid derived suppressor cells (MDSC) expressing NOS2/iNOS, and VEGFA. These transcriptomic changes have an impact on immunosuppression, decreased T cell numbers, and tumour vasculature. The researchers also stated that Renca cells had to be injected with growth factor reduced Matrigel^{TM} to obtain consistent and uniform tumours. Taken together with my data, this suggests that tumour size may be predictive of their immune profiles. Yet, this can pose great difficulty when finding variability in volumes and weights within tumour groups.

4.3 Future Directions and Significance

4.3.1 Significance

Overall, our findings are somewhat contradictory to previous reports regarding the role of KIM-1 in RCC. Although, preceding research has evidence to support both theories where KIM-1 can either be playing a protective role to patients or a harmful role by contribution to tumorigenicity. Some studies suggest that KIM-1 has oncogenic potential and is able to increase the invasiveness and progression of RCC tumours (Cuadros *et al.*, 2013). However, clinical data from TCGA database demonstrates that higher levels KIM-1 (*Havcr1*) mRNA in RCC patients is associated with greater overall patient survival (Fig 1C). Many *in vivo* studies investigating the pathophysiology of RCC used the subcutaneous murine model, due to ease of measuring the tumours and simplicity. The orthotopic model of RCC is a more clinically relevant model that mimics the natural environment (kidneys) of the tumours and their propensity to metastasize to the lungs. We have shown variance between Renca tumour phenotypes with respect to both growth kinetics and histological differences in our subcutaneous vs. orthotopic models, respectively. Despite previous research suggesting that orthotopic models allow for a greater cancer-stromal interaction (Nakano *et al.*, 2018), my data suggests that the microenvironmental niche of subcutaneous injections allow for an increased production of collagen rich matrix. Furthermore, my research demonstrates that increased KIM-1 expression positively correlates with increased *COL6A1* and *COL6A2* mRNA expression in both clinical human RCC (TCGA) data, and our Renca murine cell line. In contradiction of the prevailing view that KIM-1 promotes a more malignant phenotype of RCC, we have showed that KIM-1 expression inhibits orthotopic tumour growth in immune competent mice. This thesis work highlights the importance of the tumour model (subcutaneous vs orthotopic) in studying RCC and KIM-1.

Clinical TCGA data coupled with our data also indicates KIM-1 can possibly inhibit primary tumour growth within pre-clinical murine models of RCC.

4.3.2 Future Directions

The next phase of this project will focus on optimizing my pre-clinical orthotopic model. Results from my orthotopic - renal subcapsular RCC model – found significantly fewer lung metastatic nodules than expected within both KIM-1^{pos} and KIM-1^{neg} Renca cell injected mice. Optimizing this protocol will allow the proper analyses of whether KIM-1 is able to inhibit the process of spontaneous metastasis to the lungs in a clinically relevant model of RCC. Next, by subjecting KIM-1^{pos} and KIM-1^{neg} orthotopic Renca tumours to RNA sequencing, an analysis of identified genetic alterations could then be linked to KIM-1's ability to inhibit primary tumour growth. My previous RNA sequencing showed that KIM-1^{pos} Renca cells have significantly upregulated enriched genes involved in ECM receptor interaction. This cellular phenotype directly correlated to KIM-1^{pos} subcutaneous Renca tumours obtaining significantly thicker collagen dense stromal capsules independent of adaptive immunity. RNA sequencing on KIM-1^{pos} and KIM-1^{neg} orthotopic Renca tumours, will also help to elucidate any genetic drivers that could be altering the TME, allowing for the phenotypic differences that I have observed *in vivo*. Lastly, in my orthotopic Renca tumour models, I have been able to observe a trending towards significance in the frequency of $CD3^+$ immune cells – where KIM-1^{pos} contains more in comparison to KIM-1^{neg} Renca tumours. Although I analyzed the frequency and distribution of $CD3^+$, $CD3^+CD4^+$, and $CD3^+CD8^+$ immune cells, I did not evaluate their effector function. Analysis of orthotopic Renca tumours using flow cytometry to investigate the presence of immunomodulatory cytokines such as IFNγ and IL-2, could give rise to the functionality of the immune cells present. This analysis may also elucidate the reasoning behind the significantly reduced size of orthotopic KIM-1^{pos}

Renca tumours. These findings can also be elucidated by performing co-immunofluorescence staining for more specific immune markers such as T-cell exhaustion markers such CD44 or LY6C, to evaluate the activator state of T lymphocytes present.

Once the orthotopic Renca model is optimized, it will be possible to test the effect of an agonist anti-KIM-1 antibody (RMT1-10) on the growth, dissemination and development of primary tumours and metastatic nodules within the orthotopic model (Ichimura, Brooks and Bonventre, 2012). This may determine whether KIM-1's seemingly inhibitory effect on primary and secondary tumour growth can be enhanced with RMT1-10 delivery. When treating RMT1-10, we would expect to see stimulation of KIM-1 which may enhance its anti-tumour growth effects in RCC cells previously observed by our group (Lee *et al.*, 2021).

4.4 Conclusion

My research has revealed novel insights into the role of KIM-1 in RCC. Moreover, it has highlighted the significant differences between subcutaneous and orthotopic models used for pre-clinical oncological studies. The expression of KIM-1 in RCC tumours was associated with improved overall patient survival based on interrogation of the TCGA database. My pre-clinical orthotopic model suggests that KIM-1 may play a protective role in RCC. KIM-1 expression in RCC tumours positively correlated with transcripts for several collagen genes in human RCC patients. I observed significant discrepancies involving tumour progression and histological phenotypes between the subcutaneous and orthotopic murine RCC models. More research is required to fully discern the role of KIM-1 expression in RCC tumour progression, as KIM-1 may serve as a potential therapeutic target.

Appendices

Appendix 1. Confirmation of KIM-1 expression (KIM-1^{pos}) and absence of KIM-1 expression (KIM-1^{neg}) through total cell protein lysate, mRNA expression, and cell surface expression of KIM-1^{pos} and KIM-1^{neg} Renca cell lines.

A.

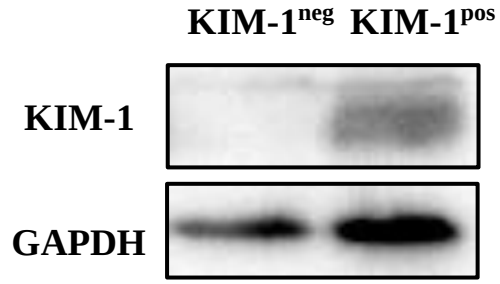

B.

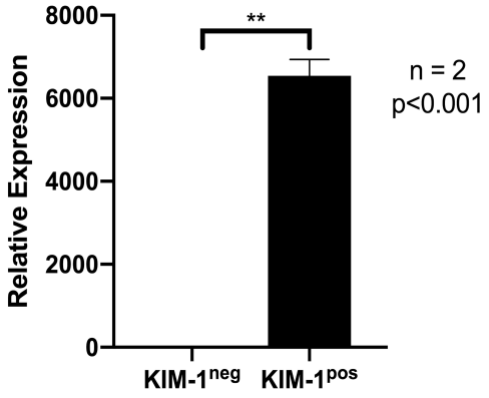

C.

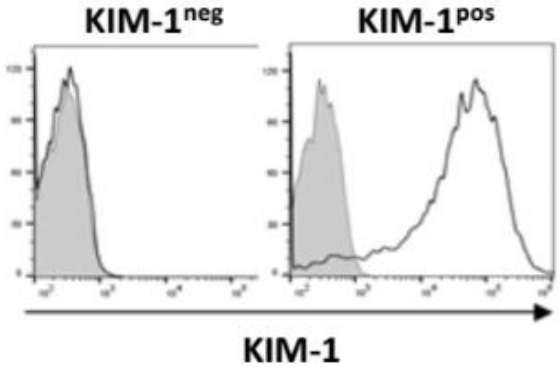

Supplementary Figure 1. Renca RCC cell line protein, mRNA and surface level expression of KIM-1, respectively.

Renca cells were transduced using a lentivirus carrying a vector encoding for murine KIM-1 cDNA (KIM-1^{pos}) or empty vector (KIM-1^{neg}). **A,** Western blot to detect murine KIM-1 in KIM-1^{pos} and KIM-1^{neg} Renca cells. **B,** Relative mRNA expression of KIM-1 (*Havcr1*) mRNA in KIM-1^{pos} and KIM-1^{neg} Renca cell lines normalized for expression of housekeeping gene GAPDH. **C,** KIM-1^{pos} and KIM-1^{neg} Renca cell line analysis of KIM-1 surface level expression by flow cytometry using anti-KIM-1 antibody.

Appendix 2. Periodate Lysine Paraformaldehyde Solution Protocol

Materials for PLP Solution:

- 0.1M Sodium Phosphate Buffer (Dibasic)
    - 14.18 g Na_2HPO_4 (Dibasic Sodium Phosphate) + 1L ddH_2O
- 0.1M Sodium Phosphate Buffer (Monobasic Sodium Phosphate)
    - 13.8g NaH_2PO_4 (Monobasic) + 1L ddH_2O
- 0.1M Phosphate Buffer (PB) – (stored RT) = 3:1 Dibasic buffer to Monobasic buffer
- L-Lysine
- Paraformaldehyde (PFA)
- Sodium M-Periodate
- Sucrose (10%, 20%, 30%) Dissolved in 0.1M Sodium Phosphate Buffer

<u>Freezing Tissue:</u>

- Dry Ice (store in Styrofoam box)
- Ethanol (put within dry ice)
- Isopentane (put in metal bin overtop of dry ice)
- Optimal Cutting Temperature Compound (OCT)
- Histology Tissue Cassettes
- Cling Wrap and Tin Foil

Citations

Ajay, A. K. *et al.* (2014) 'A bioinformatics approach identifies signal transducer and activator of transcription-3 and checkpoint kinase 1 as upstream regulators of kidney injury molecule-1 after kidney injury', *Journal of the American Society of Nephrology*, 25(1). doi: 10.1681/ASN.2013020161.

Anderson, N. M. and Simon, C. M. (2020) 'The tumor microenvironment', *Current Biology*, 60(16), pp. 921–925.

Applegate, K. G., Balch, C. M. and Pellis, N. R. (1990) 'In Vitro Migration of Lymphocytes through Collagen Matrix: Arrested Locomotion in Tumor-infiltrating Lymphocytes', *Cancer Research*, 50(22).

Arai, S. *et al.* (2016) 'Apoptosis inhibitor of macrophage protein enhances intraluminal debris clearance and ameliorates acute kidney injury in mice', *Nature Medicine*, 22(2). doi: 10.1038/nm.4012.

Aulitzky, W. *et al.* (1989) 'Successful treatment of metastatic renal cell carcinoma with a biologically active dose of recombinant interferon-gamma', *Journal of Clinical Oncology*, 7(12), pp. 1875–84.

Battelli, C. and Cho, D. C. (2011) 'MTOR inhibitors in renal cell carcinoma', *Therapy*. doi: 10.2217/thy.11.32.

Becher, O. J. and Holland, E. C. (2006) 'Genetically engineered models have advantages over xenografts for preclinical studies', *Cancer Research*. doi: 10.1158/0008-5472.CAN-05-3827.

Best, S. L. *et al.* (2019) 'Collagen organization of renal cell carcinoma differs between low and high grade tumors', *BMC Cancer*, 19(1). doi: 10.1186/s12885-019-5708-z.

Bibby, M. C. (2004) 'Orthotopic models of cancer for preclinical drug evaluation: Advantages

and disadvantages', *European Journal of Cancer*, 40(6). doi: 10.1016/j.ejca.2003.11.021.

Boehncke, W. H. and Brembilla, N. C. (2019) 'Autoreactive T-lymphocytes in inflammatory skin diseases', *Frontiers in Immunology*. doi: 10.3389/fimmu.2019.01198.

Bonazzi, V. F. *et al.* (2011) 'Cross-platform array screening identifies COL1A2, THBS1, TNFRSF10D and UCHL1 as genes frequently silenced by methylation in melanoma', *PLoS ONE*, 6(10). doi: 10.1371/journal.pone.0026121.

Bonventre, J. V. (2008) 'Kidney injury molecule-1 (KIM-1): A specific and sensitive biomarker of kidney injury', in *Scandinavian Journal of Clinical and Laboratory Investigation*. doi: 10.1080/00365510802145059.

Bonventre, J. V. (2009) 'Kidney injury molecule-1 (KIM-1): A urinary biomarker and much more', *Nephrology Dialysis Transplantation*. doi: 10.1093/ndt/gfp010.

Buchbinder, E. I. and Desai, A. (2016) 'CTLA-4 and PD-1 pathways similarities, differences, and implications of their inhibition', *American Journal of Clinical Oncology: Cancer Clinical Trials*. doi: 10.1097/COC.0000000000000239.

Cairns, P. (2011) 'Renal Cell Carcinoma', *Cancer Biomarkers*, pp. 461–473. Available at: https://www.ncbi.nlm.nih.gov/pmc/articles/PMC3308682/pdf/nihms362390.pdf.

Canadian Cancer Statistics Advisory Committee (2019) *Canadian Cancer Statistics 2019*, *Canadian Cancer Society*.

Chang, X. *et al.* (2016) 'Comparative efficacy and safety of first-line treatments in patients with metastatic renal cell cancer: A network meta-analysis based on phase 3 RCTs', *Oncotarget*, 7(13). doi: 10.18632/oncotarget.7511.

Chen, Y. *et al.* (2016) 'Identification of biological targets of therapeutic intervention for clear cell renal cell carcinoma based on bioinformatics approach', *Cancer Cell International*, 16(1).

doi: 10.1186/s12935-016-0291-8.

Chin, A. I. *et al.* (2006) 'Surveillance strategies for renal cell carcinoma patients following nephrectomy.', *Reviews in urology*, 8(1).

Cho, H. *et al.* (2016) 'On-target efficacy of a HIF-2α antagonist in preclinical kidney cancer models', *Nature*, 539(7627). doi: 10.1038/nature19795.

Choueiri, T. K. and Kaelin, W. G. (2020) 'Targeting the HIF2–VEGF axis in renal cell carcinoma', *Nature Medicine*. doi: 10.1038/s41591-020-1093-z.

Choueiri, T. K. and Motzer, R. J. (2017) 'Systemic Therapy for Metastatic Renal-Cell Carcinoma', *New England Journal of Medicine*, 376(4), pp. 354–366. doi: 10.1056/NEJMra1601333.

Cohen, H. T. and McGovern, F. J. (2005) 'Renal-cell carcinoma', *New England Journal of Medicine*, 8;353(23), pp. 2477–90.

Cox, T. R. and Erler, J. T. (2011) 'Remodeling and homeostasis of the extracellular matrix: Implications for fibrotic diseases and cancer', *DMM Disease Models and Mechanisms*. doi: 10.1242/dmm.004077.

Cuadros, T. *et al.* (2013) 'Hepatitis A virus cellular receptor 1/kidney injury molecule-1 is a susceptibility gene for clear cell renal cell carcinoma and hepatitis A virus cellular receptor/kidney injury molecule-1 ectodomain shedding a predictive biomarker of tumour progression', *European Journal of Cancer*, 49(8). doi: 10.1016/j.ejca.2012.12.020.

Cuadros, T. *et al.* (2014) 'Molecular and cellular pathobiology HAVCR/KIM-1 activates the IL-6/STAT-3 pathway in clear cell renal cell carcinoma and determines tumor progression and patient outcome', *Cancer Research*, 74(5). doi: 10.1158/0008-5472.CAN-13-1671.

Decastro, G. J. and McKiernan, J. M. (2008) 'Epidemiology, clinical staging, and presentation of

renal cell carcinoma', *The Urologic Clinics of North American*, 35(4), pp. 581–592.

Donskov, F. *et al.* (2020) 'Outcomes based on age in the phase III METEOR trial of cabozantinib versus everolimus in patients with advanced renal cell carcinoma', *European Journal of Cancer*, 126. doi: 10.1016/j.ejca.2019.10.032.

Escudier, B. *et al.* (1993) 'Combination of interleukin-2 and gamma interferon in metastatic renal cell carcinoma', *European Journal of Cancer*, 29(5). doi: 10.1016/S0959-8049(05)80354-5.

Fang, M. *et al.* (2014) 'Collagen as a double-edged sword in tumor progression', *Tumor Biology*. doi: 10.1007/s13277-013-1511-7.

Feldman, R. D. *et al.* (2016) 'Aldosterone mediates metastatic spread of renal cancer via the G protein-coupled estrogen receptor (GPER)', *FASEB Journal*, 30(6). doi: 10.1096/fj.15-275552.

Gandhi, R. *et al.* (2014) 'Accelerated receptor shedding inhibits kidney injury molecule-1 (KIM-1)-mediated efferocytosis', *American Journal of Physiology - Renal Physiology*, 307(2). doi: 10.1152/ajprenal.00638.2013.

Germano, G. *et al.* (2017) 'Inactivation of DNA repair triggers neoantigen generation and impairs tumour growth', *Nature*, 552. doi: 10.1038/nature24673.

Globocan (2020) 'No Title'.

Gnarra, J. R. *et al.* (1994) 'Mutations of the VHL tumour suppressor gene in renal carcinoma', *Nature Genetics*, 7(1). doi: 10.1038/ng0594-85.

Gomez-Cuadrado, L. *et al.* (2017) 'Mouse models of metastasis: Progress and prospects', *DMM Disease Models and Mechanisms*. doi: 10.1242/dmm.030403.

Groulx, I. and Lee, S. (2002) 'Oxygen-Dependent Ubiquitination and Degradation of Hypoxia-Inducible Factor Requires Nuclear-Cytoplasmic Trafficking of the von Hippel-Lindau Tumor

Suppressor Protein', *Molecular and Cellular Biology*, 22(15). doi: 10.1128/mcb.22.15.5319-5336.2002.

Guida, M. *et al.* (2007) 'Basal cytokines profile in metastatic renal cell carcinoma patients treated with subcutaneous IL-2-based therapy compared with that of healthy donors', *Journal of Translational Medicine*, 5. doi: 10.1186/1479-5876-5-51.

Han, W. K. *et al.* (2002) 'Kidney Injury Molecule-1 (KIM-1): A novel biomarker for human renal proximal tubule injury', *Kidney International*, 62(1). doi: 10.1046/j.1523-1755.2002.00433.x.

Han, W. K. *et al.* (2005) 'Human kidney injury molecule-1 is a tissue and urinary tumor marker of renal cell carcinoma', *Journal of the American Society of Nephrology*, 16(4). doi: 10.1681/ASN.2004070530.

Hanahan, D. and Coussens, L. M. (2012) 'Accessories to the crime: functions of cells recruited to the tumor microenvironment', *Cancer Cell*, 20(21(3)), pp. 309–22. Available at: https://pubmed.ncbi.nlm.nih.gov/22439926/.

Harlander, S. *et al.* (2017) 'Combined mutation in Vhl, Trp53 and Rb1 causes clear cell renal cell carcinoma in mice', *Nature Medicine*, 23(7). doi: 10.1038/nm.4343.

Heng, D. Y. C., Kollmannsberger, C. and Chi, K. N. (2010) 'Review: Targeted therapy for metastatic renal cell carcinoma: Current treatment and future directions', *Therapeutic Advances in Medical Oncology*. doi: 10.1177/1758834009352498.

Henke, E., Nandigama, R. and Ergün, S. (2020) 'Extracellular Matrix in the Tumor Microenvironment and Its Impact on Cancer Therapy', *Frontiers in Molecular Biosciences*. doi: 10.3389/fmolb.2019.00160.

Hillman, G. G., Droz, J. P. and Haas, G. P. (1994) 'Experimental animal models for the study of

therapeutic approaches in renal cell carcinoma', *In Vivo*.

Hu, H. *et al.* (2009) 'Gender differences in the susceptibility to renal ischemia-reperfusion injury in BALB/c mice', *Tohoku Journal of Experimental Medicine*, 218(4). doi: 10.1620/tjem.218.325.

Huang, J. and Manning, B. D. (2008) 'The TSC1-TSC2 complex: A molecular switchboard controlling cell growth', *Biochemical Journal*. doi: 10.1042/BJ20080281.

Humphreys, B. D. *et al.* (2013) 'Chronic epithelial kidney injury molecule-1 expression causes murine kidney fibrosis', *Journal of Clinical Investigation*, 123(9). doi: 10.1172/JCI45361.

Ichimura, T. *et al.* (1998) 'Kidney injury molecule-1 (KIM-1), a putative epithelial cell adhesion molecule containing a novel immunoglobulin domain, is up-regulated in renal cells after injury', *Journal of Biological Chemistry*, 273(7). doi: 10.1074/jbc.273.7.4135.

Ichimura, T. *et al.* (2008) 'Kidney injury molecule-1 is a phosphatidylserine receptor that confers a phagocytic phenotype on epithelial cells', *Journal of Clinical Investigation*, 118(5). doi: 10.1172/JCI34487.

Ichimura, T., Brooks, C. R. and Bonventre, J. V. (2012) 'Kim-1/Tim-1 and immune cells: Shifting sands', *Kidney International*. doi: 10.1038/ki.2012.11.

Ismail, O. Z. *et al.* (2016) 'G protein α12 (Gα12) is a negative regulator of kidney injury molecule-1-mediated efferocytosis', *American Journal of Physiology - Renal Physiology*, 310(7). doi: 10.1152/ajprenal.00169.2015.

Ismail, Z. O. *et al.* (2016) 'G protein α 12 (Gα 12) is a negative regulator of kidney injury molecule-1-mediated efferocytosis', *American Journal of Physiology-Renal Physiology*, 310(7), pp. F607–F620.

Keith, D. S. *et al.* (1994) 'Renal cell carcinoma in autosomal dominant polycystic kidney disease', *Journal of the American Society of Nephrology*, 4(9), pp. 1661–9.

Khanna, C. and Hunter, K. (2005) 'Modeling metastasis in vivo', *Carcinogenesis*. doi: 10.1093/carcin/bgh261.

Kobayashi, N. *et al.* (2007) 'TIM-1 and TIM-4 Glycoproteins Bind Phosphatidylserine and Mediate Uptake of Apoptotic Cells', *Immunity*, 27(6). doi: 10.1016/j.immuni.2007.11.011.

Kuczek, D. E. *et al.* (2019) 'Collagen density regulates the activity of tumor-infiltrating T cells', *Journal for ImmunoTherapy of Cancer*, 7(1). doi: 10.1186/s40425-019-0556-6.

De L Davies, C. *et al.* (2002) 'Comparison of IgG diffusion and extracellular matrix composition in rhabdomyosarcomas grown in mice versus in vitro as spheroids reveals the role of host stromal cells', *British Journal of Cancer*, 86(10). doi: 10.1038/sj.bjc.6600270.

Larkin, J. M. G. and Eisen, T. (2006) 'Renal cell carcinoma and the use of sorafenib', *Therapeutics and Clinical Risk Management*.

Lee, J. C. *et al.* (2021) 'Kidney injury molecule-1 inhibits metastasis of renal cell carcinoma', *Scientific reports*, 11(11840).

Lee, J. and Gunaratnam, L. (2019) *The role of kidney injury molecule-1 in the metastasis of renal cell carcinoma*. The University of Western Ontario.

Lee, S. *et al.* (2018) 'Specification of subject sex in oncology-related animal studies', *Acute and Critical Care*, 33(3). doi: 10.4266/acc.2017.00444.

Li, L. and Kaelin, W. G. (2011) 'New insights into the biology of renal cell carcinoma', *Hematology/Oncology Clinics of North America*. doi: 10.1016/j.hoc.2011.04.004.

Lim, S. Bin *et al.* (2019) 'Pan-cancer analysis connects tumor matrisome to immune response', *npj Precision Oncology*, 3(1). doi: 10.1038/s41698-019-0087-0.

Lin, F. *et al.* (2007) 'Human kidney injury molecule-1 (hKIM-1): A useful immunohistochemical marker for diagnosing renal cell carcinoma and ovarian clear cell

carcinoma', *American Journal of Surgical Pathology*, 31(3). doi: 10.1097/01.pas.0000213353.95508.67.

Lu, D. *et al.* (2019) 'Beyond T Cells: Understanding the Role of PD-1/PD-L1 in Tumor-Associated Macrophages', *Journal of Immunology Research*. doi: 10.1155/2019/1919082.

Lwin, T. M., Hoffman, R. M. and Bouvet, M. (2018) 'Advantages of patient-derived orthotopic mouse models and genetic reporters for developing fluorescence-guided surgery', *Journal of Surgical Oncology*. doi: 10.1002/jso.25150.

Ma, X. *et al.* (2001) 'VHL gene alterations in renal cell carcinoma patients: Novel hotspot or founder mutations and linkage disequilibrium', *Oncogene*, 20(38). doi: 10.1038/sj.onc.1204692.

Majo, S. *et al.* (2020) 'Impact of Extracellular Matrix Components to Renal Cell Carcinoma Behavior', *Frontiers in Oncology*, 10. doi: 10.3389/fonc.2020.00625.

Maller, O. *et al.* (2020) 'Tumour-associated macrophages drive stromal cell-dependent collagen crosslinking and stiffening to promote breast cancer aggression', *Nature Materials*. doi: 10.1038/s41563-020-00849-5.

Mijuskovic, M. *et al.* (2018) 'Tissue and urinary KIM-1 relate to tumor characteristics in patients with clear renal cell carcinoma', *International Urology and Nephrology*, 50(1). doi: 10.1007/s11255-017-1724-6.

Mori, K. *et al.* (2009) 'CpG hypermethylation of collagen type I alpha 2 contributes to proliferation and migration activity of human bladder cancer', *International Journal of Oncology*, 34(6), pp. 1593–602.

Mori, S. *et al.* (2014) 'Characteristic expression of extracellular matrix in subcutaneous adipose tissue development and adipogenesis; Comparison with visceral adipose tissue', *International Journal of Biological Sciences*, 10(8). doi: 10.7150/ijbs.8672.

Motzer, R. J. *et al.* (2013) 'Pazopanib versus Sunitinib in Metastatic Renal-Cell Carcinoma', *New England Journal of Medicine*, 369(8). doi: 10.1056/nejmoa1303989.

Motzer, R. J. *et al.* (2015) 'Nivolumab versus Everolimus in Advanced Renal-Cell Carcinoma', *New England Journal of Medicine*, 373(19). doi: 10.1056/nejmoa1510665.

Motzer, R. J. *et al.* (2018) 'Nivolumab plus Ipilimumab versus Sunitinib in Advanced Renal-Cell Carcinoma', *New England Journal of Medicine*, 378(14). doi: 10.1056/nejmoa1712126.

Motzer, R. J. *et al.* (2019) 'Avelumab plus Axitinib versus Sunitinib for Advanced Renal-Cell Carcinoma', *New England Journal of Medicine*, 380(12). doi: 10.1056/nejmoa1816047.

Muglia, V. F. and Prando, A. (2015) 'Renal cell carcinoma: histological classification and correlation with imaging findings', *Radiologia Brasileira*, 48(3). doi: 10.1590/0100-3984.2013.1927.

Murphy, G. P. and Hrushesky, W. J. (1973) 'A murine renal cell carcinoma', *Journal of the National Cancer Institute*, 50(4). doi: 10.1093/jnci/50.4.1013.

Murphy, K. A. *et al.* (2017) 'A syngeneic mouse model of metastatic renal cell carcinoma for quantitative and longitudinal assessment of preclinical therapies', *Journal of Visualized Experiments*, 2017(122). doi: 10.3791/55080.

Nagata, S. *et al.* (2016) 'Exposure of phosphatidylserine on the cell surface', *Cell Death and Differentiation*. doi: 10.1038/cdd.2016.7.

Nakano, K. *et al.* (2018) 'Difference in morphology and interactome profiles between orthotopic and subcutaneous gastric cancer xenograft models', *Journal of Toxicologic Pathology*, 31(4). doi: 10.1293/tox.2018-0020.

National Cancer Institute (2020) 'Renal Cell Cancer Treatment (PDQ®)–Patient Version', *National Institutes of Health*. Available at: https://www.cancer.gov/types/kidney/patient/kidney-

treatment-pdq.

National Human Genome Research Institute (2004) 'Scientists Compare Rat Genome With Human, Mouse Analysis Yields New Insights into Medical Model, Evolutionary Process', *National Institutes of Health*. Available at: https://www.genome.gov/11511308/2004-release-scientists-compare-rat-genome#:~:text=Humans have 23 pairs of,patterns across the organisms' chromosomes.

Nissen, N. I., Karsdal, M. and Willumsen, N. (2019) 'Collagens and Cancer associated fibroblasts in the reactive stroma and its relation to Cancer biology', *Journal of Experimental and Clinical Cancer Research*, 38(115).

Owusu-Ansah, K. G. *et al.* (2019) 'COL6A1 promotes metastasis and predicts poor prognosis in patients with pancreatic cancer', *International Journal of Oncology*, 55(2). doi: 10.3892/ijo.2019.4825.

Pardoll, D. M. (2012) 'Immunology beats cancer: A blueprint for successful translation', *Nature Immunology*. doi: 10.1038/ni.2392.

Pause, A. *et al.* (1997) 'The von Hippel-Lindau tumor-suppressor gene product forms a stable complex with human CUL-2, a member of the Cdc53 family of proteins', *Proceedings of the National Academy of Sciences of the United States of America*, 94(6). doi: 10.1073/pnas.94.6.2156.

Peng, D. H. *et al.* (2020) 'Collagen promotes anti-PD-1/PD-L1 resistance in cancer through LAIR1-dependent CD8+ T cell exhaustion', *Nature Communications*, 11(1). doi: 10.1038/s41467-020-18298-8.

Porta, C., Paglino, C. and Mosca, A. (2014) 'Targeting PI3K/Akt/mTOR signaling in cancer', *Frontiers in Oncology*. doi: 10.3389/fonc.2014.00064.

Ravaud, A. *et al.* (2016) 'Adjuvant Sunitinib in High-Risk Renal-Cell Carcinoma after Nephrectomy', *New England Journal of Medicine*, 375(23). doi: 10.1056/nejmoa1611406.

Rechsteiner, M. P. *et al.* (2011) 'VHL gene mutations and their effects on hypoxia inducible factor HIFα: identification of potential driver and passenger mutations', *Cancer Research*, 71(16). doi: 10.1158/0008-5472.CAN-11-0757.

Reznek, R. H. (2004) 'CT/MRI in staging renal cell carcinoma', *Cancer Imaging*, 4. doi: 10.1102/1470-7330.2004.0012.

Richmond, A. and Yingjun, S. (2008) 'Mouse xenograft models vs GEM models for human cancer therapeutics', *DMM Disease Models and Mechanisms*. doi: 10.1242/dmm.000976.

Romano, M. *et al.* (2019) 'Past, present, and future of regulatory T cell therapy in transplantation and autoimmunity', *Frontiers in Immunology*. doi: 10.3389/fimmu.2019.00043.

Rosenberg, S. A. (2007) 'Interleukin 2 for patients with renal cancer', *Nature Clinical Practice Oncology*. doi: 10.1038/ncponc0926.

Sabbisetti, V. S. *et al.* (2014) 'Blood kidney injury molecule-1 is a biomarker of acute and chronic kidney injury and predicts progression to ESRD in type I diabetes', *Journal of the American Society of Nephrology*, 25(10). doi: 10.1681/ASN.2013070758.

Sahni, V. A. and Silverman, S. G. (2009) 'Biopsy of renal masses: when and why.', *Cancer imaging : the official publication of the International Cancer Imaging Society*. doi: 10.1102/1470-7330.2009.0005.

Salmon, H. *et al.* (2012) 'Matrix architecture defines the preferential localization and migration of T cells into the stroma of human lung tumors', *Journal of Clinical Investigation*, 122(3). doi: 10.1172/JCI45817.

Salup, R. R., Herberman, R. B. and Wiltrout, R. H. (1985) 'Role of natural killer activity in

development of spontaneous metastases in murine renal cancer', *Journal of Urology*, 134(6). doi: 10.1016/S0022-5347(17)47702-0.

Sandock, D. S., Seftel, A. D. and Resnick, M. I. (1997) 'Adrenal metastases from renal cell carcinoma: Role of ipsilateral adrenalectomy and definition of stage', *Urology*, 49(1). doi: 10.1016/S0090-4295(96)00388-3.

Santiago, C. *et al.* (2007) 'Structures of T Cell Immunoglobulin Mucin Receptors 1 and 2 Reveal Mechanisms for Regulation of Immune Responses by the TIM Receptor Family', *Immunity*, 26(3). doi: 10.1016/j.immuni.2007.01.014.

Sasaki, H. *et al.* (2015) 'An improved intrafemoral injection with minimized leakage as an orthotopic mouse model of osteosarcoma', *Analytical Biochemistry*, 486. doi: 10.1016/j.ab.2015.06.030.

Scelo, G. *et al.* (2018) 'KIM-1 as a blood-based marker for early detection of kidney cancer: A prospective nested case–control study', *Clinical Cancer Research*, 24(22). doi: 10.1158/1078-0432.CCR-18-1496.

Seager, R. J. *et al.* (2017) 'Dynamic interplay between tumour, stroma and immune system can drive or prevent tumour progression', *arXiv*. doi: 10.1088/2057-1739/aa7e86.

Seidel, J. A., Otsuka, A. and Kabashima, K. (2018) 'Anti-PD-1 and Anti-CTLA-4 Therapies in Cancer: Mechanisms of Action, Efficacy, and Limitations', *Frontiers in Oncology*, 8(86). Available at: https://www.ncbi.nlm.nih.gov/pmc/articles/PMC5883082/#:~:text=CTLA-4 upregulation on T,order to kill malignant cells.

Şenbabaoğlu, Y. *et al.* (2016) 'Tumor immune microenvironment characterization in clear cell renal cell carcinoma identifies prognostic and immunotherapeutically relevant messenger RNA signatures', *Genome Biology*, 17(1). doi: 10.1186/s13059-016-1092-z.

Shao, N. *et al.* (2019) 'Causes of Death and Conditional Survival of Renal Cell Carcinoma', *Frontiers in Oncology*, 9. doi: 10.3389/fonc.2019.00591.

Siegel, R. L., Miller, K. D. and Jemal, A. (2020) 'Cancer statistics, 2020', *CA: A Cancer Journal for Clinicians*, 70(1). doi: 10.3322/caac.21590.

Sobczuk, P. *et al.* (2020) 'Choosing The Right Animal Model for Renal Cancer Research', *Translational Oncology*. doi: 10.1016/j.tranon.2020.100745.

Sordat, B. C. M. (2017) 'From Ectopic to Orthotopic Tumor Grafting Sites: Evidence for a Critical Role of the Host Tissue Microenvironment for the Actual Expression of the Malignant Phenotype', in *Patient-Derived Mouse Models of Cancer Molecular and Translational Medicine*. Humana Press, Cham, pp. 43–53. doi: https://doi.org/10.1007/978-3-319-57424-0_4.

Stitzlein, L., Rao, P. S. S. and Dudley, R. (2019) 'Emerging oral VEGF inhibitors for the treatment of renal cell carcinoma', *Expert Opinion on Investigational Drugs*. doi: 10.1080/13543784.2019.1559296.

Tang, F. *et al.* (2018) 'Anti-CTLA-4 antibodies in cancer immunotherapy: Selective depletion of intratumoral regulatory T cells or checkpoint blockade?', *Cell and Bioscience*, 8(1). doi: 10.1186/s13578-018-0229-z.

Tau, G. and Rotherman, P. (2001) 'Biologic functions of the IFN-γ receptors', *Allergy*, 54((12)), pp. 1233–1251. Available at: https://www.ncbi.nlm.nih.gov/pmc/articles/PMC4154595/#:~:text=IFN-γ is primarily secreted,%2C regulate Th1%2FTh2 balance%2C.

The American Joint Committee on Cancer (AJCC) (2017) *AJCC Cancer Staging Manual*.

Vachhani, P. and George, S. (2016) 'VEGF inhibitors in renal cell carcinoma', *Clinical Advances in Hematology and Oncology*, 14(12).

Verine, J. *et al.* (2010) 'Hereditary renal cancer syndromes: An update of a systematic review', *European Urology*. doi: 10.1016/j.eururo.2010.08.031.

De Vivar Chevez, A. R., Finke, J. and Bukowski, R. (2014) 'The role of inflammation in kidney cancer', *Advances in Experimental Medicine and Biology*, 816. doi: 10.1007/978-3-348-837-8_9.

Walker, C., Mojares, E. and Del Río Hernández, A. (2018) 'Role of extracellular matrix in development and cancer progression', *International Journal of Molecular Sciences*. doi: 10.3390/ijms19103028.

Wan, F. *et al.* (2015) 'Upregulation of COL6A1 is predictive of poor prognosis in clear cell renal cell carcinoma patients', *Oncotarget*, 6(29). doi: 10.18632/oncotarget.4860.

Weinstock, M. and McDermott, D. (2015) 'Targeting PD-1/PD-L1 in the treatment of metastatic renal cell carcinoma', *Therapeutic Advances in Urology*. doi: 10.1177/1756287215597647.

Wojciechowicz, K. *et al.* (2013) 'Development of the Mouse Dermal Adipose Layer Occurs Independently of Subcutaneous Adipose Tissue and Is Marked by Restricted Early Expression of FABP4', *PLoS ONE*, 8(3). doi: 10.1371/journal.pone.0059811.

Wolf, M. M., Kimryn Rathmell, W. and Beckermann, K. E. (2020) 'Modeling clear cell renal cell carcinoma and therapeutic implications', *Oncogene*. doi: 10.1038/s41388-020-1234-3.

World Health Organization (2018) 'No Title', (Cancer-Key Facts).

Wynn, T. A. (2008) 'Cellular and molecular mechanisms of fibrosis', *Journal of Pathology*. doi: 10.1002/path.2277.

Xu, F. *et al.* (2017) 'The Oncogenic Role of COL23A1 in Clear Cell Renal Cell Carcinoma', *Scientific Reports*, 7(1). doi: 10.1038/s41598-017-10134-2.

Xu, S. *et al.* (2019) 'The role of collagen in cancer: From bench to bedside', *Journal of Translational Medicine*. doi: 10.1186/s12967-019-2058-1.

Yang, L. *et al.* (2015) 'KIM-1-mediated phagocytosis reduces acute injury to the kidney', *Journal of Clinical Investigation*, 125(4). doi: 10.1172/JCI75417.

Yang, P. *et al.* (2014) 'Renal cell carcinoma in tuberous sclerosis complex', *American Journal of Surgical Pathology*, 38(7). doi: 10.1097/PAS.0000000000000237.

Yu, J. W. *et al.* (2018) 'Tumor-immune profiling of murine syngeneic tumor models as a framework to guide mechanistic studies and predict therapy response in distinct tumor microenvironments', *PLoS ONE*, 13(11). doi: 10.1371/journal.pone.0206223.

Yuzhalin, A. E. *et al.* (2018) 'A core matrisome gene signature predicts cancer outcome', *British Journal of Cancer*, 118(3). doi: 10.1038/bjc.2017.458.

Zemek, R. M. *et al.* (2020) 'Bilateral murine tumor models for characterizing the response to immune checkpoint blockade', *Nature Protocols*, 15(5). doi: 10.1038/s41596-020-0299-3.

Zhang, P. L. *et al.* (2014) 'Urine kidney injury molecule-1: A potential non-invasive biomarker for patients with renal cell carcinoma', *International Urology and Nephrology*, 46(2). doi: 10.1007/s11255-013-0522-z.

Zhang, W. *et al.* (2019) 'Comparative Study of Subcutaneous and Orthotopic Mouse Models of Prostate Cancer: Vascular Perfusion, Vasculature Density, Hypoxic Burden and BB2r-Targeting Efficacy', *Scientific reports*, 9(1). doi: 10.1038/s41598-019-47308-z.

Zheng, X. *et al.* (2019) 'Prognostic value of TIM-1 expression in human non-small-cell lung cancer', *Journal of Translational Medicine*, 17(1). doi: 10.1186/s12967-019-1931-2.